Effects of heterogeneity of concrete on the mechanical behavior of structures at different scales

Maria Ghannoum

Communauté
UNIVERSITÉ Grenoble Alpes

THÈSE

Pour obtenir le grade de

DOCTEUR DE LA COMMUNAUTE UNIVERSITE GRENOBLE ALPES

Spécialité : **2MGE : Matériaux, Mécanique, Génie civil, Electrochimie**

Arrêté ministériel : 25 mai 2016

Présentée par

Maria GHANNOUM

Thèse dirigée par **Julien BAROTH**

préparée au sein du **Laboratoire Sols, Solides, Structures et Risques**
dans **l'École Doctorale I-MEP2-Ingénierie-Matériaux, Mécanique, Environnement, Energétique, Procédés, Production**

Effets des hétérogénéités du béton sur le comportement mécanique des structures à plusieurs échelles

Thèse soutenue publiquement le **18 septembre 2017**,
devant le jury composé de :

M. Alain Sellier
Professeur, Université Paul Sabatier, Rapporteur
M. Denis BREYSSE
Professeur, Institut de mécanique et d'ingénierie-Bordeaux, Rapporteur
M. Pierre ROSSI
Dr IFSTTAR, Examinateur
M. Jacky MAZARS
Professeur émérité, Université Grenoble-Alpes, Président
Mme Sylvie MICHEL-PONNELLE
Ingénieur de recherche, EDF, Examinateur
M. Julien BAROTH
Maître de conférences, Université Grenoble-Alpes, Directeur de thèse
Mme Claude ROSPARS
CR IFSTTAR, Co-directeur de thèse
M. Alain MILLARD
Ingénieur-Chercheur, CEA Saclay, Encadrant de thèse

To Mom and Dad, who encourage me to go on this adventure.

"Trust in dreams, for in them is hidden the

gate of eternity", *Khalil Gibran*

Acknowledgements

First and foremost, I would like to express my appreciation to my advisor Julien BAROTH for the continuous support of my Ph.D study and related research, for his patience, motivation, and immense knowledge. His guidance helped me in all the time of research and writing of this thesis. I am, also, grateful for our many and valuable scientific and non scientific conversations those three years period that I will keep as a pleasant memory. I could not have imagined having a better advisor and mentor for my Ph.D study. It was an honor to be his first Ph.D student.

Besides, I would like to express my sincere gratitude to my supervisors Alain MILLARD and Claude ROSPARS, who, despite being in Paris, were available these 3 years with their constructive advices. It was a great opportunity for me to work at their side and guidance they have provided which has always been very pleasant, positive and constructive. I would like also to thank them for giving me the opportunity of being a part of IFSTTAR lab and CEA Saclay, where i met great researchers, I mention in particular Antoine LLAU.

I would like to thank the jury members for their interest and participation in this thesis. Special thanks go to Mr. Denis BREYSSE and Mr. Alain SELLIER, for their constructive comments on the thesis script. I am also very grateful to Mr. Pierre Rossi, Mrs Sylvie MICHEL-PONNELLE for examining my thesis. And finally, My deepest thank go to Mr Jacky MAZARS for accepting to be the president of my jury.

My Ph.D was founded by the ANR project MACENA, that is to be thanked deeply for giving me the opportunity to be a part of this project.

My sincere thanks also goes to Mr. Cino VIGGIANI for offering me the opportunity to come to France and achieve my dreams.

In the 3SR Lab, I was grateful to meet many people, who were more than friends to me and made my stay in Grenoble very pleasant. Special thank to Eleni KOUFOUDI, for our endless talks and laughters, to Reem ABDULRAHMAN for our endless breaks and gossips. My sincere thanks go also to Rodaina, Abdallah, Mohamad Y., Mohamd D., Maxime, Alexandra, Eleni S., Fabio, Timos, Bratislav.

Outside the lab, I met amazing friends, with who i shared wonderful memories in France and more precisely in Grenoble. My sincere thanks go to Raymonda, Ranime, Reine, Jimmy, Christelle, Chirine, Joseph ...

A very special thanks go to my flatmate, my best friend and my travel companion Nahia. She filled the every day routine of the thesis with laughter and fun.

I am, also, deeply grateful to my family (my mom, my dad, Bashir, Mirna and Nahed) and friends (Laura, Karine, Dima, Amani and Yasmine) in Lebanon who supported me and encouraged me during my stay abroad which help me to overcome all the difficulties I affronted.

Finally, my deepest thanks go to my husband for almost unbelievable support throughout this thesis and all these years. Thank you for making my life abroad easier.

Abstract

This thesis aims to model concrete heterogeneities and their consequences on the mechanical behavior of concrete or Reinforced Concrete (RC) structures. These heterogeneities lead to the spatial variability of the concrete tensile strength depending on the volume of concrete under tension. Thus, the influence of this spatial variability on the mechanical behavior and concrete cracking pattern is particularly enhanced using a Stochastic Finite Element (SFE) method accounting for statistical size effect. More precisely, an analytical size effect law and random fields generation are used in two steps:

First, in order to evaluate the reduction of the mean concrete tensile strength at different scales, an analytical probabilistic approach of the Weakest Link and Localization (WL2) method (Sellier and Millard [2014]) is proposed. This method is able to estimate the distribution of the tensile strength, at different scales, accounting for stress redistributions around the weakest point. However, it depends on a scale length, whose identification is discussed and identified using experimental concrete series. This scale length accounts for spatial variability of the concrete tensile strength.

Secondly, the capability of reproducing the size effect on the mean concrete tensile strength, in Finite Element (FE) models, by accounting for the variability of this parameter is discussed using SFE method. This method consists on generating discretized autocorrelated random fields realizations, using the mean tensile strength estimated from the analytical approach of WL2. Moreover, the choice of autocorrelation parameters, used to define the random fields, is discussed.

The ability of both methods to reproduce the size effect on tensile strength, more particularly the statistical one, is evaluated using various experimental series. Furthermore, the SFE method is applied to the concrete of the simplified model of a containment building. The variability of concrete tensile strength, at this scale, is modeled using independent autocorrelated random field at each lift, that are identified from in-situ measurements. The SFE method shows its pertinence in the estimation of crack positions.

Keywords: tensile strength . size effect . variability . WL2 . stochastic finite element . random fields . scale length . autocorrelation length

Résumé de la thèse

Cette thèse contribue à la modélisation des hétérogénéités du béton et leurs conséquences sur le comportement mécanique des structures en béton ou en béton armé. Ces hétérogénéités conduisent à la variabilité spatiale de la résistance à la traction, dont l'effet dépend du volume du béton sollicité en traction. Ainsi, l'influence de cette variabilité spatiale sur le comportement mécanique et sur la fissuration du béton est particulièrement étudiée à l'aide d'une méthode d'Eléments Finis Stochastiques (EFS) reprśentant l'effet d'échelle statistique. En particulier, une loi d'effet d'échelle analytique et des champs aléatoires sont utilisés en deux étapes :

Premièrement, afin d'évaluer la réduction de la résistance moyenne à la traction du béton à différentes échelles, une approche analytique probabiliste de la méthode Weakest Link and Localization (WL2) (Sellier and Millard [2014]) est proposée. Cette méthode estime la distribution de la résistance à la traction, à différentes échelles, en tenant compte des redistributions des contraintes autour du point le plus faible. Cependant, cela dépend d'une longueur d'échelle, dont l'identification est discutée. Cette longueur d'échelle rend compte du caractère aléatoire de la résistance à la traction du béton.

Deuxièmement, la capacité de reproduire l'effet d'échelle sur la résistance moyenne à la traction du béton, dans les modèles EF, en tenant compte de la variabilité de ce paramètre, est discutée à l'aide de la méthode EFS. La méthode consiste à générer des réalisations de champs aléatoires autocorrelés discrétisés, en utilisant la résistance à la traction réduite estimée à partir de l'approche analytique de WL2. En outre, le choix des paramètres d'autocorrélations, utilisés pour définir les champs aléatoires, est discuté.

La capacité des deux méthodes à reproduire l'effet d'échelle sur la résistance à la traction, et plus particulièrement l'effet d'échelle statistique, est évaluée à l'aide de différentes séries expérimentales. En outre, la méthode EFS est appliquée au modèle simplifié du béton d'une enceinte à double paroi. Les incertitudes sur la résistance à la traction, à cette échelle, sont modélisées à l'aide d'un champ aléatoire autocorrelé indépendant à chaque levée et identifiable à partir des données recueillies sur chantier. La propagation des incertitudes, à l'état initial, montre sa pertinence dans l'estimation des positions de fissures.

Mots clés: Résistance à la traction . effet d'échelle . variabilité . WL2 . élément fini stochastique . champs aléatoires . longueur d'échelle . longueur d'autocorrélation

Contents

List of Figures

List of Tables

Abbreviations

CDF	**C**umulative **D**ensity **F**unction
FE	**F**inite **E**lement
FPZ	**F**racture **P**rocess **Z**one
HSV	**H**ighly **S**tressed **V**olume
ITZ	**I**terfacial **T**ransition **Z**one
LEFM	**L**inear **E**lastic **F**racture **M**echanic
MFSL	**M**ulti-**F**ractal **S**caling **L**aw
RC	**R**einforced **C**oncrete
REV	**R**epresentative **E**lementary **V**olume
SEL	**S**ize **E**ffect **L**aw
SFE	**S**tochastic **F**inite **E**lement
USEL	**U**niversal **S**ize **E**ffect **L**aw
W/C	**W**ater/**C**ement
WEV	**W**eibull **E**ffective **V**olume
WL2	**W**eakest **L**ink and **L**ocalization

Symbols

Symbols	Definition	Units
f_t	Tensile strength	Pa
f_{ctm}	Tensile strength measured on a cylindrical specimen	Pa
$f_{ct,sp}$	Splitting tensile strength measured on a cylindrical specimen	Pa
$_{ct,fl}$	Flexural strength	Pa
$f_{ct,0.05}$	Characteristic tensile strength with 5 % quantile	Pa
$\mu(f_t)$	Mean value of the tensile strength	Pa
$Std\,(f_t)$	Standard deviation of the tensile strength	Pa
$CV(f_t)$	Coefficient of variation of the tensile strength	Pa
$f_{cy}(D)$	Compressive strength of a cylindrical specimen of diameter D	Pa
$f_{cu}(d)$	Compressive strength of a cubic specimen of size d	Pa
f_c	Compressive strength of standard cylinder (15×30 cm^2)	Pa
σ_{max}	Maximum value of the principal stresses	Pa
$\sigma_I, \sigma_{II}, \sigma_{III}$	Principal stresses	Pa
$f_{t/ref}$	Tensile strength of a reference structure	Pa
f_{t0}	Tensile strength for a HSV of 1 cm^3	Pa
σ_0	Material strength or yield limit	Pa
f_{r^∞}	Nominal strength for very large beams with no statistical size effect	Pa
E	Young's modulus	Pa
E_{ci}	Young's modulus at 20^{o}C	Pa
$E_{ci}(T)$	Young's modulus at temperature T	Pa
V	Total volume of the specimen	m^3
V_A	Volume of the largest aggregate	m^3
V_{ref}	Effective volume of a reference structure	m^3
V_E	Effective volume	m^3

A	Cross section area	m^2
L	Span of the beam	m
b	Thickness of the beam	m
H	Height of the beam	m
L_s	Shear span	m
L_b	Bending span	m
l_{ch}	Irwin length	m
D_b	Approximately equal to the FPZ length	
l_p	Material characteristic length	m
l_s	Statistical characteristic length	m
l_I	Scale length	m
υ	Scale of fluctuation	m
a	Gaussian autocorrelation length	m
b	Exponential autocorrelation length	m
c	Sinusoidal autocorrelation length	m
l_{cc}	Characteristic correlation length	m
d_{max}	Max aggregate size	mm
$P_{f/v}$	Probability of failure of a loaded volume V	%
$P_{f/ref}$	Probability of failure of a reference structure	%
r	Reinforcement ratio	%
G_f	Fracture energy	$J.m^{-2}$
m	Weibull parameter	-
K	Severity factor	-
ε_{D0}	Damage threshold	-
B, D_0	Empirical dimensional parameters	-
F_α, F_β	Functions of the compressive strength	-
$C_{VV}(x, x')$	Autocovariance function	-
$\rho_v(x, x')$	Autocorrelation function	-

Chapter 1

General introduction

1.1 Industrial context

France electricity production is based on its majority on nuclear energy. The protection of radionuclide dispersion in the environment, in case of the breakdown of a nuclear reactor such as the accident of the power plant of Fukushima-Daïchi, remains a crucial issue. Therefore, it is important to control the tightness of nuclear power plants, during their service life that is over 40 years. Two types of nuclear power plant exist, in France: reactor buildings of 900 MWe with a simple Reinforced Concrete (RC) containment and a steel liner and reactor buildings of 1300 and 1450 MWe with double RC containments and without steel liner. Both types of containment must insure the protection of the reactor from any external impact and protect the environment from any radionuclide leakage. Hence, to limit the radionuclide leakage, the nuclear power plants are composed by three barriers: the fuel cladding, the primary cooling system and the nuclear containment vessel. In case of breakdown of the two first barriers, the 900 MWe nuclear power plant is constituted of pre-stressed concrete and an inner steel liner. It provides, then, the reactor and the environmental protection. However, in the case of double wall nuclear power plant, the environmental protection is insured by the inner pre-stressed concrete wall and the protection of the reactor is insured by the external RC wall.

Safety analysis of nuclear power plants is provided with a "Severe accident" loading (with an internal pressure of 4.2 bars and a temperature of 180^{o}C), instead of "Lost of coolant accident" loading. Moreover, a regulatory criterion is imposed on the leakage rate (1 % per volume per day) of the inner wall of thickness generally equal to 1.2 m.

In the objective of the extension of the operating life of the nuclear power plants, EDF decided in 2010 to study the aging mechanism of a reactor building of 1300 MWe with double wall, by mean of a 1/3 scaled mock-up VeRCoRs.
In addition, Ceos.fr [2009] project underlined the necessity to account, in the design codes (CEN [2005] and Code [2012]), for the influence of Thermo-Hydro-Mechanical (THM) effect and size effect on the behavior of massive structures, such as nuclear containment. These effects are crucial for the estimation of load stress and strain and concrete crack pattern. Following this path, MACENA (MAitrise du Confinement d'une ENceinte en Accident – Confinement assessment of a vessel during an accident) project was built, in order to better understand the behavior of nuclear containment, under severe accident. Research work and experimental comparisons are based on VeRCoRs mock-up. This mock-up is constructed, in order to study its behavior at early age, the effect of aging and its influence on the evolution of leak tightness. Moreover, the behavior of this mock-up under severe accident conditions, modeled by thermo-mechanical loading maintained several days, is studied (Corbin and Garcia [2015]).

1.2 MACENA project

This PhD thesis is founded by French ANR (Association Nationale de Recherche) and is part of MACENA project. More specifically, this work is a part of the working package WP1 (Assessment of structural state before an accident) that aims to develop mechanical models for the initial state of a nuclear containment vessel (before the occurrence of a severe accident). The major objective of this project is to propose appropriate methodologies, based on constitutive simplified laws and results from the knowledge of the structure, to evaluate the mechanical degradation of concrete due to aging and the residual tension of the pre-stessing cables. WP1 should provide, then, answers on the influence of the variability of concrete mechanical properties on the mechanical behavior of a nuclear containment, at initial state (just before an accident). This work should be included, further in the WP4 package (Structural analysis during an accident). In particular, the main task of this thesis is to develop scaling methods to propagate uncertainties, since the behavior of the structure is influenced by the variability of material characteristics and/or of model parameters. However, time-dependency of aging effect is not included in the modeling.

1.3 Problematic of the thesis

Concrete mechanical properties are generally measured, using conventional tests, on small specimens tested in laboratory (mean compressive strength at 28 days f_{cm}, mean direct tensile strength at 28 days f_{ctm}, splitting tensile strength $f_{ct,sp}$, flexural strength $f_{ct,fl}$). However, due to the heterogeneous composition of the concrete, several laboratory tests conducted on specimens with the same concrete mix lead to different measured concrete characteristics. Thus, a main problematic is to study the effect of this variability (a coefficient of variation on the tensile strength varying from 10 % to 20%), measured on laboratory tests, on the behavior of large RC structures. In addition, the heterogeneity of the concrete leads to a reduction of the tensile strength at first crack observed or measured when the loaded volume is high. This effect, known as size effect, therefore results in a change of the tensile strength at first crack f_t, in large structures, compared to the mean value of the tensile strength f_{ctm} measured at the specimen scale, which can be divided by 2. This estimation was noticed in Ceos.fr [2009] project, the work supported by Mefisto [2012] and Sellier and Millard [2014], when dealing with large structures such as massive beams representative of RC structures, subjected mainly to direct tension which is the most severe loading for concrete. Hence, the mechanical properties of concrete, measured at the specimen scale, and more precisely the tensile strength f_{ctm} can not be representative of the tensile strength of concrete at larger scale f_t. Until now, this tensile strength can not be easily measured in situ (destructive or non-destructive methods). However, it represents one of the most relevant properties in large concrete or RC structures.

1.4 Objectives and methodology

The main objective of this thesis is then to better characterize the concrete properties at the structural scale based on the measured mechanical properties obtained on small laboratory specimens, and more precisely the measured tensile strength f_{ctm}, obtained by conventional tests.

Hence, an analytical method that estimates the average size effect on f_t, that should be introduced in the structure model considering its volume and a numerical method that

accounts for the spatial variability of f_t is proposed.

The methodology used in this PhD thesis can be summarized, then, into two tasks:

- The estimation of the mean, dispersion and distribution of the tensile strength at first crack, for structures of different sizes.
- The propagation of the variability on the tensile strength in Finite Elements (FE) models.

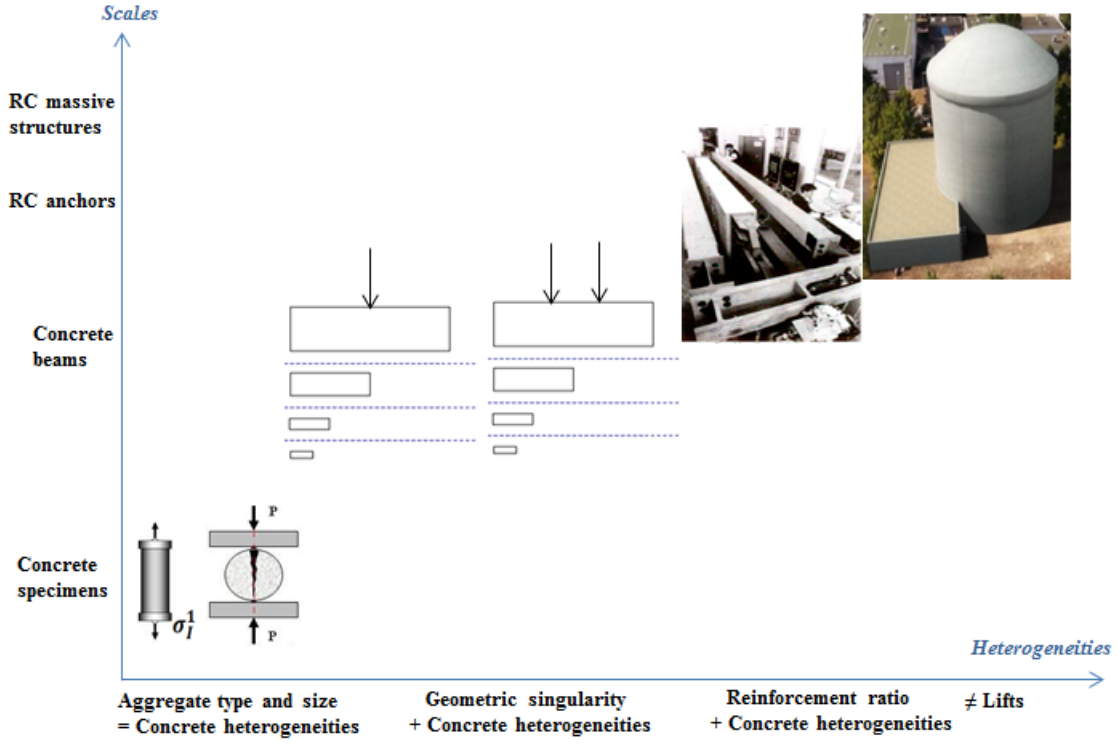

FIGURE 1.1: Different types of studied structures.

Figure 1.1 displays the different structural scales, studied in this thesis, from laboratory tests to large massive structures. Each scale presents various types of heterogeneities from material scales (aggregate size and type, cement, porosity ...) to structural scale that includes construction joints.

Briefly, concrete is a heterogeneous material that induces variability in the measurement of its mechanical properties. Moreover, this concrete strength variability can be the cause of the decrease of concrete tensile strength when the structural volume increases (Weibull [1951], Torrent [1977], Rossi et al. [1994], Sellier and Millard [2014] ...). Therefore, the focus of this thesis is only on statistical size effect of concrete.

1.5 Organization of the thesis manuscript

After this introductory chapter, the manuscript is composed by four additional chapters:

- Chapter 2 is a presentation of the state of the art on different existing methods aiming to solve the problematic raised before. This chapter is divided into three main sections. The first section presents three different scales of concrete structures and introduces the tensile strength at first crack, as an important mechanical property for concrete. The second section focuses on the modeling of size effect on tensile strength in concrete and presents the different methods developed to reproduce the size effect in structures of different sizes. The third and final section elaborates different numerical methods consisting on modeling the variability of the mechanical properties of concrete using random fields.

- Chapter 3 is dedicated to the proposal of a simplified analytical method for modeling size effect in concrete. An analytical probabilistic approach of WL2 method is developed in order to give a fast estimation of the mean and the dispersion of the tensile strength at first crack for concrete or reinforced concrete structures, having different volumes and subjected to different loadings. For validation purposes, experimental campaigns, found in the literature, of series of concrete structures under uniaxial tension, 3-point bending loading and 4-point bending loading are considered. Moreover, validations on large scale structures, such as Mivelaz anchor (Mivelaz [1996]), Malpasset dam (Bažant et al. [2007]) and containments (Michelle-Ponnelle [2015]) are presented.

- Chapter 4 deals with SFE models using discretized random fields. The proposed method which consists on modeling the spatial variability of the tensile strength in concrete is described. A sensitivity analysis is done to characterize the parameters of the discretized random field. Furthermore, in order to validate the methodology, it is also applied to series of concrete structures under 4-point bending loading and 3-point bending loading. Finally, the SFE method using discretized random fields is applied to a concrete vessel using concrete properties of the 1/3 mock-up VeRCoRs (but with no reinforcement or presstressed cables).

- Chapter 5 gives conclusions and perspectives of the present work.

Chapter 2

State of the art

Reliability and durability of Reinforced Concrete (RC) or prestressed concrete structures can be preserved by the control of concrete cracking. Thus, the modeling of concrete cracking is a key issue, for civil engineering structures and more precisely structures under tension as nuclear containments. However, concrete is a heterogeneous material. This heterogeneity is the source of the distribution of different weak zones in concrete provoking different sensitivity of cracking per zone and variability on the concrete mechanical properties. This chapter raises, then, the issue of the influence of concrete variability on the mechanical behavior of RC structures and their cracking, depending on the scale study. Size effect on tensile strength of concrete is particularly dealt with. First, cracking of concrete or RC structures at different scales: the micro, meso and structural scales of concrete are introduced. Thus, it is shown that the heterogeneities of concrete at micro-scale induces a scattering of the concrete tensile strength measured at the meso-scale. Moreover, size effect phenomenon is manifested by the decrease of the tensile strength of concrete for large scaled structures, in comparison with the value measured at meso-scale. Therefore, the different existing methods allowing the prediction of the statistical, energetic and energetic-statistical size effects on tensile strength are presented. Finally, since spatial variability of concrete is directly linked to size effect phenomenon, stochastic finite element (SFE) methods using discretized random fields are mentioned, in order to predict the fracture in concrete and RC structures at different scales.

2.1 Cracking of concrete or RC structures at different scales

Quasi-brittle materials such as rock, ceramics, concrete ... are characterized by micro-cracking, when increasing loading or deformation is applied. Gradual development of macroscopic crack can result from the localization of micro-cracking in a narrow region called Fracture Process Zone (FPZ). Reasonable control of cracking is provided using the available design codes. Cracks in concrete depend on different parameters, such as tensile strength of concrete, drying shrinkage, thermal contraction, restraint (external or internal) to shortening ... Thus, tensile strength is of primary importance to control concrete cracking. However, tensile strength of concrete f_t is characterized by its scattering at meso and structural scales. This scattering is highly influenced by the concrete heterogeneities. These heterogeneities can be linked directly to the concrete mix such as aggregate size, aggregate shape and porosity (Rossi et al. [1994], Van Vliet and Van Mier [2000]) or to the construction conditions, such as boundary conditions, friction, reinforcement ratio and construction joints (Momayez et al. [2005], Farra [1994] and Briffaut [2010]). Figure 2.1 presents the heterogeneities of the concrete at the material (aggregates and specimens) and the structural scales. Thus, the heterogeneities of concrete can be presented at three main scales:

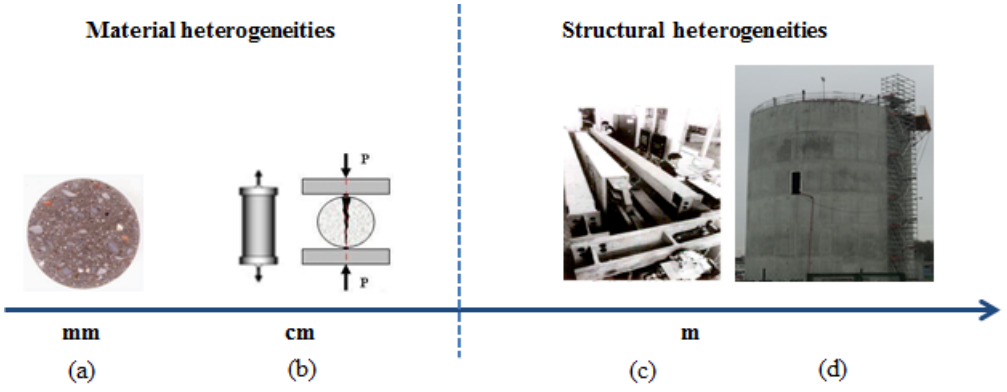

FIGURE 2.1: Heterogeneities at different scales of concrete: (a) at micro scale (Kanos et al. [2006]), (b) at meso scale (REV), (c) at structural scale (Mivelaz [1996] anchor), (d) VeRcoRs (Michelle-Ponnelle [2015]).

- The scale of aggregate, the water/cement ratio (W/C), porosity leading to significantly different characteristics for the same mixture. In particular, Interfacial Transition Zones (ITZ) are considered to be more or less porous areas. Moreover,

they are known to be often most porous and weak among the phases composing concrete (Wong et al. [2009], Grassl et al. [2010] and Nemati and Gardoni [2005]).

- The scale of the concrete (Sebsadji and Chouicha [2012], Stroeven et al. [2004] and Le et al. [2011]), more precisely at the Representative Elementary Volume (REV) scale (defined in Section 2.1.2.1), having variable mechanical properties, depending on the distribution of the aggregates in the mix, the porosity...

- The scale of the structure on which the mechanical behavior, damage, or widths and spacing of cracks should be known (Ceos.fr [2009]). The results obtained at this scale are often deterministic, because of the time-consuming numerical models which are based on the average values of material parameters.

The variability in the mechanical properties at REV scale is the consequence of the heterogeneities of concrete at micro-scale. Consequently, this variability stands at several scales, thus the size effect on f_t at the structural scale is highlighted. In the following, each scale is detailed and explained.

2.1.1 Concrete at micro-scale: a heterogeneous media

Concrete is a composite phase-material which contains mainly aggregates, cement matrix and voids containing water or air. Thus, the concrete has a heterogeneous structure and it is considered as brittle or quasi-brittle material. An important scale, in the concrete specimen, is the scale of its heterogeneities due to the presence of defects, such as voids, micro-cracks and ITZ. Figure 2.2 shows the different components of concrete and an example of the occurrence of a crack, thus the evidence of a FPZ in mode I is highlighted. As coarse aggregates occupy more than one third of the volume of concrete, changes in coarse aggregates induce changes on the strength and fracture properties of concrete (Wong et al. [2009]). In addition, cement paste shrinkage, autogeneous shrinkage and thermal shrinkage can induce micro-cracking in concrete. Also, ITZ present an important effect on the concrete properties (Nemati and Gardoni [2005]). As this thesis focuses on the mechanical behavior of concrete, the influence of the aggregates and the ITZ on the concrete properties are discussed.

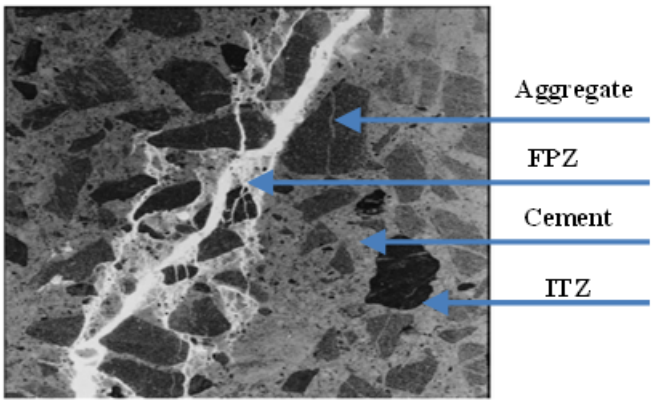

FIGURE 2.2: Different components of concrete and the occurrence of cracking (Dufour [2017]).

2.1.1.1 Influence of the Interfacial Transition Zones (ITZ)

The properties of concrete, at the REV scale, are directly linked to the ITZ which tends to act as the weak link in the chain compared to the bulk cement paste and the aggregate particles. Indeed, among the phases composing the concrete, ITZ phase is known to be often more porous and weak, where first micro-cracks occur (Nemati and Gardoni [2005]). Thus, the low tensile strength and stiffness of concrete can be due to the low strength and stiffness of the ITZ.

2.1.1.2 Influence of Aggregates size

It is widely understood that a link exists between the structure at micro-scale and the properties of the structure at macro-scale, rather between micro-cracking and transport properties. For example, increasing aggregate size at constant aggregate fraction induces an increase of permeability (Wong et al. [2009]). Thus, the diameter of the aggregate plays an important role on the prediction of the durability and service life. The aggregate size is directly associated to the length of micro-cracks and the average crack width. In conclusion, the influence of concrete components, and more precisely the aggregates and the ITZ, on the appearance of a weak zone is highlighted. Thus, the crack propagation of concrete is linked to the the concrete heterogeneities at the micro-scale.

2.1.2 Concrete at specimen scale: Variability of material properties

This meso scale level corresponds to the REV of the concrete. The mechanical properties of concrete (direct tensile strength at 28 days f_{ctm}, compressive strength at 28 days f_c and Young's modulus E) should be determined at this scale. However, at first, a definition for the REV of concrete should be adopted. Some authors tried to give a definition for the REV corresponding to cementitious materials (Sebsadji and Chouicha [2012] and Stroeven et al. [2004]). Conventionally, the size of the REV of the concrete must be at least 3-5 times the size of the largest aggregate when the measured properties concern the mechanical behavior of concrete (Le et al. [2011]).

2.1.2.1 What is the REV for concrete?

A REV is considered as a small volume of a heterogeneous material, which is capable of obtaining an appropriate homogenized behavior. Bornert et al. [2001] stated that the REV must satisfy these two following conditions:

- Larger than the characteristic size of the heterogeneity (the largest aggregate size, for example), in order to allow a correct statistical representation of the studied material.
- Smaller than the characteristic size of a mechanical structure (beam, anchor, structure, building ...), in order to represent an equivalent homogeneous material.

For example, Wu [2015] estimated a REV equal to $7d_{max}^3$ as representative of concrete related to the desorption isotherm, where d_{max} is the largest aggregate. In addition, it is worth noting that standard test specimens have a diameter D equal to 150 or 160 mm and a length L equal to three and five times the maximum aggregate size d_{max} but is usually larger. Also, the splitting (or Brazilian) test is considered as a standard test method to measure the splitting tensile strength $f_{ct,sp}$ of concrete (ASTM [2004], CEN [2005] and Code [2012]) since it is the simplest and the most reliable method to estimate the tensile strength. The direct tensile strength f_{ctm} is approximately equal to $0.9f_{ct,sp}$ (CEN [2005]).

Even though a standard REV is chosen for concrete, performing several compression tests or splitting tests to same mixture of concrete leads to different curve of stress-strain or

force-displacement. Generally, the averaging behavior is the only one considered, but scattering is an important feature that should be taken into account in constitutive laws. Mesureur [1989] determined the scattering linked to the used test method. He showed that the tensile strengths measured on N specimens subjected to splitting tests present a coefficient of variation twice as large as the compressive strengths measured on N specimens subjected to compressive tests. Simultaneously, the variability of the mechanical properties of concrete REV is directly linked to the heterogeneities of concrete at the micro scale (see Figure 2.3). Table 2.1 gives intervals for the mean values and the coefficient of variations of the compressive strength, the tensile strength, the Young's modulus, the steel yield stress and the concrete density, in the case of concrete. Hence, the scattering in the mechanical properties of concrete is highlighted. For cur-

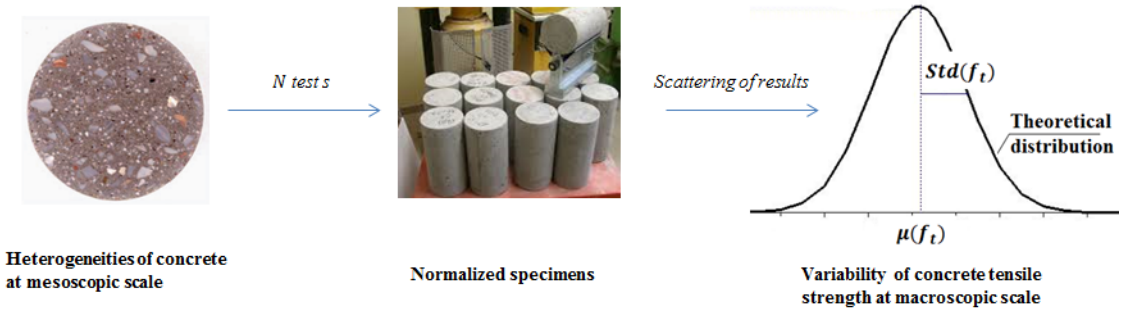

FIGURE 2.3: Scattering in the mechanical response of concrete due to heterogeneities.

rent structures, the scattering of the tensile strength is implicitly taken into account in Code [2012] and CEN [2005] using the characteristic value $f_{ct,0.05}$ that guarantees that at most 5 % of the values encountered are less than $f_{ct,0.05}$. This scattering is due not only to the size of the specimen, but also to its geometry and its boundary conditions effect. One approach used by Rossi and Piau [1988] consists on considering that the

TABLE 2.1: Mean values and coefficient of variations of physical and mechanical characteristics in RC structures (Sudret [2007]).

Uncertain Parameter	Mean	CV (%)
Compressive strength (f_c)	30-130 MPa	7-15
Tensile strength (f_t)	3-5 MPa	10-20
Young's modulus (E)	38-47 GPa	5-8
Steel yield stress (f_y)	420 MPa	5
Concrete density	2500 kg/m^3	10

mechanical properties of concrete follow a random distribution, before performing the numerical simulations. Consequently, Breysse [1990] assumed an elastic-brittle behavior for this representative micro volume, modeled using a spring having a randomly distributed probability of fracture.

In addition, for concrete specimens subjected to direct tension, Rossi et al. [1994] showed that the mechanical properties of the concrete (tensile strength f_t and Young's modulus E) depend on the maximum diameter of the granulate. In consequence, the influence of the concrete heterogeneity on the macroscopic behavior of the specimen increases for the small specimens, where micro-structural effects, which depend on the presence or absence of large aggregates in the critical section, dominate. Consequently, Rossi et al.

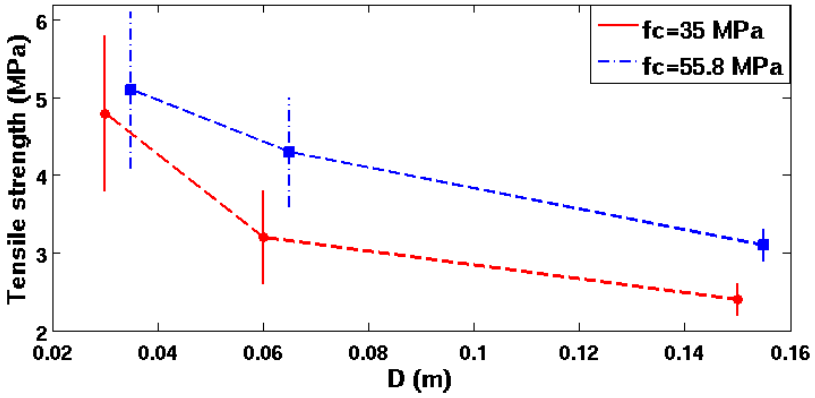

FIGURE 2.4: Experimental dispersion of concrete tensile strength as function of the diameter of the specimen, for two different concrete mix (Rossi et al. [1994]).

[1994] showed that the mean and the standard deviation of the tensile strength decreases as the volume of the specimen increases (see Figure 2.4). However, the mean value of the Young's modulus was found independent of the size of the specimen. Thus, a size effect on the tensile strength is observed at this meso-scale.

2.1.2.2 Shape effect on concrete specimens

The concrete specimens used to test the mechanical properties of the concrete differ in sizes and shapes from country to another and compressive strength showed a dependency on both size and shape of the used specimen. Some authors experimentally investigated the effect of the size and shape of the specimen on the compressive strength by conducting both cubic and cylindrical specimens having different volumes (Del Viso et al. [2007] and Yi et al. [2006]). Figure 2.5 shows the evolution of the ratio between the compressive

strength $f_{cy}(D)$ of a cylinder, having a diameter D, and the compressive strength of standard cylinder (in this case, 15×30 cm^2) f_c as function of the cylinder diameter D and the evolution of the ratio between the compressive strength $f_{cu}(d)$ of a cubic specimen, having a dimension d, and f_c as function of the cube size d. The size effect for cubes was observed to be stronger than cylinders. In addition, Del Viso et al. [2007] showed an influence of the size shape on the pre-peak and post peak of the curves $\sigma - \varepsilon$. Cylinder specimens present a strong failure localization and frictional contact strength compared to the cubic specimens that present a mild failure localization.

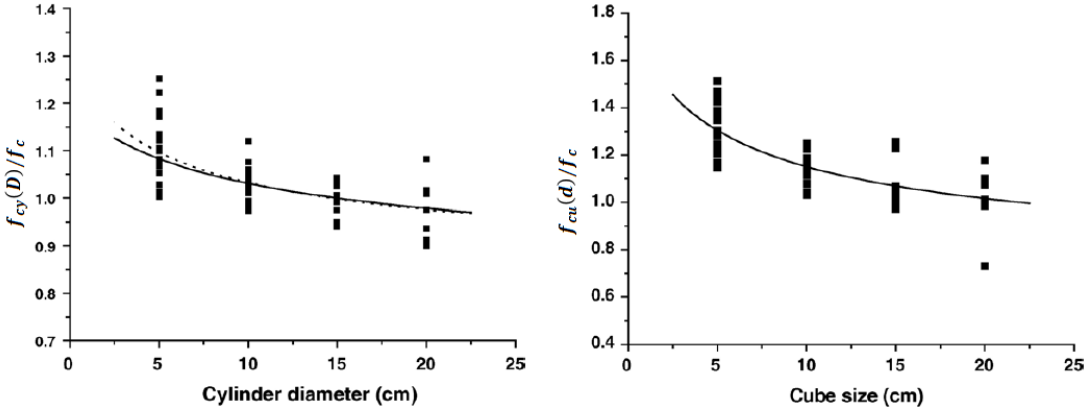

FIGURE 2.5: Size effect on compressive strength for cylindrical (left) and cubic (right) specimens (Yi et al. [2006]).

2.1.2.3 Boundary conditions effect on splitting tests

Several authors highlighted the decrease of the splitting tensile strength $f_{ct,sp}$ as the volume of the specimen increases and its boundary condition differs. Thus, the size effect on the measured value of $f_{ct,sp}$ is introduced by Bažant et al. [1991], Torrent [1977], Hasegawa et al. [1985], Kadleček and Modrỳ [2002], Carmona et al. [1998] and Rocco et al. [2001]. These tests were conducted on specimens having diameter ranging between 19 and 3000 mm. The maximum tensile strength $f_{ct,sp}$ is shown to decrease as the width b_s of the load-bearing strips increases. Rocco et al. [2001] showed, for example, that a variation of only 4 % of $f_{ct,sp}$ is obtained on standardized specimens having $b_s/D = 12$. In conclusion, REV scale should account for the heterogeneity composition of concrete at micro-scale.

Consequently, several size effects on concrete such as the boundary layer effect, the

geometry of the specimen, the randomness of the material strength and the stress redistribution affect the mechanical properties of concrete at the structural scale, as described hereafter.

2.1.3 Concrete at structural scale: size effects phenomena

The variation of the tensile strength f_t with a characteristic size of a structural member is an important property when dealing with concrete, in which the tensile structural strength decreases and the material brittleness increases when the element size under tension increases. In order to highlight the severe problem arising from size effect phenomenon, tensile strength corresponding to specimens and anchors under uniaxial tension are studied. The used experimental concrete specimen series correspond to Rossi et al. [1994] and Van Vliet and Van Mier [2000] and the used anchors correspond to Clement [1987], Farra [1994] and Mivelaz [1996]. Details on each experimental test are given in Appendix A. Figure 2.6 presents the different results of the tensile strength obtained on each specimen and tensile strength at first crack for the case of anchors as function of the smallest dimension of the specimen or anchor. The results are presented as the ratio between the tensile strength of the considered structure and the reference tensile strength corresponding to the first specimen of the series. For the case of anchors, the refrence tensile strength corresponds to the splitting tensile strength. This

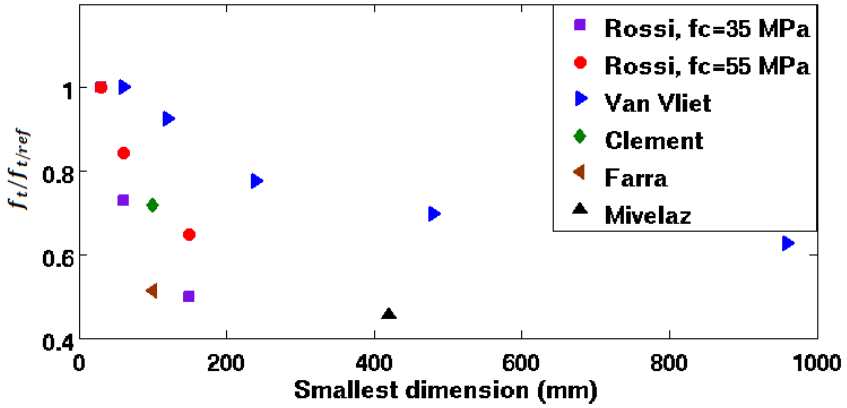

FIGURE 2.6: Values of the tensile strength for series of specimens or anchors under uniaxial tension as function of the smallest dimension of the specimen (Rossi et al. [1994], Van Vliet and Van Mier [2000], Clement [1987], Farra [1994] and Mivelaz [1996]).

figure highlights the size effect on the tensile strength. As underlined before, the tensile strength f_t decreases when the volume increases and it is almost divided by 2 for large structures.

Thus, the tensile strength corresponding to the appearance of the first macro-crack represents one of the most relevant properties in large concrete or RC structures. In the following, the parameters influencing the global response of the structures at different scales are discussed.

2.1.3.1 Sources of size effect

The national project Ceos.fr [2009] and the works supported by Mefisto [2012] project showed that a loss of 50 % of the tensile strength value measured on splitting test can be obtained when dealing with large structures such as anchors and nuclear containments, both subjected mainly to direct tension (Sellier and Millard [2014]). Hence, these projects allow significant advances concerning the prediction of the tensile strength for large structures. This reduction is the consequence of not only "the size effect" phenomenon, but also some other aspects, such as the geometry, the stress state, the material composition, the boundary effects and the load rate (Bažant [1999], Van Vliet and Van Mier [2000] and Grégoire et al. [2013]). Figure 2.7 shows the different input parameters that influence the response variability of the structure. Other than the size

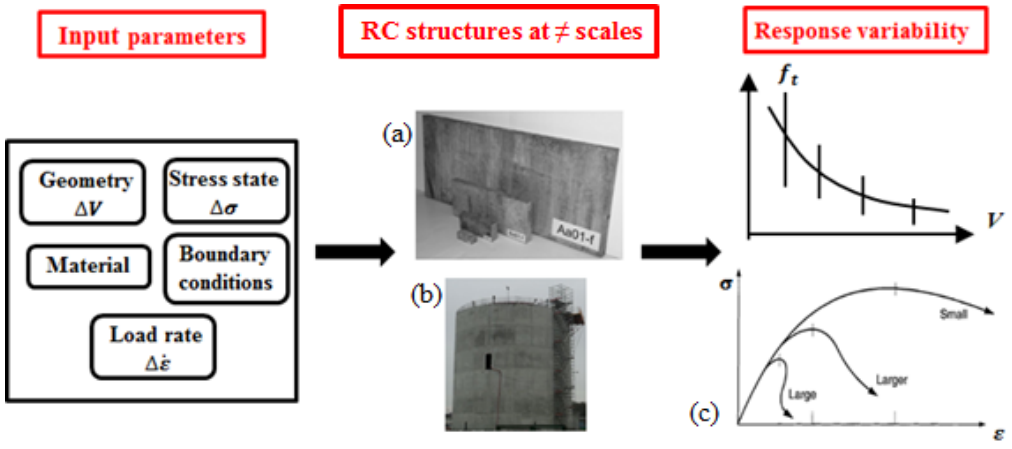

FIGURE 2.7: Size effect phenomenon: sources and typologies ((a): Hoover and Bažant [2014a], (b): Michelle-Ponnelle [2015], (c): Bažant [1999]).

effect on f_t, there is a size effect on the shape of the postpeak in $\sigma - \varepsilon$ plots. In very large structures, a snapback may occur. As for small structures, the postpeak curves decrease slowly. Hence, the ductility of the material is characterized by the shape of the postpeak curves, as the larger the specimen is smaller the ductility is (Bažant [1999]). The size effect on the postpeak shape is mainly due to the load rate and the boundary conditions.

2.1.3.2 Statistical and energetic size effect

The concrete composition, the volume of the specimen and its stress state influence directly the fracture properties. Thus, the thesis focuses on the size effect due to fracture mechanics. The boundary conditions and the load rate are not taken into account. The size effect can be distinguished by two different features; the weakest link theory analyzed by Weibull [1951] due to material strength randomness (statistical size effect) and the energy release when a large crack or a large FPZ containing damage material develops before the maximum load is reached (energetic size effect) (Hillerborg et al. [1976a]). Consequently, the study of the global behavior of a structure induces the use of a coefficient of reduction on the tensile strength measured at the specimen scale. On the one hand, the statistical size effect is observed in structures having different volume ΔV and subjected to uniform stress field σ. On the other hand, structures having different volumes ΔV and subjected to non uniform stress $\Delta\sigma$ are affected by energetic-statistical size effect. Moreover, for the case of splitting tests, cautions should be taken for the boundary conditions also (see section 2.1.2.3). For example, Figure 2.8 shows very clear size effect trend on the splitting tensile strength for diameters between 50 and 500 mm (Kadleček and Modrỳ [2002]). For specimens having D higher than 500 mm, Bažant et al. [1991] and Hasegawa et al. [1985] showed that the splitting tensile strength is not influenced by the volume of the specimen. However, when dealing with

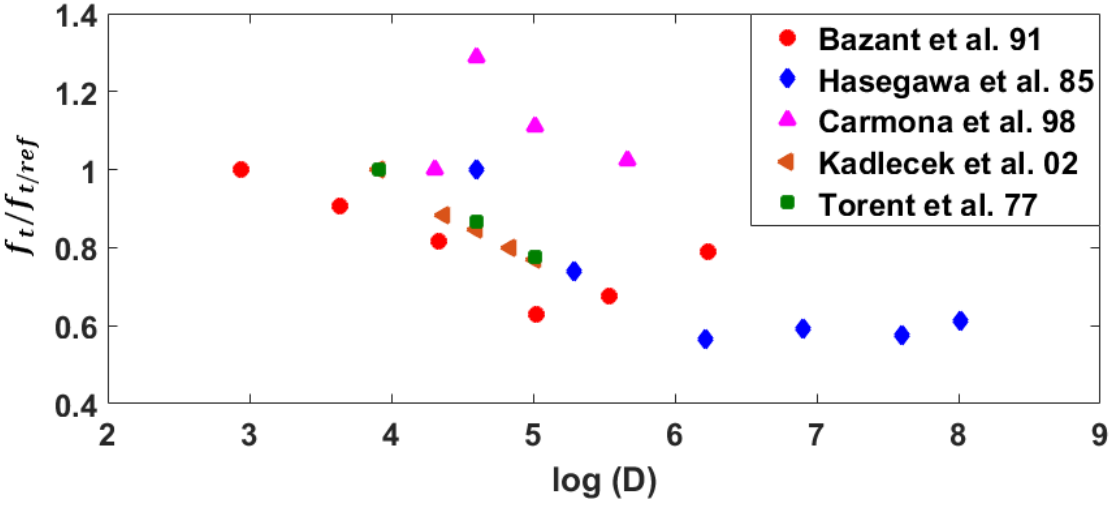

FIGURE 2.8: Experimental results of average splitting tensile strengths deduced from experiments from Torrent [1977], Bažant et al. [1991], Hasegawa et al. [1985], Kadleček and Modrỳ [2002] and Carmona et al. [1998].

notched beams or splitting test, the statistical size effect becomes negligible due to the

strong stress concentration.

Briefly, the study of the mechanical heterogeneities of concrete that lead to the variation of the tensile strength is of a main interest in the characterization of large massive structures, at initial state, during severe accident and fluid transfers. Therefore, the main problem is the definition of a law that predicts the best the tensile strength of concrete.

2.2 Modeling of size effect on tensile strength in concrete

After Griffith [1921] observations, the statistical size effect was the major interest of many authors who tried to fit a statistical theory to the problem, which ended up by the appearance of the weakest-link theory and the extreme value statistics (Peirce [1926], Tippett [1925], Fisher and Tippett [1928], Fréchet [1928] and Von Mises [1936]).

The weakest-link theory was finally characterized by Weibull [1951], who developed a law to describe the distribution of the statistical strength by mean of a power law with a threshold. Until 1985, size effect was only from a statistical origin. Therefore improvements of the Weibull law and applications to metal and ceramics were conducted (Lamon and Evans [1983], Kittl and Diaz [1988] and Kittl and Diaz [1990]). Also, application to concrete specimens in which the size effect is preponderant were one of the main interest (Carpinteri [1989], Mihashi and Izumi [1977] and Wittmann and Zaitsev [2013]).

First, the simple scaling applicable to all physical systems (without a characteristic length) is explained. Then, models that reproduces the statistical or the energetic or a combination of energetic-statistical size effect, in order to better predict the failure occurrence of concrete structure, are introduced (e.g. Weibull [1951], Torrent [1977], Mazars [1984], Lamon [1988], Sellier and Millard [2014],Hoover and Bažant [2014b] and Carpinteri et al. [1995]). Finally, a synthesis table that resumes the advantages and disadvantages of each method is given.

2.2.1 Power scaling laws

It is worth noting, at first, that no characteristic length is defined in the power scaling laws. In order to explain these laws, an example of geometrically similar series of

notched beams subjected to 3-point bending is taken (see Figure 2.9). The objective is to deduce the response Y (maximum deflection, maximum strength ...) as function of the structure size D. Thus, (Y_0, Y, Y') are the responses of the beams having a depth equal respectively to 1, D and D'. Hence, by taking the smallest beam as the reference beam, the response of the second and the third beam are defined respectively by $Y/Y_0 = f(D)$ and $Y'/Y_0 = f(D')$. Since there is no characteristic length, D can also be taken as the reference size and the response of the third beam can be evaluated as $Y'/Y = f(D'/D)$. Therefore, the following equation can be deduced:

$$\frac{f(D')}{f(D)} = f\left(\frac{D'}{D}\right) \tag{2.1}$$

This equation has the Equation 2.2 as an only solution (the power law solution).

$$f(D) = \left(\frac{D}{c_1}\right)^s \tag{2.2}$$

where s is a constant and c_1 is considered as a unit of length measurement.

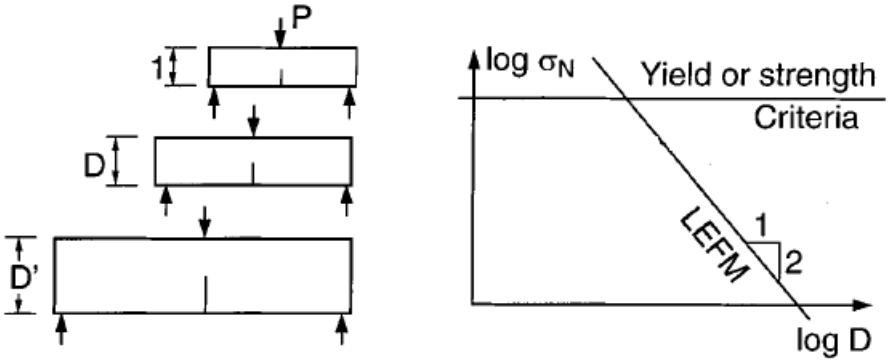

FIGURE 2.9: Power scaling laws (Bažant [1999]).

This power scale is applied to failure theories that consider the FPZ as simplified to a point and no characteristic length is involved (elasticity with a strength limit, elasto-plasticity, viscoplasticity, linear elastic fracture mechanic (LEFM)). To determine the power scale laws, exponent s must be estimated. It can be done using the failure criterion of the material. For small sizes, $s = 0$ represents elasticity with a strength limit or plasticity with a yield surface. Thus, the response Y represents the nominal stress at failure. Hence, failure of all geometrical similar structures occurs at the same nominal stress (no size effect). As for large sizes, LEFM is considered with $s = -1/2$, for similar geometrical structures with similar notches or cracks. This is resumed in Figure

2.9, where in a logarithmic scale $\log \sigma_N$ versus $\log D$ (σ_N is the nominal strength), the power scale is a straight line and s is the corresponding slope. For quasi-brittle materials, an intermediate relation between the two asymptotes describing the power laws is a definition of their size effect.

Hillerborg et al. [1976a] introduced a cohesive crack model for concrete characterized by a softening stress-displacement law for the crack opening. Hence, a deterministic size effect starts to appear as a main reason for the failure of plain concrete beams. Bažant [1976] showed a size effect on the post-peak deflection and energy dissipation induced from the localization of strain-softening damage. Simultaneously, Bažant [1984] developed, for quasi-brittle materials, a size effect law based on energy released analysis. In conclusion, very large beams exhibit only statistical size effect as the deterministic size effect curve has an horizontal asymptote at its end.

2.2.2 Weibull effective volume methods

Weibull effective volume (WEV) method based on the weakest link theory is developed in order to account for the decrease of the tensile strength in brittle and quasi-brittle materials. Moreover, many size effect approaches were derived from the WEV method, in order to improve this latter method and account for the energetic size effect (Highly stressed volume approach (Kuguel [1961] and Torrent [1977]), Lamon and Evans [1983] approach, Mazars [1984] approach, Weakest Link and Localisation method (Sellier and Millard [2014]).

2.2.2.1 Principles

Weibull effective volume (WEV) methods (Kuguel [1961], Quinn [2003a], Quinn [2003b]) have been developed to compare the rupture strength for structures with different types of solicitation (loaded in tension, pure bending, 3-point and 4-point bending) and different volumes. An example that illustrates the WEV concept is a beam loaded in 4-point bending, as shown in Figure 2.10. The effective volume V_E is an equivalent volume with the same material having the same probability of rupture as the initial volume if it is subjected to the maximum stress in a uniform way (see Equation 2.3).

$$V_E = \int_V \left(\frac{\langle \sigma \rangle}{\sigma_{max}} \right)^m dV \tag{2.3}$$

where σ is the applied stress over the volume V and $\langle . \rangle$ accounts for the positive part only, σ_{max} is the maximum value of the principal stresses in the structure and m is the Weibull modulus (this parameter will be discussed in Chapter 3).

The maximum stress corresponds to the maximum one in a stress field subjected to given solicitations:

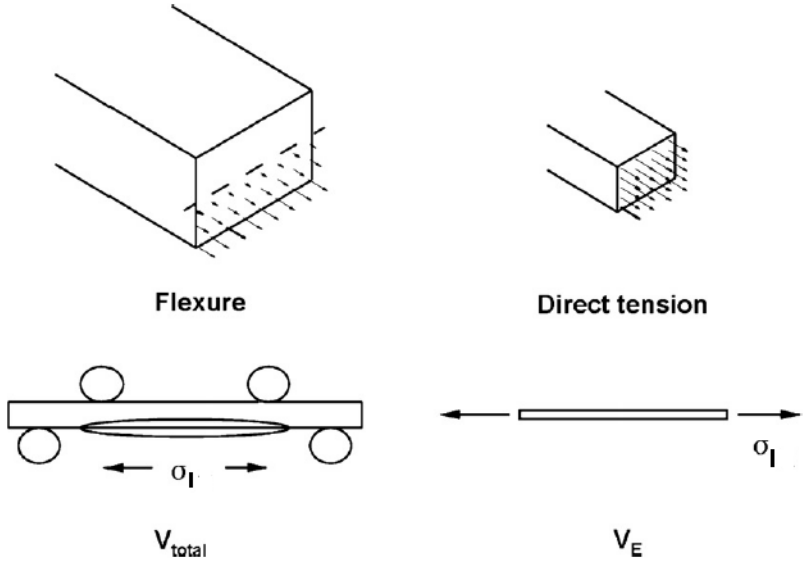

FIGURE 2.10: WEV concept (Wu et al. [2012]).

$$\sigma_{max} = \max\left(\sigma_I, \sigma_{II}, \sigma_{III}\right) \tag{2.4}$$

where σ_I, σ_{II} and σ_{III} are the principal stresses in an elastic loading ($\sigma_I \geq \sigma_{II} \geq \sigma_{III}$). The statistical Weibull distribution is based on the weakest link model and the occurrence of failure from a single crack or critical flaw by crack growth. The flaws have similar shape and orientation, in which the critical flaw is statistically distributed. As a consequence, the tensile strength seems to be controlled by these flaws. This method is applicable to brittle materials. The probability of presence of defaults depends on the size of the structure, i.e. it increases when the size of the structure becomes larger, which implies the problem of dependency of the tensile strength on the loaded volume, this phenomenon is called Weibull weakest link theory (Weibull [1951]). The Weibull theory is considered as a one dimensional chain in which each link can break with the same probability. The location of the failure is unknown because all the volumes dV are considered with the same probabilistic weight.

$$\ln\left(1 - P_{f/v}\right) = \int_V \frac{\ln\left(1 - P_{f/ref}\right)}{V_{ref}} dV \tag{2.5}$$

where $P_{f/v}$ is the probability of failure of a loaded volume V and $P_{f/ref}$ is the probability of failure of a reference structure, with V_{ref} its effective volume .
Using the Weibull statistical approach, the rupture probability can be written in the following form:

$$P(\underline{\underline{\sigma}}, V) = 1 - \exp\left(-\frac{1}{V_{ref}} \int_V \left(\frac{\langle\sigma\rangle}{f_{t/ref}}\right)^m dV\right) \tag{2.6}$$

where $f_{t/ref}$ is the tensile strength of the reference structure.

The WEV approach developed is applicable for structures having different types of loading. Applications to structures subjected to uniaxial uniform stress field and uniaxial non uniform stress field will be presented. The effective volume V_E, computed using Equation 2.3 is defined as equal to the volume subjected to uniform stress field, and is equal to zero if the volume is subjected to compressive stress field. As a result, traction is the most severe loading mode that leads to the highest probability of rupture.
Therefore, in the case of uniaxial uniform stress field, the effective volume is equal to the total volume of the structure. Thus, the rupture probability, deduced from Equation 2.6, for two different volumes V^1 and V^2 of samples subjected to uniform stress field is given by the following equation, for $i = 1, 2$:

$$P_{fi} = 1 - \exp\left(-\frac{V^i}{V_{ref}} \left(\frac{f_t^i}{f_{t/ref}}\right)^m\right) \tag{2.7}$$

where f_t^i is the tensile strength in the volume V^i.
From these previous equations, the following relation can be obtained:

$$\frac{f_t^2}{f_t^1} = \left(\frac{V^2}{V^1}\right)^{-1/m} \left(\frac{\ln(1 - P_{f2})}{\ln(1 - P_{f1})}\right)^{-1/m} \tag{2.8}$$

The previous equation can be reduced to the following relation.

$$\frac{f_t^2}{f_t^1} = \left(\frac{V^2}{V^1}\right)^{-1/m} \tag{2.9}$$

As for the case of non-uniform stress field, the probability of rupture for two different volumes is expressed as function of the effective volume. Thus, V^1 and V^2, corresponding to $i = 1$ and $i = 2$ in Equation 2.7 are replaced by V_E^1 and V_E^2 respectively. Therefore, the volume effect on the rupture stress for a given probability ($P_{f1} = P_{f2}$) can be written

using a similar equation deduced in the uniform case:

$$\frac{f_t^2}{f_t^1} = \left(\frac{V_E^2}{V_E^1}\right)^{-1/m} \tag{2.10}$$

Thus, the rupture strength ratios vary as the inverse of the effective volume ratio. The effective volume depends the total loaded volume and the severity factor K (Kuguel [1961], Quinn [2003a], Quinn [2003b]):

$$V_E = KV \tag{2.11}$$

Thus, the severity factor depends on the type of loading; for traction $K = 1$, for 3-point bending $K = \frac{1}{2(m+1)^2}$, for 4-point bending $K = \frac{m+3}{6(m+1)}$ and for pure bending $K = \frac{1}{2(m+1)}$.
In conclusion, the original WEV methods present some limits, as:

- The presence of default increases indefinitely as the size of the structure becomes larger, so a null tensile strength is attributed to very large structures.
- It does not take into consideration the stress redistribution phenomena, i.e the failure in a limited zone does not lead to the failure of the structure.
- It ignores the deterministic size effect, which makes the Weibull theory valid only if, as soon as the microcracks become macrocrack, the failure will occur.

2.2.2.2 Highly stressed volume approach

A particular WEV uses the highly and elastically stressed volume as the reference volume (Kuguel [1961]). This highly stressed volume (HSV) approach is based on the fact that in the fracture of quasi-brittle materials such as ceramics or concrete-like materials, it is not necessary to analyze what happens in the whole volume of the specimen, but only in its most critical area. Therefore, the HSV is defined by the volume where the tensile stress is greater arbitrarily than 90 or 95 % of σ_{max} (Torrent [1977]), it is equal to the total volume of a specimen subjected only to tensile strength (see Figure 2.11). Hence, the definition of the HSV can also be assumed as the definition of the critical section where the crack leading to failure will occur.

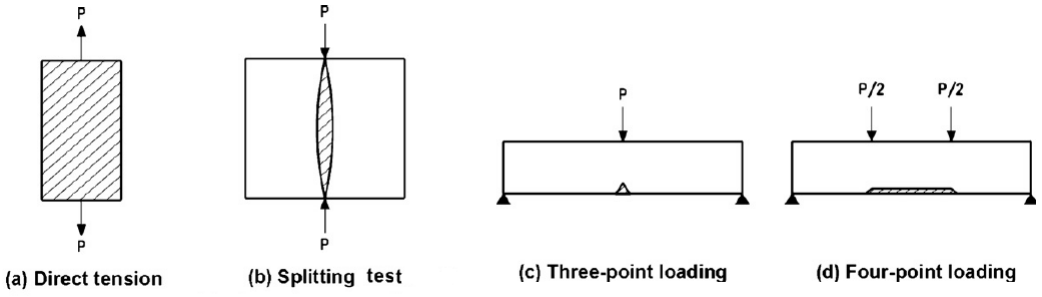

FIGURE 2.11: The contour of the highly stressed volume HSV (Wu et al. [2012]).

TABLE 2.2: Concrete mix compositions (Torrent [1977]), where $f_c = 42.3$ MPa

Water/Cement ratio	0.45	0.55	0.55	0.55	0.67	0.8	0.8
Aggregates type	EC	FNS	EC	MNS	FNS	EC	FNS
f_{t0} (MPa)	7.17	5.92	6.17	5.29	4.4	3.67	3.38
m	10.4	12.2	11.6	13.3	9.5	11.1	9.7

Noticing that the maximum tensile strength of the tested sample will decrease with increasing HSV, Torrent [1977] fitted an exponential expression such as:

$$f_t = f_{t0}.\left(\frac{HSV}{HSV_0}\right)^{-1/m} \tag{2.12}$$

where f_{t0} is considered as the tensile strength for a HSV of 1 cm^3, denote HSV_0. Torrent [1977] wanted to study the effect of the mix characteristics, mainly the type of aggregate and W/C ratio, on parameters f_{t0} and m. He chose to work with mortar and conducted an experimental campaign of tests by considering 7 mixes and 9 types of test (splitting cylindrical tests with a diameter $D = 50, 100, 150$ mm and a slenderness of 2, beams with different volumes ($25 \times 25 \times 106$ mm^3, $25 \times 25 \times 240$ mm^3, $40 \times 40 \times 106$ mm^3, $150 \times 150 \times 450$ mm^3) subjected to 3-point bending and one beam having the same volume as the largest one and subjected to 4-point bending). Table 2.2 provides numerical values of f_{t0} and m, fitted from experiments conducted on various beams and cylindrical concrete specimens, using different concrete mix compositions. Torrent [1977] showed that parameter m does not depend on the mix characteristics, thus it is a parameter of the material and characterizes the size effect. Moreover, he showed that the size effect is closely quantified by the Equation 2.12. These conclusions can be derived for concrete and validation were conducted by many works (Wright and Garwood [1952], Malhotra [1970] and Neville [1995]).

For example, Wu et al. [2012] applied original WEV approach and HSV approach on

concrete specimens subjected to different types of loading (direct tension, splitting test and 4-point bending) and he showed that HSV approach is more accurate in reproducing the experimental tensile strength than the WEV approach. Original WEV method tends to give smaller values of the tensile strength, thus it is an inadequate method to reproduce the failure of the concrete.

2.2.2.3 Rossi's approach

For concrete specimens subjected to tensile strength, Rossi et al. [1994] presented a size effect method based on the WEV method. Under the hypothesis of dependency between the concrete tensile strength and the cement paste, which is where there are the most weak points, Rossi et al. [1994] underlined a possible relation between f_t and the ratio volume of specimen to volume of coarsest grain. This ratio presents an estimation of the quantity of cement paste, thus the presence or not of defaults. Therefore, the size effect is governed by the quality of cement paste. In conclusion, the size effect is reflected by those two equations:

$$\mu\left(f_t\right) = F_\alpha\left(\frac{V_S}{V_A}\right) \tag{2.13}$$

$$Std\left(f_t\right) = F_\beta\left(\frac{V_S}{V_A}\right) \tag{2.14}$$

where $\mu\left(f_t\right)$ and $Std\left(f_t\right)$ are respectively the mean and the standard deviation values of the tensile strength, V_A is the volume of the largest aggregate, V_S is the volume of the specimen and F_α and F_β are functions of the compressive strength.
Based on an optimization program that aims to fit the best with experimental tests, the Equations 2.13 and 2.14 are rewritten in the following form:

$$\mu\left(f_t\right) = a\left(\frac{V_S}{V_A}\right)^{-1/m} \tag{2.15}$$

$$Std\left(f_t\right) = A\left(\frac{V_S}{V_A}\right)^{-B} \tag{2.16}$$

where $a = 6.5$, $A = 0.35$ and m and B are functions of the compressive strength, since the size effect depends directly on this mechanical property. The relation between the Weibull modulus m and the compressive strength f_c is given in Chapter 3 (Equation 3.11).

2.2.2.4 Mazars' approach

Mazars [1984] derived from the WEV and HSV methods a size effect approach based on the strain instead of the stress. A local strain $\tilde{\varepsilon}_D$ is associated for each element ΔV. In the total volume V of the specimen, the local strains $\tilde{\varepsilon}_D$ are distributed randomly. $f\left(\tilde{\varepsilon}_D\right)$ is the probability density function of the random variable ε_D. The rupture probability of the element ΔV is written as follow:

$$P_f(\varepsilon_D, \Delta V) = \int_0^{\tilde{\varepsilon}} f\left(\tilde{\varepsilon}_D\right) d\varepsilon_D \tag{2.17}$$

The elements ΔV are considered independent and the Weibull function of repartition of the stress in a volume ($f(S) = k(\sigma - \sigma_i)^m$) is used. Thus, in the case of non uniform solicitation (denoted $\tilde{E}$), the rupture probability is considered as an integral on the total volume V, as follow:

$$P_f(\tilde{E}, V) = 1 - \exp\left(-k \int \tilde{\varepsilon}^m dV\right) \tag{2.18}$$

By considering the concrete behavior as linear and elastic before reaching the threshold strain, the solicitation $\tilde{\varepsilon}$ in an element can be considered as function of the maximum local solicitation $\tilde{\varepsilon}_M$ as shown in Figure 2.12. The function $g(x, y, z)$ depends only on

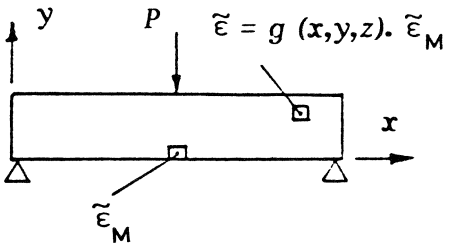

FIGURE 2.12: Computation of the effective volume (Mazars [1984]).

the geometry of the specimen and the type of loading. Based on the assumption that the maximum strain threshold $\tilde{\varepsilon}_{D0}$ is reached in the most loaded volume ($\int_V \tilde{\varepsilon} dV = W_0$), the mean value of the strain threshold can be deduced using the following equation:

$$\varepsilon_{D0} = \left(\frac{W_0}{\int_V g(x, y, z)^m dV}\right)^{1/m} \tag{2.19}$$

where W_0 and m are material characteristics.

2.2.2.5 Lamon's approach

Lamon [1988] developed a size effect method based on the WEV method and applicable only to ceramics. His method can be considered as an extension of the WEV method to the case of multiaxial elementary stress. Since the defaults in a structure have random orientation with respect to the stress field, the elementary stress is defined as the equivalent stress of the multiaxial stress field subjected to the default or the fracture. It is, then, a combination of a normal component σ_n and a tangent one τ. The equation of the elementary stress σ_E is given by the following equation:

$$\sigma_E = \left(\sigma_n^4 + 6\tau^2\sigma_n^2 + \tau^4\right)^{1/4} \tag{2.20}$$

The local stress field (σ_n, τ) are determined from the imposed loading evaluated using the principal stresses field (σ_I, σ_{II}, σ_{III}), as shown in Figure 2.13. Furthermore, the

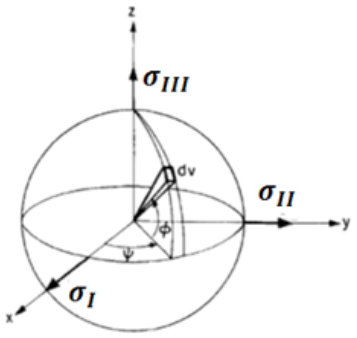

FIGURE 2.13: Elementary sphere in the principal stresses space for determining the local stresses (Lamon [1988]).

rupture probability given by the multiaxial elementary stress model is expressed as function of the maximum stress:

$$P(\underline{\underline{\sigma}}, V) = 1 - \exp\left(-\frac{1}{V_{ref}}\int\left(\frac{\sigma}{\sigma_{max}}\right)^m I_v\left(m, \frac{\sigma_{II}}{\sigma_I}, \frac{\sigma_{III}}{\sigma_I}\right)\right) \tag{2.21}$$

Thus the method of multiaxial stress field defines an effective volume that depends not only on the state of stress but also on the direction of stress by introducing a parameter I_v, which depends on the orientation of the defects in all directions.

2.2.2.6 Weakest link and localization method

Based on the experimental tests done on the Mivelaz anchor (Mivelaz [1996]), Sellier and Millard [2014] outlined the reduction of the tensile strength for large concrete or RC structures by 50 % compared to the experimental tensile strength measured on splitting test. The weakest link and localization method WL2 was developed in the framework of a finite element (FE) code, in which, the tensile strength is not known at the beginning of the analysis, it is determined automatically during the step-by-step analysis considering both the random properties of the material and the current stress state. A weighting function is introduced in the WL2 theory to balance the probabilistic influence of each point x of a structure.

$$\Psi(x, l_I) = \exp\left(-\frac{x^2}{2.l_I^2}\right) \tag{2.22}$$

where l_I is the length that characterizes the spatial decrease of the probabilistic weighting function, it was determined by inverse analysis and x is the distance between a current point M and the integrated point S.

Ψ can be understood as a localization function, which prevents the continually increasing probability of finding a defect when the volume increases, which is the case of WEV method, and it allows the stress redistribution around the "weakest link" by taking into account the effect of the point S on the current point M as shown in Figure 2.14. In the case of $\Psi = 1$ as in Lamon and Evans [1983], the WEV method is applicable to homogeneous materials such as ceramics in which the crack develops at the presence of a defect contrary with concrete, where there is possibility of stress redistribution that prevents the rupture of the specimen.

Thus, the WL2 method gives improvement to the WEV method by introducing the weighting function in the Weibull integral (Equation 2.23), which leads to:

$$\ln\left(1 - P_{fv/M}\right) = \int_V \frac{\ln\left(1 - P_{fref}\right)}{V_{ref}} \Psi(x, l_I) dv \tag{2.23}$$

In this method, the chosen reference volume is a cylindrical splitting test of dimensions 11×22 cm^2. This assumption is convenient since l_I is higher than the dimensions of the reference volume, estimated in the order of 3×10^{-4} m^3.

Sellier and Millard [2014] have determined l_I by inverse analysis, in the particular case of a 5 m-long reinforced concrete brace (Mivelaz [1996]), they found an order of magnitude of l_I around $30 - 50$ cm (see Figure 2.15).

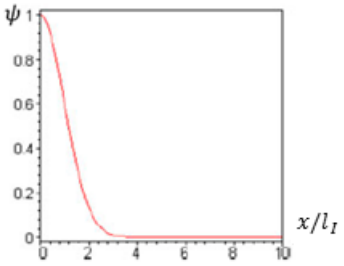

FIGURE 2.14: Evolution of the probabilistic weighting function (Sellier and Millard [2014]).

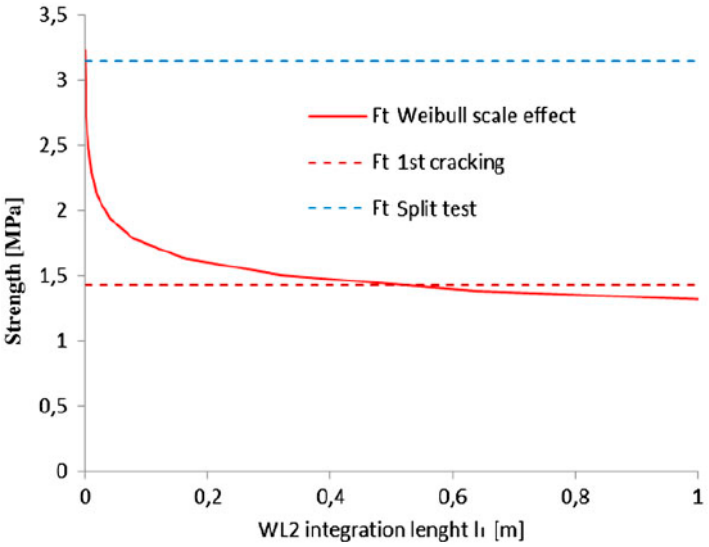

FIGURE 2.15: Evolution of the mean tensile strength f_t at first crack as function of l_I (Sellier and Millard [2014]).

Briefly, the spatial randomness of the mechanical properties of concrete is the key to study and predict the size effect. Thus, alternative FE models, based on the assumption that the tensile strength or the Young's modulus are not constant values are developed.

2.2.3 Bažant size effect law

In section 2.2.1, quasibrittle materials such as concrete are characterized by two power scaling laws having no characteristic length: material strength or yield limit characterized by σ_0 for small sizes and LEFM characterized by the fracture energy G_f for large sizes. However, the bridging between plasticity and LEFM is satisfied with the presence of characteristic length. Thus, Irwin [1960] characteristic length l_{ch} is a mean to combine the two power laws.

$$l_{ch} = \frac{E.G_f}{\sigma_0^2} \tag{2.24}$$

where E is the Young's modulus.

Bažant [1976] analyzed the crack damage distribution and he showed a deterministic size effect on the postpeak deflection and the energy dissipation due to the damage localization into a crack band. In consequence, Bažant [1999] considered the Irwin length as a material length in the order of the length of the FPZ. Thus, in concrete materials, characteristic length must be involved to account for size effect due to the large number of inhomogeneities in concrete.

On the one hand, he developed first a size effect law (SEL), derived from energy release analysis, for type 2 structures, which contain initially a notch larger than the FPZ. Thus, the statistical size effect, in this case, is negligible (Bažant [1984]). Therefore, the bridging between small sizes and large sizes is given by Equation 2.25.

$$f_t = \frac{B f_{t/ref}}{\sqrt{1 + D/D_0}} \tag{2.25}$$

where B and D_0 are empirical dimensional parameters determined by experimental fitting.

This equation is the transition between a horizontal asymptote for small structures and an inclined asymptote of slope $-1/2$ for large structures, in the size effect plot of $\log f_t$ vs $\log D$ (see Figure 2.16). Based on the assumption of the importance of the characteristic length in concrete materials, Equation 2.25 can be rewritten in the following form:

$$f_t = \sqrt{\frac{E' G_f}{g_0 D + g_0' c_f}} \tag{2.26}$$

where E' is the Young's modulus ($= E$ for plane stress and $= E(1-\nu)$ for plane strain where ν is the Poisson coefficient), $c_f = \gamma_s . l_0$ is the characteristic length where γ_s is material dependent, g_0 and g_0' are energy release rate functions, that depend on the initial crack or notch (Bažant and Kazemi [1991]).

In addition, Saouma et al. [2003] and Saouma and Fava [2006] gave analytical explanation of the parameter B based on local stress intensity factors and cohesive stresses. Saouma and Fava [2006] derived a fractal size effect from the original Bažant SEL.

On the other hand, structures having no notches are subjected either to energetic-statistical size effect or statistical size effect, depending on the applied stress. This type of structures, corresponding to type 1, fails when the macrocrack initiates from a smooth surface. However, for the case of 4-point bending beams for example, the statistical

size effect is not negligible due to the large part of failure occupied in the structure. Therefore, to ensure the presence of the Weibull statistical size effect, the size of the specimen must be larger than the size of the REV equal to 2-3 times the size of material inhomogeneities in the case of uniaxial tensile loading (Le et al. [2013]). Therefore, for the case of energetic-statistical size effect, large sizes are defined by an asymptote of slope $-n/m$ in the logarithmic size effect plot (see Figure 2.16). In conclusion, for Type

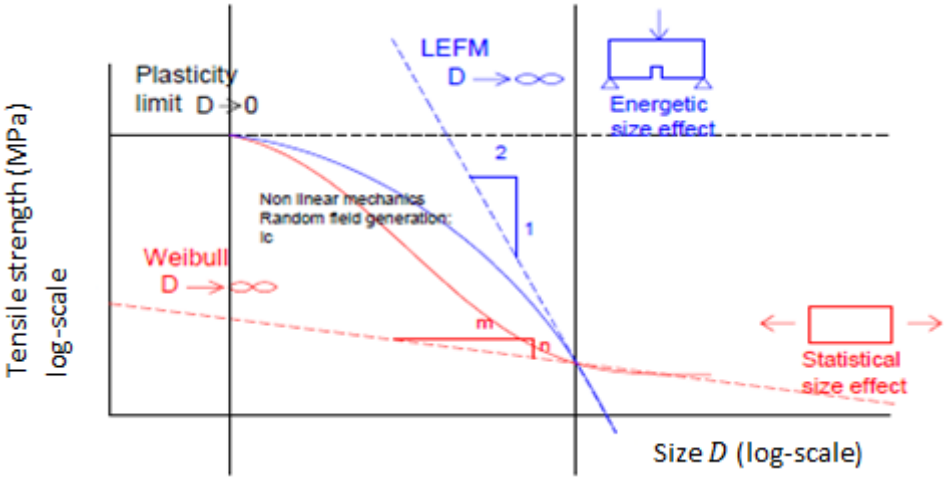

FIGURE 2.16: Logarithmic size effect plot for Type 1 and type 2 according to Hoover and Bažant [2014b].

1 size effect, two SEL equations are defined:

- Energetic size effect:

$$f_t = f_{r\infty}\left(1 + \frac{rD_b}{D + l_p}\right)^{1/r} \tag{2.27}$$

- Energetic-statistical size effect

$$f_t = f_{r\infty}\left(\left(\frac{l_s}{l_s + D}\right)^{rn/m} + \frac{rD_b}{D + l_p}\right)^{1/r} \tag{2.28}$$

where $f_{r\infty}$ is the nominal strength for very large beams (for example flexural strength or modulus of rupture), D_b is approximately equal to the FPZ length. l_p is a material characteristic length in the order of 15 cm controlling the point of transition to a horizontal asymptote of the $\log(f_t)$ versus the $\log(D)$ curve and l_s is a statistical characteristic length, in the order of 28 cm, which refers to the spatial variability of failure probability (Bažant et al. [2007]).

Figure 2.16 shows the asymptote corresponding to small and large structures in the standardized logarithmic plot of size effect for type 2 structures corresponding to notched beams and type 1 structures. In this figure, the statistical size effect is not negligible in the type 1 structures.

Hoover and Bažant [2014b] attempted to develop a universal size effect law (USEL), since the previous attempt to bridge the Type 1 and 2 was not accurate enough. His attempt to develop USEL was based on strain gradient. The USEL has the following form:

$$f_t = \left(\frac{E' G_f}{g_0 D + (1-\lambda)\, c_f g_0' + \lambda E' G_f / f_{r\infty}^2} \right)^{1/2} \left(\left(\frac{\lambda l_s}{l_s + D} \right)^{rn/m} + \frac{r \lambda D_b}{\bar{D} + l_p} \right)^{1/r} \tag{2.29}$$

where λ and $\bar{D}$ are parameters that depend on strain gradient.

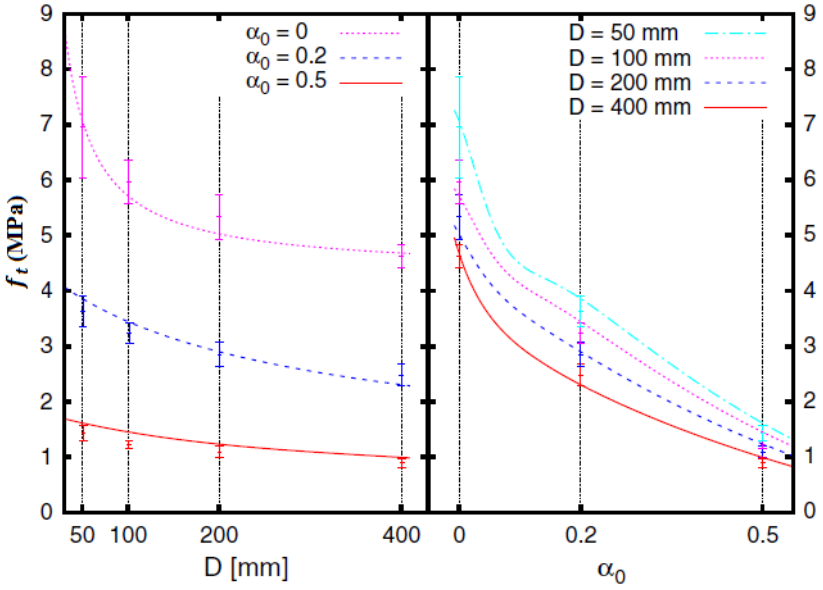

FIGURE 2.17: Evolution of the nominal strength for beams subjected to 3-point bending load as function of the height of the beam D (left) and the notch-to-depth ratio α_0 (right) (Grégoire et al. [2013]).

Hoover and Bažant [2014b] proved on a series of notched and unnotched beams subjected to 3-point bending that the USEL allows to predict the nominal strength with a coefficient of variation of only 2.3%. However, it depends on many numerical parameters that need to be fitted experimentally. In conclusions, Bažant USEL was applied to some experimental series mainly to beams subjected to 3-point bending. An important example corresponds to the study of Grégoire et al. [2013] who conducted tests on beams under 3-point bending loading, having different sizes and 3 types of notches referred

to by the notch-to-depth ratio α_0, where $\alpha_0 = 0$ corresponds to unnotched beams (see Appendix A). In Figure 2.17, the curves correspond to the values of the tensile strength computed using the USEL of Bažant and the experimental values are presented using vertical bars. The USEL proved to be an accurate law to characterize the size effect as shown in Figure 2.17. Also, it is worth noting that as the notch-to-depth ratio increases, the tensile strength decreases.

2.2.4 Carpinteri size effect law

A different model for the size effect is presented by Carpinteri et al. [1995]. Its model is based on the assumption of the decrease of the effect of microstructural disorder, as the volume increases. In contrary with Bažant SEL, it is considered, for this fractal method, that the small structures sizes are governed by LEFM with a slope of $-1/2$ and large structures are governed by a constant stress, without accounting for fractal and disorder. Thus, a multi-fractal scaling law (MFSL) is qualitatively postulated, it is given by the following equation:

$$f_t = f_{r\infty} \left(1 + \frac{l_{ch}}{D}\right)^{1/2} \tag{2.30}$$

In Equation 2.30, $f_{r\infty}$ and l_{ch} represent two constants, determined from the best fit of the experimental data. In Carpinteri and Cornetti [2002], it was observed that the MFSL is more accurate than Bažant SEL for the cases of unnotched beams, whereas Bažant SEL is valid when a strong energy-driven fractal process is activated. However, as seen in Saouma and Fava [2006], the MFSL can be criticized for several reasons. On the one hand, Irwin [1960] and Hillerborg et al. [1976a] defeated the applicability of LEFM for small sizes. On the other hand, the MFSL does not have an upper bound for the tensile strength as size is reduced.

2.2.5 Synthesis

Finally, a synthesis table that resumes the capability of each method to account for either statistic or energetic or energetic-statistical size effect is given in Table 2.3. Table 2.3 shows that Bažant USEL and Carpinteri MFSL seem to account for the different types of size effect. However, both methods are based on experimental calibration depending

on more than 3 empirical constants. In addition, these methods are available only for geometrically similar structures.

In this thesis, the focus is on structures failing mainly due to tension. Hence, structures with strong stress concentration, as notched concrete beams and splitting tests are not in the study domain. Thus, our interest is to model both statistical size effect or energetic-statistical size effect. Therefore, since WL2 depends only on two parameters and is capable on reproducing rather statistical size effect and if possible energetic-statistical size effect (Sellier and Millard [2014] and Ceos.fr [2009]), an analytical-probabilistic version of this method is developed in Chapter 3.

TABLE 2.3: Synthesis of the different size effect methods.

SE methods	Statistical	Energetic	Energetic-statistical	Number of empirical constants
Original WEV method	✓	×	×	1
HSV method	✓	×	✓	1
Rossi approach	✓	×	×	2
Mazars approach	✓	×	✓	3
Multiaxial elementary method	✓	×	×	3
WL2	✓	×	✓	2
Bažant USEL	✓	✓	✓	5
Carpinteri MFSL	✓	✓	✓	3

2.3 Modeling spatial variability of concrete

Statistical tools and probabilistic approaches have often been developed to model the behavior of heterogeneous materials. As mentioned previously, the heterogeneities of concrete at micro-scale (ITZ, aggregates, cement matrix, porosity ...) lead to the variability of the mechanical properties of concrete at the REV scale and larger (see Figure

2.3). Thus, the material properties of concrete are randomly distributed. In the following, different methods to describe the spatial variability of concrete will be presented, particularly Stochastic Finite Elements (SFE) using discretized random fields. Therefore, random fields are described. Finally, the eventual relation between SFE models and size effect is discussed.

2.3.1 Methods accounting for spatial variability of concrete

The simplest approach consists on attributing to each volume of material, using Monte-Carlo procedure, properties (f_t and E) which follows a given distribution and then to perform the numerical simulation. Another way is to consider a given distribution of defects within the volume of the material. Each defect is supposed to possess a probabilistic elastic-brittle behavior and the macro behavior results as a sum of all these elementary defects.

Moreover, a possible approach is the one proposed by Breysse [1991], which is based upon the modelisation of the micro-structural geometry and topology onto a discrete representation then performing FE simulations. However, analyzing the damage behavior of large structures and the mapping of the micro-structure becomes almost impossible. Thus, the material disorder is taken at the macro-scale material properties by considering them as randomly distributed in space (Carmeliet and de Borst [1995]). As a consequence, spatial variability of input parameters are represented by random variables or random fields characterized by autocorrelation functions. Hence, a better representation of the spatial heterogeneity of the concrete and its effect on the cracking should be taken into account, both at the scale of the fracturing zone and at the scale of the structure.

Some authors pointed out the usefulness of accounting for the spatial randomness of concrete mechanical properties in the FE models, where usually the concrete is supposed as homogeneous material. Rossi et al. [1996] accounted for the initial heterogeneity of the material (f_t and E) with respect to the size of the structure in order to accurately represent the crack propagation. As for Tang et al. [2010], he introduced a spatial correlation length factor into Weibull distribution law by defining the mechanical property as a 2D random field discretized into n finite elements.

As a consequence, SFE models using random fields are used to investigate the uncertainty propagation of the mechanical properties of the concrete (f_t or E) on the outputs of interest parameters (rupture force or strength). In this way the fluctuations of the

material parameters are modeled by means of random fields and the cracking process is represented using finite element discretization. Some authors used discretized random fields to model the randomness of the concrete properties (Carmeliet and de Borst [1995], Colliat et al. [2007], Vořechovskỳ [2007], Małecki et al. [2007], De Larrard et al. [2010], Giry [2011] and Syroka-Korol et al. [2013]). Syroka-Korol et al. [2013] modeled unnotched beams subjected to 3-point bending load, they used a regularization method and an original technique for the random field generation. It is worth noting that for unnotched beams under uniaxial tension, the difference in the response between a deterministic material strength and a stochastic strength grew with increasing size. Hence, the importance of the generation of random fields in FE models rises to represent material spatial randomness, and then capture this effect on mechanical behavior such like tensile strength, damage and crack pattern. Breysse [1991] discussed the choice of the mechanical property modeled as random field (E orf_t). Based on this choice, different behaviors can be obtained. On the one hand, if f_t is random, the disorder and the heterogeneous behavior will appear only after the rupture of the first element. On the other hand, if E is random, the material is heterogeneous since the initial phase. However, Rossi et al. [1994] showed that E is independent of the volume of the specimen. Thus, in this thesis, f_t is chosen to be randomly distributed.
Briefly, the method to model the variability of the tensile strength in concrete, used in this thesis, is discrete random fields. Therefore, the definition of random filed is discussed, in the next section.

2.3.2 Random fields

A random field $V(x)$ is defined as a collection of random variables indexed by a continuous parameter $x \in \Omega$, where Ω is an open set of R^d $(d = 1, 2, 3)$ describing the geometry. The Gaussian random field is completely defined by its mean function $\mu(x)$ and its autocovariance function $C_{VV}(x, x')$ that depends on an autocorrelation function $\rho_v(x, x')$, as shown in Equation 2.31.

$$C_{VV}(x, x') = Std(x)Std(x')\rho_v(x, x') \tag{2.31}$$

The modeling of the tensile strength of concrete f_t requires the use of univariate multi-dimensional fields, whose autocorrelation function depends only on the relative length, called autocorrelation length, between two points. The higher the autocorrelation length is, the stronger the statistical correlation between two points of the field is and for a very large autocorrelation length, the random field tends to a random variable. Thus, the dependency of the material characteristics of the concrete is provided by the use of autocorrelation functions. Different types of autocorrelation functions is found in the literature, commonly Gaussian, exponential and sinusoidal functions (Carmeliet and de Borst [1995], De Larrard et al. [2010], Colliat et al. [2007], Giry [2011] and Sudret [2007]). These autocorrelation functions are detailed in Chapter 4. The main question to model the spatial variability of the mechanical properties of concrete is the choice of the autocorrelation function and its corresponding length. Thus, to compare the different values of autocorrelation lengths found in the literature and the different shapes of autocorrelation functions, an equivalence between the different autocorrelation length must be found.

One used method to find an equivalence between the different autocorrelation lengths corresponding to different autocorrelation functions is the scale of fluctuation, proposed by Vanmarcke [2010] and given by the following Equation:

$$\upsilon = 2\int_0^\infty \rho(x)dx \tag{2.32}$$

Another method that can be used to compare different autocorrelation functions is the variogram. The variogram is defined using the following equation:

$$\gamma(h) = \frac{1}{2}var\left[Z(x+h) - Z(x)\right] \tag{2.33}$$

where $Z(x)$ and $Z(x+h)$ are two random variables considered respectively at x and $x+h$, h is a chosen distance that separate these two random variables.

Thus, the variogram $\gamma(h)$ is usually presented as function of h. Figure 2.18 is an example of the theoretical variogram fitted from the experimental measurements of the ultrasonic pulse velocity (the points) on a wall of a thermal power plant for the national project of research EVADEOS, in order to evaluate the concrete properties and its spatial randomness. This variogram presents, then, the ultrasonic pulse velocity at different locations

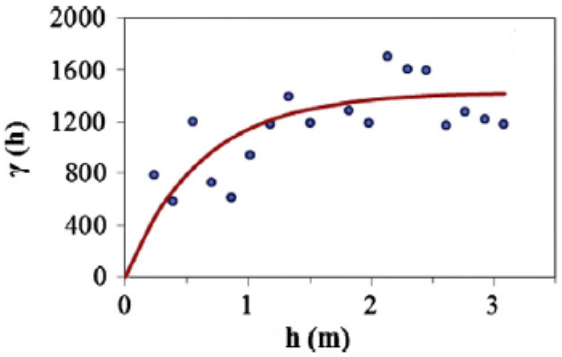

FIGURE 2.18: Variogram showing the experimental and theoretical variation of the ultrasonic pulse velocity in a RC wall (Gomez-Cardenas et al. [2015]).

of the wall (Gomez-Cardenas et al. [2015]).

The variogram reaches a level that is equal to 95 % of the variance of the variable for a distance called characteristic correlation length l_{cc}. In addition, a direct relation between the variogram and the autocorrelation function is given by the following equation:

$$\gamma(h) = Std^2 (1 - \rho(x)) \tag{2.34}$$

Thus, for $\rho(x) = 0.05$, the characteristic correlation length l_{cc} is reached. In consequence, l_{cc} is considered as another criteria to compare the different types of autocorrelation lengths. Different methods used for the random field discretization are presented in Appendix B.

2.3.3 SFE models and size effect

As the decrease of the tensile strength when the volume increases is associated to the spatial randomness of the local material strength, Weibull [1951] developed the weakest link concept, which gives a relationship between the volume of the structure and its average strength which is called size effect. Thus, in FE models, it is necessary to model the spatial variability of the concrete leading to the localization process and the redistribution of defects around the micro crack. Thus, random fields are defined as a tool to reproduce the size effect on tensile strength for quasi-brittle materials (Vořechovskỳ [2007], Syroka-Korol et al. [2013] and Colliat et al. [2007]). Vořechovskỳ [2007] showed that modeling spatial variability of local material strength accounts for the statistical part of the size effect. In addition, Colliat et al. [2007] used random fields as a tool to model quasi-brittle materials size effect and they demonstrated that probabilistic

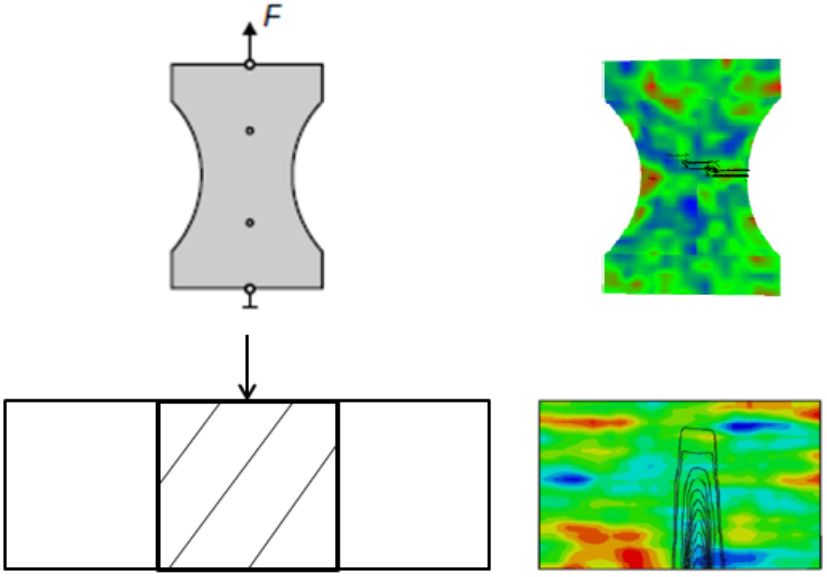

FIGURE 2.19: Spatial variability of tensile strength and crack patterns for a dog-bone specimen subjected to direct tension (Vořechovskỳ [2007]) and the central part of a beam subjected to 3-point bending (Syroka-Korol et al. [2013]).

approach using correlated random fields is capable to link continuum damage mechanics for small structures and LEFM for larger structures. Figure 2.19 shows examples of random fields from Vořechovskỳ [2007] (Gaussian random field on f_t for Van Vliet and Van Mier [2000] series) and Syroka-Korol et al. [2013] (Gaussian random fields on f_t for concrete series under 3-point bending loading).

2.3.4 Synthesis

The generation of discretized random fields involves many problems as the choice of the uncertain parameter, the probabilistic method, the autocorrelation function and the autocorrelation length. Usually, the random field models the uncertainty propagation on a parameter corresponding to the material behavior (f_t, E, damage threshold in Mazars damage model $\varepsilon_{D0} = f_t/E$, strength related parameter in a microplane model K_1, elastic yield stress σ_y, gap between the maximum stress and the elastic yield stress e_f ...). Table 2.4 presents a brief summary of the characteristics of the discretized random fields used to characterize the spatial randomness in concrete. It is worth noting that theses parameters are chosen arbitrary by the authors. As in this chapter, the variability and the size effect on f_t are highlighted, the tensile strength seems to be an important uncertain parameter, which may influence the global response of the structure and more precisely its cracking pattern. Therefore, SFE method using discretized random fields

TABLE 2.4: Synthesis of the different characteristics of discretized random fields used by some authors (Carmeliet and de Borst [1995], Vořechovskỳ [2007], Syroka-Korol et al. [2013], De Larrard et al. [2010], Colliat et al. [2007], Małecki et al. [2007] and Giry [2011]).

Reference	Type of structure	Probabilistic method	Law	Variability	Autocorrelation function and length	Size effect ($+m$)
Carmeliet and de Borst [1995]	Cylindrical tensile specimen	Midpoint	Non Gaussian	ε_{D0}	$\exp\left(-\frac{x^2}{2l^2}\right)$, $l = 5$ mm	No
Vořechovskỳ [2007]	Dog-bone tensile specimen	Latin hypercube sampling	Gaussian	K_1	$\exp\left(-\frac{x^2}{l^2}\right)$, $l = 8$ cm	Yes, $m = 7$
Syroka-Korol et al. [2013]	3-point bending beams	Latin hypercube sampling	Gaussian	f_t	$\exp\left(-\frac{x^2}{2l^2}\right)$, $l = 5$ cm	Yes, $m = 24 - 48$
De Larrard et al. [2010]	Nuclear containment	Karuhnen-Loève	Lognormal	E	$\exp\left(-\frac{x^2}{l^2}\right)$, $l = 30 - 60$ m	No
Colliat et al. [2007]	1D truss under tensile load	Karuhnen-Loève	Lognormal	σ_y and e_f	$\exp\left(-\frac{x}{l}\right)$, $l = 10$ cm	Yes
Małecki et al. [2007]	RC bar under tensile load	-	Gaussian	f_t	-	No
Giry [2011]	Cylindrical tensile specimen	Turning bands	Gaussian	ε_{D0}	$\exp\left(-\frac{x}{l}\right)$, $l = 1$ cm	No

on tensile strength is developed in this thesis. Comparisons with experimental results are carried on to give explanation for the choice of each parameter of the random field. Moreover, the pertinence of using such SFE method on the reproduction of size effect is discussed.

2.4 Conclusion

The heterogeneities of concrete at micro-scale are reflected by the variability of its mechanical properties at larger scale. Thus, the 16×32 cm^2 specimens are considered as a REV for concrete. However, the tensile strength measured on this specimen should

be used with caution when dealing with large structures. This chapter highlights the important size effect on tensile strength which should be accounted in massive structures such as nuclear containments in which the prevision of cracks is a critical issue. Different size effect methods have been presented in this chapter. These size effect methods suffer either from the tendency to underestimate the experimental tensile strength for large structures or the presence of different numerical parameters. One main objective of the thesis is to estimate the coefficient of reduction of concrete tensile strength in nuclear containments, mainly subjected to uniaxial tension. Thus, the focus is on statistical size effect. WL2 method developed by Sellier and Millard [2014] is retained because of its simplicity and capability of accounting for stress redistribution. Moreover, this method seems capable of reproducing energetic-statistical size effect. However, the scale length introduced, in this method, is identified only on an example of Mivelaz [1996] anchor. Therefore, it is important to identify this parameter on a wider experimental concrete test series. This numerical method is used in Chapter 3 to develop an analytical probabilistic size effect method.

Moreover, different methods have been used to account for the spatial variability of the mechanical properties of concrete, in FE models. These methods are mainly based on random field generations. However, each author works on its own structure type, using its own random field characterization (generation method, distribution, autocorrelation function and parameter), due the necessity of defining one random field valid for different types of structures. Therefore, in Chapter 4, the objective is to develop a SFE method that uses a discretized random field, in which a simple autocorrelation function and discretization method are chosen and applied to a wide range of case studies.

Chapter 3

Prediction of size effect in concrete structures using an analytical approach

A challenge for massive Reinforced Concrete (RC) structures is to identify the tensile strength corresponding to the first crack at their scale considering the measured tensile strength obtained in laboratories on concrete specimens. Several models to describe the dependency of the tensile strength of the sample on its size have been presented in Chapter 2. The objective is, then, to better understand the crack initiation in structures of large dimensions, taking into account the size effect, i.e. the reduction on the mean tensile strength and the associated uncertainties.

This chapter aims to develop an analytical-probabilistic approach of the Weakest Link and Localization (WL2) method developed by Sellier and Millard [2014]. WL2 method introduces a nonlocal formulation which allows the redistribution of the stresses at each step which means that a defect in a small area usually does not lead to a failure of the structure due to the redistribution capacity around the "weakest link". Moreover, Chapter 2 highlights the relevance of WL2 method, developed as Finite Element (FE), in accounting for statistical size effect. Our main objective is, then, to derive an analytical and simple WL2 method, denoted $\mathrm{WL2}_A$.

Briefly, the aim is to apply this analytical-probabilistic version $\mathrm{WL2}_A$ of size effect

method to different types of structures, from concrete structures (specimens under uniaxial tension, 3-point bending loading and 4-point bending loading) to massive structures (anchors, dams, nuclear containments ...). Consequently, the method is carried out, in order to provide tensile strength corresponding to the first macroscopic crack and to reproduce the main properties of size effect characterized by the decrease of the mean and the standard deviation of the tensile strength when the volume increases.

This chapter is organized as follows; first, the principle of the analytical-probabilistic method are described. Then, the different parameters of the method (the properties of the reference structure, the Weibull modulus m and the scale length l_I) are determined for various experimental tests. The capability of this approach to reproduce the mean and the standard deviation of the tensile strength at first crack is validated using concrete specimens under uniaxial tension (Rossi et al. [1994] and Van Vliet and Van Mier [2000]), 3-point bending loading (Torrent [1977], Hoover and Bažant [2014a] and Grégoire et al. [2013]) and 4-point bending loading (Koide et al. [2000], Mazars [1984] and Torrent [1977]). Finally, the method is applied to large massive structures such as the Mivelaz anchor, the Malpasset dam and nuclear containments vessels.

3.1 Analytical-probabilistic approach WL2$_A$

This section presents the development of the analytical method derived from the WL2 method developed by Sellier and Millard [2014] and denoted hereafter WL2$_{EF}$. The principles and originalities of the approach are first introduced. Then, the two unkown parameters of the method (Weibull modulus m and scale length l_I) are discussed. The Weibull modulus constitutes a main parameter for this method. However, it can be determined using different methods (empirical formula (Rossi et al. [1994]), Weibull definition (Sellier and Millard [2014]), maximum likelihood (Lamon and Evans [1983]) and the regression method (Wu et al. [2012])). Thus, the applicability of these three methods is discussed and a range of validation is proposed for this parameter. In addition, an interval of validation for the scale length is determined using an inverse analysis based on experimental results of Rossi et al. [1994] series and Hoover and Bažant [2014a] series.

3.1.1 Principle of the analytical-probabilistic approach

This approach is based on the WEV method. Recapitulating the definition of an effective volume V_E, it corresponds to a volume subjected uniformly to the maximum principal stress and having the same probability of failure as the total volume of the structure subjected to the actual stress field. It can be considered, then, as the volume containing the heterogeneities of the concrete.

Weibull distribution defines the probability of failure P_f of a structure subjected to non-uniform multi-axial stress $\underline{\underline{\sigma}}$, it is given by Equation 2.6.

As mainly loading cases which produce tension in the loaded structures are considered in this thesis, only the case of non-uniform uniaxial load is considered. Thus, the elastic principal stresses ($\sigma_I \geq \sigma_{II} \geq \sigma_{III}$) are reduced to only one stress component σ_I and the probability of failure can be written as follows:

$$P_f(\underline{\underline{\sigma}}, V) = 1 - \exp\left(-\frac{1}{V_{ref}} \int_V \left\langle \frac{\sigma_I(x,y,z)}{f_{t/ref}} \right\rangle^m dV\right) \tag{3.1}$$

where $\langle . \rangle$ accounts for the positive part, m is the Weibull modulus and V_{ref} and $f_{t/ref}$ are the volume and the tensile strength of the reference structure respectively. This volume usually corresponds to a normalized (e.g. cylindrical or cubic (see section 2.1.2)) specimen.

However, a main disadvantage of this theory is that its characteristic length ($\sqrt[3]{V_{ref}}$) does not seem to account for the stress redistribution phenomenon. In addition, the failure of concrete can be viewed as a statistical process, since the mechanical properties of concrete present a spatial randomness character. The ultimate load capacity, then, depends on the distribution of flaws within the concrete. Thus, a rearrangement of the Weibull integral can be considered. Hence, the size effect can be described with a nonlocal formulation of the Weibull theory and the spatial variability of the material strength (Sellier and Millard [2014]). For this purpose, a weighting function $\psi(l_I, x)$ (Equation 3.2) is introduced to the Weibull integral, in order to balance the probabilistic influence of each point of a structure by considering its distance x from another point.

$$\psi(l_I, x) = \exp\left(-\frac{x^2}{2l_I^2}\right) \tag{3.2}$$

where x is the distance between the integrated point and an arbitrary point of the volume V and l_I is a scale length defined in the direction of the first principal stress.

This weighting function is intended to account for the variability of the tensile strength in concrete. This concrete variability is controlled by the appearance of a weak zone, usually piloted by the absence of aggregates or the presence of an unexpected porosity. Moreover, among the phases composing the concrete, the interfacial transitional zone (ITZ) is known to be porous, weak and the site of initial microcrack occurrence (Nemati and Gardoni [2005]). The inelastic behavior of concrete often begins before the development of a macrocrack, and failure starts within this weak local zone. Because concrete is not perfectly brittle, stress redistribution should therefore occur around this weakest zone. If another weak zone were to exist in the structure, then crack propagation would depend on the distance x between two weak points. Hence, scale length l_I characterizes the spatial decrease in the function $\Psi(l_I, x)$. This scale length is responsible to account for the stress redistribution around the weakest spot. As, for stress redistributions, one can distinguish two cases: the attenuation of the elastic stresses, depending on the distance to the weak zone or the development of a highly nonlinear zone around the weakest point (i.e. the development of a fracture process zone FPZ). However, the case of high concentration of stresses (as in the splitting test or in notched beams) is not taken into account, in this thesis.

The originality of the method is that it limits the domain of the Weibull integral and avoids using a too small tensile strength for very large elements. Thus, the probability of failure is obtained by introducing the Equation 3.2 into the Equation 3.1:

$$P_f(\underline{\underline{\sigma}}, V) = 1 - \exp\left(- \int_V \left\langle \frac{\sigma_I(x,y,z)}{f_{t/ref}} \right\rangle^m \psi(l_I, x) \frac{dV}{V_{ref}} \right) \tag{3.3}$$

Consequently, the effective volume V_E, given in Equation 3.4, depends on m, the stress field, the total volume V of the studied structure and the weighting function $\Psi(l_I, x)$. V_E is given by the following equation:

$$V_E = \int_V \left\langle \frac{\sigma_I(x,y,z)}{\sigma_{max}} \right\rangle^m \psi(l_I, x)\, dV \tag{3.4}$$

where σ_{max} is the maximum value of the principal stresses in the structure.

For the estimation of the first principal stress $\sigma_I(x,y,z)$, the Rankine's formula is used. Thus, the first principal stress is computed as a relation between normal stress σ_{11} and shear stress σ_{12}:

$$\sigma_I = \frac{\sigma_{11}}{2} + \frac{1}{2}\sqrt{\sigma_{11}^2 + 4\sigma_{12}^2} \tag{3.5}$$

Finally, using the Weibull weakest-link model, the tensile strength f_t can thus be defined as a strength dependent on component size:

$$f_t = f_{t/ref} \left(\frac{V_{ref}}{V_E} \right)^{1/m} \tag{3.6}$$

The aim of this approach is to predict the tensile strength of a (reinforced) concrete structure, not only on an averaged basis but also in terms of dispersion. We have opted to account for uncertainties relative to the tensile strength of the smallest specimen $f_{t/ref}$ using a random variable Y_1 and the Weibull modulus m through a random variable Y_2. The Weibull modulus is directly linked to the mechanical properties of concrete, which are considered as variables, its estimation will be discussed in the following section. The tensile strength of the structure thus also becomes a random variable, Z. From Equation 3.6, we deduce:

$$Z = Y_1 \left(\frac{V_{ref}}{V_E} \right)^{1/Y_2} \tag{3.7}$$

Our focus is not only on the mean but also the coefficient of variation of Z, which depends on the means and coefficients of variation of both Y_1 and Y_2. In the following discussion, such uncertainty propagation studies are conducted using Monte Carlo methods. Moreover, the effective volume depends on the scale length l_I, which is directly correlated with concrete variability, as pointed out in Sellier and Millard [2014]. One objective of this approach therefore is to identify the scale length l_I for series of concrete specimens under uniaxial tension (Rossi et al. [1994]) and 3-point bending loading (Hoover and Bažant [2014a]).

In conclusion, a simplified approach is proposed, in order to estimate:

- The scale length l_I from series of concrete specimens under uniaxial tension or 3-point bending loading. For each concrete series, different volumes of concrete specimens are studied (V_i, V_j ...). As a consequence, ratios of V_{Ei}/V_{Ej} are studied for all the possible couples $(f_{t,i}, f_{t,j})$, using Equation 3.6. The only unknown parameter remaining is the scale length l_I.

- The mean, the standard deviation and the distribution of the tensile strength, by propagating the experimental variability of the reference tensile strength $f_{t/ref}$ and the variability of the Weibull modulus m using Monte-Carlo simulations.

Furthermore, in order to make it easier to state the size effect for the different studied geometries and the different loading cases, a reference x-axis has to be chosen. In most studies, the smallest size of the specimen (usually the diameter in the case of cylindrical specimens or the height in the case of rectangular beams) is used to emphasize the size effect in the studied series. Torrent [1977] estimated the Highly Stress Volume (HSV) (see Chapter 2), which corresponds to the volume that contains 90 or 95 % of the maximum stress σ_{max}, for different loading cases. Therefore, the use of log HSV as the x-axis in the size effect plot seems to be more accurate, specially for beams under 3-point and 4-point bending loading, where the stress is not uniform. Figure 3.1 presents the three different geometries subjected to 3 different types of loading studied in this chapter (cylindrical specimens (Rossi et al. [1994]), dog bone specimens (Van Vliet and Van Mier [2000]), and rectangular beams (Hoover and Bažant [2014a], Grégoire et al. [2013], Torrent [1977], Koide et al. [2000] and Mazars [1984])) and their corresponding outlined HSV. In the case of cylindrical specimens under uniaxial tension, the HSV is

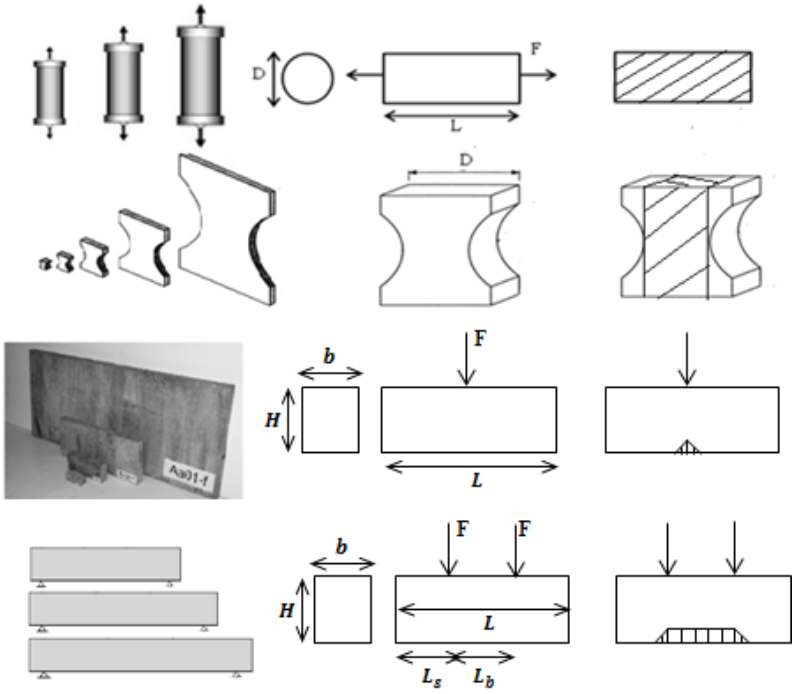

FIGURE 3.1: Different studied geometries: cylindrical specimen (Rossi et al. [1994]), dog bone specimen (Van Vliet and Van Mier [2000]), 3 points bending beams (Torrent [1977], Hoover and Bažant [2014a], Grégoire et al. [2013]) and 4-point bending beams (Mazars [1984] and Koide et al. [2000]) and their corresponding HSV (hatched area).

equal to the total volume of the specimen, whereas for dog-bone specimens, the HSV is equal to a rectangular volume whose cross-section equals that of the central part of the dog bone (i.e. smallest section) and whose length is that of the specimen. Moreover, in

the case of 3-point bending beams, Torrent [1977] defined the HSV as a triangle, of a height and length equal respectively to $h = \frac{H}{40}$ and $l = \frac{L}{20}$, extruded through the beam width, such that:

$$HSV = \frac{bHL}{1600} \tag{3.8}$$

where b, H and L are respectively the thickness, the height and the length of the beam. Finally, in the case of 4-point bending loading, the HSV corresponds to the extrude over the total width of the beam of the shaded area in Figure 3.1. The shaded area is composed by a rectangle of height $h = \frac{H}{40}$ and length equal to the bending length of the beam L_b and two triangles of height $H/40$ and length $L_s/20$ where L_s is equal to the shear length of the beam, which corresponds to the distance between the support and the point of application of the force. Thus, the HSV, in the case of 4-point bending loading could be estimated as follow:

$$HSV = \frac{bHL_b}{40} + \frac{bHL_s}{800} \tag{3.9}$$

3.1.2 Synthesis of experimental campaigns of concrete structures

This section briefly presents the experimental tests conducted on concrete specimens of different volumes under uniaxial tension or 3-point bending loading or 4-point bending loading. In a cylindrical specimen under uniaxial tension, the tensile strength is uniform and equal to $\sigma_{max} = \frac{F}{S}$, where S is the cross-sectional area. In the case of 3-point bending loading, stress is not uniform in the beam and only the bottom part is under tension; maximum tensile stress, in the elastic phase, is equal to $\sigma_{max} = \frac{3}{2}\frac{FL}{bH^2}$, where L, b, H are the span, the width and the height respectively. As for the case of 4-point bending, the maximum tensile stress is equal to $\sigma_{max} = \frac{6FL_s}{bH^2}$, where L_s is the shear span.

Table 3.1 gives the different concrete mix compositions for all the studied test series and their main properties. The details of the series mentioned are presented in Appendix A. For the case of direct tensile tests, two series of concrete specimens, with different volumes, are presented; Rossi et al. [1994] series present the advantage of studying two different concrete mixtures for three volumes of cylindrical specimens, they showed a decrease of the mean and the standard deviation of the tensile strength as the volume increases and the lower the compressive strength of the concrete is, the lower the tensile

TABLE 3.1: Concrete mix composition and main properties for each test series (Rossi et al. [1994], Van Vliet and Van Mier [2000],Hoover and Bažant [2014a], Grégoire et al. [2013], Torrent [1977], Mazars [1984] and Koide et al. [2000]).

Available data	Rossi et al. [1994]	Van Vliet and Van Mier [2000]	Hoover and Bažant [2014a]	Grégoire et al. [2013]	Torrent [1977]	Mazars [1984]	Koide et al. [2000]
Number of specimens	> 26	> 20	> 128	> 34	unknown	> 17	> 45
Geometry	Cylind.	Dog-bone	Rect.	Rect.	Rect.	Rect.	Rect.
Diameter D (mm)	30-60-150	60-120-240-480-960	-	-	-	-	-
Height H (mm)	-	-	40-93-215-500	50.6-101-200-400	25-25-40-150	100-220	100-100-100
Type of loading	Direct tension	Direct tension	3-point bending	3-point bending	3-point bending	4-point bending	4-point bending
Length L (mm)	2D	150-300-600-1200-2400	96-223-516-1200	177-353-700-1400	106-240-106-450	300-1400	600-800-1000
Bending span L_b (mm)	-	-	-	-	-	100-600	200-400-600
Shear span L_s (mm)	-	-	-	-	-	100-400	200
Thickness b (mm)	-	-	40-40-40-40	50-50-50-50	25-25-40-150	100-150	100-100-100
d_{max} (mm)	20	8	10	10	5	10	20
W/C	0.6-0.45	0.5	0.41	0.6	0.55-0.67-0.8	-	-
f_{c28} (MPa)	35-55.8	37	45.7	42.3	> 44.3	30	30

strength is. However, Van Vliet and Van Mier [2000] focused on dog bone shape series that were conducted on concrete cured under varying humidity conditions. In this study, the size effect was found to depend on three phenomena: the presence or absence of large aggregates in the critical cross section of small specimens, the classical Weibull statistical size effect on strength for large specimens and the fluctuation of material strength when strain or stress gradients occur.

In the case of 3-point bending tests, Hoover and Bažant [2014a] and Grégoire et al. [2013] conducted experimental tests on both notched and unnotched beams, they both showed a dependency between the tensile strength and the structure size (height of the beam) and a difference between notched and unnotched specimens response. Moreover, Torrent [1977] conducted tests on unnotched beams having various mixes of concrete with different W/C ratios. In this study, only three mixes are used

However, the literature presents few experimental series on concrete beams subjected to 4-point bending. For example, Koide et al. [2000] studied the influence of scaling the bending span on the flexural resistance. Experiments correspond to 3 types of beams subjected to 4-point bending. For each type of beams, the same cross section and shear span are kept and only the bending span is scaled. Koide et al. [2000] emphasized the decrease of flexural resistance when the bending span increases. However, the three beams present the same tensile strength. In addition, Mazars [1984] conducted two beams having the same geometry but different cross section, shear span and bending span and subjected to 4-point bending. These two beams have the same characteristics of concrete. He showed that the bigger beam is weaker in term of tensile strength.

Figures 3.2 and 3.3 present the evolution of the tensile strength as function of log HSV for the case of the studied concrete specimens under uniaxial tension and the studied concrete beams under 3-point bending loading respectively. In both cases, the problematic of size effect on the tensile strength at first crack is emphasized. Thus, it is important to develop a simple method to estimate this mechanical property.

In all concrete series tested, the crack corresponds to a mode I mechanism in tension. A crack thus appears whenever the first principal stress σ_I reaches the local randomly-distributed tensile strength f_t (Rossi and Ulm [1997]):

$$\sigma_I \leq f_t \tag{3.10}$$

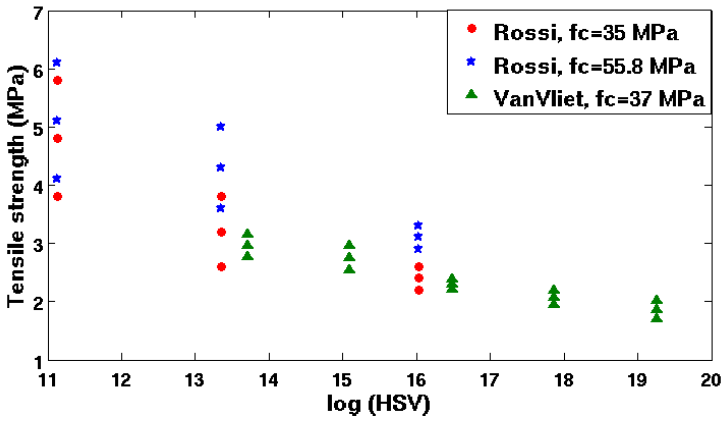

FIGURE 3.2: Mean values of the tensile strength as function of log HSV for specimens under uniaxial tension (Rossi et al. [1994] and Van Vliet and Van Mier [2000]).

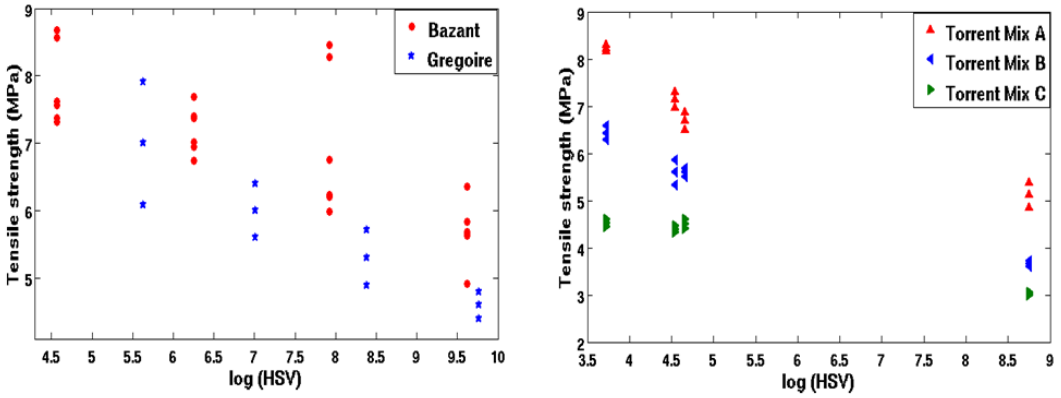

FIGURE 3.3: Mean values of the tensile strength as function of log HSV for beams under 3-point bending loading (Hoover and Bažant [2014a], Grégoire et al. [2013] and Torrent [1977]).

3.1.3 Estimation of the Weibull modulus

Modulus m is widely used in studies dedicated to the size effect in brittle materials such as ceramics but also in (reinforced) concrete structures. m is correlated with the shape of the tensile strength statistical distribution. The greater the value of m, the less scatter in the data. It is also well-known that estimating such a parameter is a tricky endeavor. A Weibull distribution is not expected to be valid for brittle materials containing bi- or multi-modal flaw distributions, displaying a high defect density. Estimations of m also change slightly with the type of test: 3 or 4-point bending vs. direct tensile tests (Warren [2001]). In addition, Afferrante et al. [2006] showed that the Weibull modulus depends on interactions between the crack distribution and the stress field. Moreover, Bergman [1984] demonstrated that the coefficient of variation of tensile strength decreases with an increasing value of m. In these latter cases, the Weibull modulus depended on the

applied stress amplitude and was no longer a constant.

To estimate the Weibull modulus, several methods can be found in the literature, including the maximum likelihood (Lamon and Evans [1983]), the regression method (Wu et al. [2012]), the Weibull definition (Sellier and Millard [2014]), and Rossi et al. [1994] formula. Even though m is considered as a statistical parameter (Le et al. [2011], Le et al. [2013]), beams under 3-point bending loading can still be considered affected by the energetic-statistical size effect and a value of m can be assessed to this type of loading. For example, m was evaluated at 10 for a series of beams under 3-point bending loading in Sellier and Millard [2014]. A brief explanation of the methods used to evaluate m is given hereafter.

Rossi et al. [1994] showed that this modulus depends on the compressive strength f_c of concrete, based on series of cylindrical concrete specimens under direct tensile tests and having different concrete compositions and volumes ($30 < f_c < 130$ MPa and $30 < D < 160$ mm), plus a maximum aggregate diameter equal to 20 mm, according to the following formula:

$$m = (0.25 - 3.6 \times 10^{-3} \times f_c + 1.3 \times 10^{-5} \times f_c^2)^{-1} \tag{3.11}$$

It is also possible to deduce the Weibull modulus directly from experimental results since it depends statistically on the mean value and coefficient of variation of the tensile strength. The relation between the Weibull modulus m and the coefficient of variation of the experimentally measured tensile strength $CV(f_t)$ is given by the following equation and illustrated in Table 3.2 (Sellier and Millard [2014]):

$$CV = \frac{\sqrt{\Gamma(1+\frac{2}{m}) - \Gamma^2(1+\frac{1}{m})}}{\Gamma(1+\frac{1}{m})} \tag{3.12}$$

where Γ is the Gamma function.

Also, Figure 3.4 gives the evolution of the Weibull modulus m as function of $CV(f_t)$. Therefore, the Weibull modulus depends on the concrete mix, which explains the relevance of considering this modulus as variable in Equation 3.7.

Other widespread statistical methods for estimating m are the maximum likelihood and regression methods (Lamon and Evans [1983], Wu et al. [2012]). It is worth noting that these last two statistical estimations require a sufficient amount of data, which tends not to be available in most cases. Danzer et al. [2007] studied the effect of the number

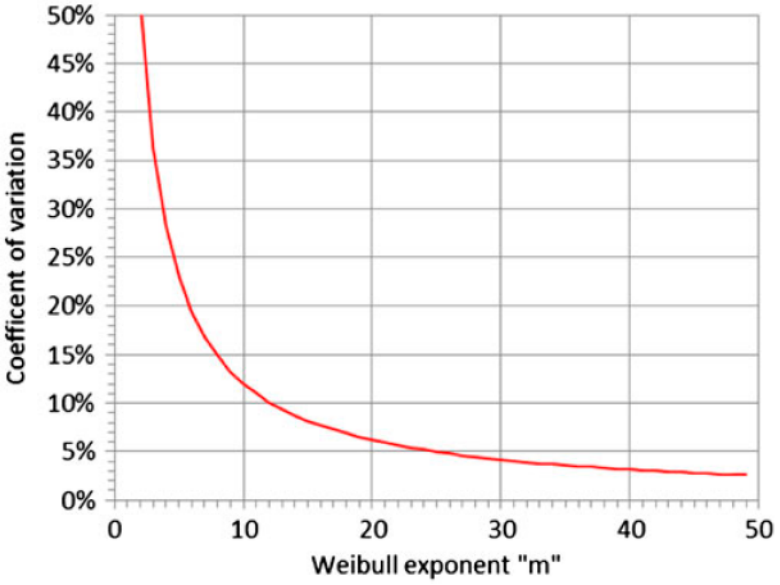

FIGURE 3.4: Evolution of m as function of $CV(f_t)$ (Sellier and Millard [2014]).

TABLE 3.2: Weibull modulus estimation for usual values of coefficients of variation of f_t using Equation 3.12

$CV(f_t)$	23	19	17	15	13	12	11	10	9.4	8.7	8.2	7.7	6.9	6.2	5.2	4	2.6
m	5	6	7	8	9	10	11	12	13	14	15	16	18	20	24	31	48

of strength tests on estimating the mean of m: for a set of 30 tests, the 90% confidence interval of m is typically ±30% around the mean value.

In conclusion on the choice of the Weibull modulus, Table 3.3 summarizes the values estimated from various methods, and confidence intervals are proposed for each experimental series. A value of m between 6 and 12 seems on average to be reasonable for ordinary concrete, since it reproduces a coefficient of variation of f_t varying from 10 to 20 %. Let's note that this result raises suspicion about the choice of values, such as 24 or 48, that can be found in other works (Bažant et al. [2007], Syroka-Korol et al. [2013] ...). Moreover, Table 3.2 shows that $m = 24 - 48$ refers to a coefficient of variation of a tensile strength varying between 2.6 and 5.2 %, which does not represent the reality for concrete material (whose coefficient of variation for tensile strength lies on the order of 10%). In addition, Bažant and Novak [2000] estimated a value of m equal to 24 using an iterative nonlinear optimization algorithm, with three optimized parameters of the energetic-statistical SEL and reliance on different experimental series under 3-point and 4-point bending loading. However, an advantage of the estimation, done in this thesis, is the use and comparison of three methods to estimate m for each experimental

TABLE 3.3: Weibull modulus estimation for each series of tests (Hoover and Bažant [2014a], Grégoire et al. [2013], Torrent [1977], Van Vliet and Van Mier [2000])

	Torrent [1977]	Hoover and Bažant [2014a]	Grégoire et al. [2013]	Van Vliet and Van Mier [2000]
Rossi et al. [1994] formula	10.1	8.9	8.23	7.4
Torrent	9-13	-	-	-
Maximum likelihood	6.5	7.9	7.1	6.5
Regression method	6	7.8	6.1	6
Weibull definition	< 12	8.5	6.5	7
Proposed range	6.5-12	8-9	6-8	6.5-7.5

series, with a consistent value of m being found for each series. Thus, the values of m estimated by Bažant and Novak [2000] are questionable and the values of m equal to 24 or 48 should not be used to describe the concrete material having variable mechanical properties. In conclusion, m is a material parameter linked to the variability on concrete tensile strength and it can be estimated independently for each experimental series, i.e. for each concrete mix.

3.1.4 Experimental identification of the scale length

In order to estimate the scale length, an inverse analysis has been carried out on series of concrete specimens under uniaxial tension (Rossi et al. [1994]) as well as on series of unnotched concrete beams loaded in 3-point bending (Hoover and Bažant [2014a]). Table 3.4 summarizes the main results of these 2 series where $\mu(f_t)$ and $Std(f_t)$ are respectively the mean and the standard deviation values of the tensile strength. The underlying notion here is to simply study the ratio of all specimen couples i and j (see Figure 3.5) to volumes $(V_{E,i}, V_{E,j})$ using Equation 3.6, which corresponds to the strength couple $(f_{t,i}, f_{t,j})$.

First, Rossi et al. [1994] series is used. In the case of a direct tensile load on cylindrical specimens, stress is uniformly distributed within the volume. Equation 3.4 can thus be

TABLE 3.4: Experimental results for Rossi et al. [1994] and Hoover and Bažant [2014a]

	Rossi et al. [1994] (f_c=35 MPa)			Rossi et al. [1994] (f_c=55.8 MPa)			Hoover and Bažant [2014a] (f_c=45.7 MPa)			
D (mm)	30	60	150	30	60	150	40	93	215	500
$\mu(f_t)$ (MPa)	4.8	3.2	2.4	5.1	4.3	3.1	7.8	7.2	6.9	5.7
$Std(f_t)$ (MPa)	1	0.6	0.2	1	0.7	0.2	0.6	0.3	1.1	0.5

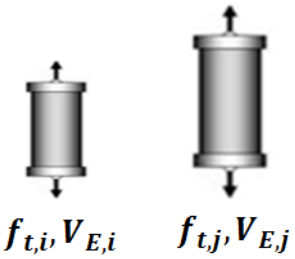

FIGURE 3.5: Two different sizes of specimens.

rewritten in the following form:

$$V_E = \pi D^2 \times \int_0^L \exp\left(-\frac{x^2}{2l_I^2}\right) dx \tag{3.13}$$

where D and L are respectively the diameter and the length of the cylinder.

In the case of the cylindrical specimens of Rossi et al. [1994], the ratio between the tensile strengths of two different specimens is reduced to the following equation:

$$\frac{f_{t,i}}{f_{t,j}} = \left(\frac{D_j^2 \times \int_{L_j} \exp\left(-\frac{x_j^2}{2.l_I^2}\right) dx}{D_i^2 \times \int_{L_i} \exp\left(-\frac{x_i^2}{2.l_I^2}\right) dx} \right)^{1/m} \tag{3.14}$$

In order to have accurate evaluation of the mean and the standard deviation of the tensile strengths ratios, we suppose that the tensile strength follows a log-normal distribution law, thus the ratio of two tensile strengths follows a lognormal distribution law (Mesureur [1989]) and its mean $\mu\left(\frac{f_{t,i}}{f_{t,j}}\right)$ and its standard deviation $Std\left(\frac{f_{t,i}}{f_{t,j}}\right)$ can be calculated using the following equations:

$$\mu\left(\frac{f_{t,i}}{f_{t,j}}\right) = \frac{\mu\left(f_{t,i}\right)\sqrt{1+CV\left(f_{t,j}\right)^2}}{\mu\left(f_{t,j}\right)\sqrt{1+CV\left(f_{t,i}\right)^2}} \sqrt{\left(1+CV\left(f_{t,i}\right)^2\right)\left(1+CV\left(f_{t,j}\right)^2\right)} \tag{3.15}$$

$$Std^2\left(\frac{f_{t,i}}{f_{t,j}}\right) = \left(\left(1+CV\left(f_{t,i}\right)^2\right)\left(1+CV\left(f_{t,j}\right)^2\right)-1\right)\times\mu^2\left(\frac{f_{t,i}}{f_{t,j}}\right) \tag{3.16}$$

where $CV\left(f_{t,i}\right)$ and $CV\left(f_{t,j}\right)$ are the coefficient of variations of the tensile strength corresponding respectively to specimen i and specimen j.

Moreover, the Weibull modulus is defined using Equation 3.11, which is directly deduced from this concrete series based on compressive tests performed on 16×32 cm^2 cylindrical concrete specimens. The value of m equals 7.4. For example, Figure 3.6 shows the numerical evolution of $\frac{f_{t,3}}{f_{t,1}}$ (i.e. ratio of tensile strengths corresponding to the highest and lowest volumes) as a function of parameter l_I. The horizontal line establishes the experimental mean value of the ratio $\frac{f_{t,3}}{f_{t,1}}$; like for the dotted lines, this indicates the experimental confidence interval for the given ratio. As seen in Figure 3.6, the analytical approach WL2$_A$ reproduces the experimental mean value of $\frac{f_{t,3}}{f_{t,1}}$ for a scale length equal to 0.2 m. From the two concrete mixes of Rossi et al. [1994] study, a mean scale length of 0.2 m and a standard deviation of 0.1 m are deduced.

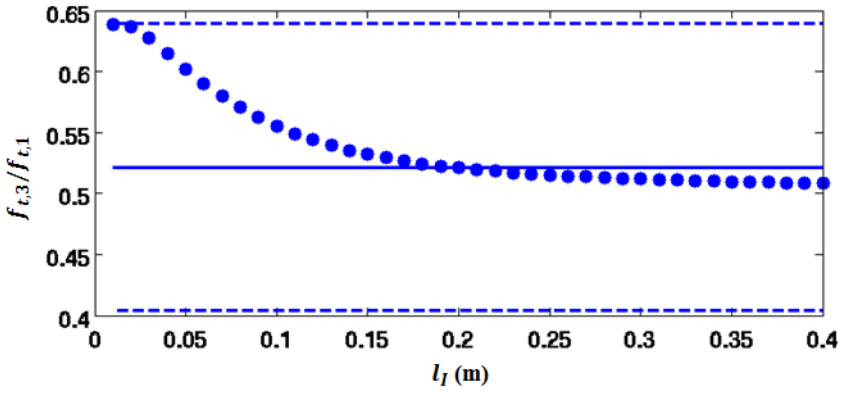

FIGURE 3.6: Evolution of the ratio of $\frac{f_{t,3}}{f_{t,1}}$ for $f_c = 35$ MPa (case of Rossi et al. [1994] series) as function of the scale length l_I.

Secondly, an inverse analysis was applied to the case of unnotched beams under 3-point bending loading, with different volumes and a constant thickness. The Hoover and Bažant [2014a] series are studied to evaluate the scale length l_I corresponding to this case of loading.

However, in this case, the stress is not uniform as in the case of direct tensile load. As mentioned before, the aim of this analytical method is to be applied in the elastic domain and for mode I rupture, thus the Rankine criteria (maximum-principal stress criteria) is chosen to ensure these hypothesis. Therefore, it is important to evaluate the first principal stress, in the case of a rectangular beam under 3-point bending loading.

Consequently, σ_I depends on both the normal stress σ_{11} and the shear stress σ_{12}, as seen in Figure 3.7. Moreover, the shear stress is affected by a correction factor α, which depends on the ratio width-to-depth (b/H) of the rectangular section (Barretta and Barretta [2010]). Under such hypothesis, Equation 3.17 gives an estimation of the α coefficient.

$$\alpha = \frac{7}{10} + \frac{3}{10}\frac{b}{H} \tag{3.17}$$

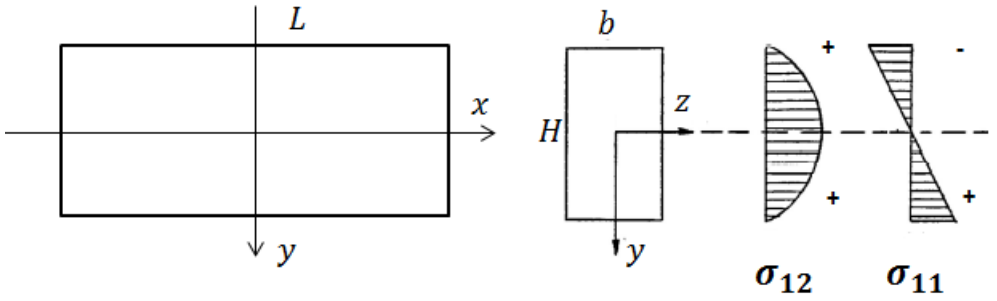

FIGURE 3.7: Evolution of the normal stress σ_{11} and the shear stress σ_{12} in a rectangular section subjected to 3-point bending.

As the effective volume depends only on the positive part of the first principal stress σ_I, it is not the same under and above the neutral axis ($x = 0$). Thus, using Equations 3.4 and 3.5 and by recalling the maximum stress in the case of 3-point bending ($\sigma_{max} = \frac{3FL}{2bH^2}$), the effective volume is deduced:

- For $0 < y < H/2$:

$$V_E = b \times \int_0^{H/2} \int_0^L \left(\frac{1}{HL} \left(Ly + \sqrt{L^2y^2 + 4\alpha^2 \left(\frac{D^2}{4} - y^2 \right)^2} \right) \right)^m \exp\left(-\frac{x^2}{2.l_I^2} \right) dxdy \tag{3.18}$$

- For $-H/2 < y < 0$:

$$V_E = b \times \int_{-H/2}^0 \int_0^L \left(\frac{2\alpha}{HL} \left(\frac{H^2}{4} - y^2 \right) \right)^m \exp\left(-\frac{x^2}{2.l_I^2} \right) dxdy \tag{3.19}$$

In the following, the same steps, done in the case of tensile load, are repeated for this Hoover and Bažant [2014a] series. The six different strength couples, which correspond to the Hoover and Bažant [2014a] series, are estimated using three different estimations of the Weibull modulus. Thus, in the case of 3-point bending loading, a mean value of 0.2 m and a standard deviation of 0.18 m can be derived for the scale length. Moreover,

the method chosen to estimate the Weibull modulus exerts negligible influence on the scale length. The increase in standard deviation of the scale length, in the case of 3-point bending loading compared to the uniaxial case, may be ascribed to the occurrence of a stress concentration and to the small thickness of the studied beams (b =40 cm).

3.2 Prediction of the size effect for various series of concrete structures

In this section, the analytical-probabilistic approach WL2$_A$ is applied to different types of structure subjected to direct tension (Rossi et al. [1994] and Van Vliet and Van Mier [2000]), 3-point bending (Torrent [1977], Hoover and Bažant [2014a] and Grégoire et al. [2013]) and 4-point bending (Koide et al. [2000] and Mazars [1984]). The mean and the standard deviation of the tensile strength at first crack are predicted for different series of concrete specimens or beams. Then, the method is applied to large massive structures.

3.2.1 Prediction of the mean of the tensile strength

Different studies have been conducted to emphasize the size effect of series of concrete specimens having different geometries. The aim of this study is to predict the tensile strength to be used for the different concrete specimens using Equation 3.6 by taking into account the tensile strength of the smallest specimen and its effective volume as the reference input parameters ($f_{t/ref}$, V_{ref}).

3.2.1.1 Series under uniaxial tension

Van Vliet and Van Mier [2000] series are studied herein. The analytical size effect approach is applied to the dry dog-bone series by considering the smallest specimen as the reference volume. The purpose of this study is to estimate the tensile strength of larger specimens using different values for both the scale length and the Weibull modulus (based on its proposed range of validity given for each series in Table 3.3). Figure 3.8 shows the different estimations of tensile strength for the four concrete specimens in this series, with various scale lengths l_I ranging between 0.1 m and 0.2 m and two values

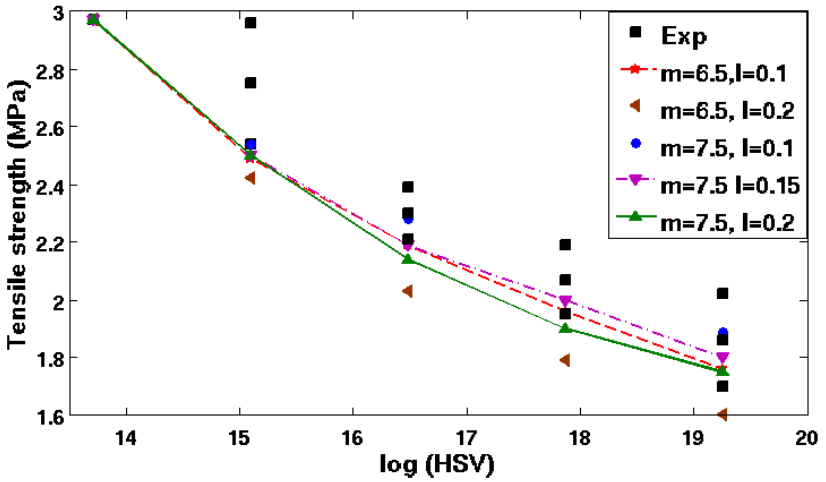

FIGURE 3.8: Estimation of the tensile strength as function of the HSV of the specimens (D=100, 200, 400, 800 and 1600 mm) for different values of the scale length l_I and the Weibull modulus m

of m corresponding to the minimum and maximum of the interval in Table 3.3. It is worth noting, first, the small number of tests experimentally done. For the second specimen for example, where the scattering in the results is the most obvious, only four specimens were tested. By comparing just the Weibull modulus, we first deduce that $m = 7.5$ is capable of more accurately reproducing the experimental results. This value corresponds to Rossi's formula, which considers m as a material parameter since it is related to f_c (Equation 3.11). Therefore, since Rossi et al. [1994] and Van Vliet and Van Mier [2000] concrete compositions are close to one another, Equation 3.11 provides the appropriate method for the case of Van Vliet and Van Mier [2000] test series. The scale length is studied next. The best fit with experimental results corresponds to a value of approximately 0.15 m. This decrease in scale length is perhaps due to a concentrated deformation gradient stemming from the dog-bone geometry.

3.2.1.2 Series under 3-point bending loading

The first series studied correspond to the work by Torrent [1977], who studied different concrete types featuring different water/cement (W/C) ratios. The HSV concept was applied to various experimental tests and revealed that Equation 2.12 quantifies the size effect phenomenon quite accurately. Torrent [1977] estimated the Weibull modulus m for each concrete mix as a function of W/C ratio as shown in the Table 3.5. A constant scale length equal to 0.2 m and three Weibull modulus estimation methods are used in

this section to highlight the influence of m on the tensile strength prediction. Tables 3.6, 3.7 and 3.8 provide the ratios of numerical to experimental tensile strength values for the three Torrent mixes using three m estimations for each mix. The choice of m estimation method exerts an influence on tensile strength. When the parameter is estimated by Weibull and the maximum likelihood method, the tensile strength is underestimated for the largest volume. For the two smallest beams, both the maximum likelihood method and Weibull definition are able to predict a mean tensile strength close to the experimental results, yet these two methods yield tensile strength values very close to one another. The choice of m estimation method thus seems to have negligible influence.

TABLE 3.5: Fitting of the Weibull modulus m by Torrent [1977]

	Mix A	Mix B	Mix C
W/C	0.55	0.67	0.8
m	12.2	9.5	9.7

The final test series stem from Hoover and Bažant [2014a] and Grégoire et al. [2013].

TABLE 3.6: Estimation of the ratio of the numerical and experimental tensile strength for the mix A of Torrent series using three methods to estimate m

	$\frac{f_t(V_2)num}{f_t(V_2)exp}$	$\frac{f_t(V_3)num}{f_t(V_3)exp}$	$\frac{f_t(V_4)num}{f_t(V_4)exp}$
$m = 12.2$ (Torrent)	1.1	1.13	1.1
$m = 12$ (Weibull)	1.05	1.08	0.85
$m = 6.5$ (Max likelihood)	1.03	1.07	0.86

TABLE 3.7: Estimation of the ratio of the numerical and experimental tensile strength for the mix B of Torrent series using three methods to estimate m

	$\frac{f_t(V_2)num}{f_t(V_2)exp}$	$\frac{f_t(V_3)num}{f_t(V_3)exp}$	$\frac{f_t(V_4)num}{f_t(V_4)exp}$
$m = 9.5$ (Torrent)	1.05	1.03	1.06
$m = 12$ (Weibull)	1	0.99	0.75
$m = 6.5$ (Max likelihood)	1.03	1	0.9

TABLE 3.8: Estimation of the ratio of the numerical and experimental tensile strength for the mix C of Torrent series using three methods to estimate m

	$\frac{f_t(V_2)num}{f_t(V_2)exp}$	$\frac{f_t(V_3)num}{f_t(V_3)exp}$	$\frac{f_t(V_4)num}{f_t(V_4)exp}$
$m = 9.7$ (Torrent)	0.95	0.9	0.9
$m = 12$ (Weibull)	0.95	0.89	0.83
$m = 6.5$ (Max likelihood)	0.95	0.9	0.96

These series offer the advantage of larger test specimens (up to 1.4 m in length). The same procedure implemented for the Van Vliet and Van Mier [2000] series was applied to these series. In the case of Hoover and Bažant [2014a] series, the first beam was rejected due to its very small dimensions (96×40 mm^2) with respect to the largest aggregate (d_{max}=10 mm), and the second beam was chosen as the reference volume. In addition, the mean of the tensile strengths corresponding to the three beams of the series are estimated using the HSV method, the WEV method and the USEL of Bažant (Hoover and Bažant [2014b]). Figure 3.9 shows the different estimations of the mean of the tensile strength using HSV method, WEV method, USEL of Bažant and the analytical approach WL2$_A$ with two different values of l_I. On the one hand, the HSV method and the WEV method tend to decrease continually the tensile strength as the volume increases and underestimate the tensile strength for the largest beams. On the other hand, the USEL of Bažant reproduces the size effect for this series. However, this method requires the optimization of different numerical parameters (see Equation 2.27). As for the analytical approach WL2$_A$, l_I=0.1 m represent the best fit for this experimental series.

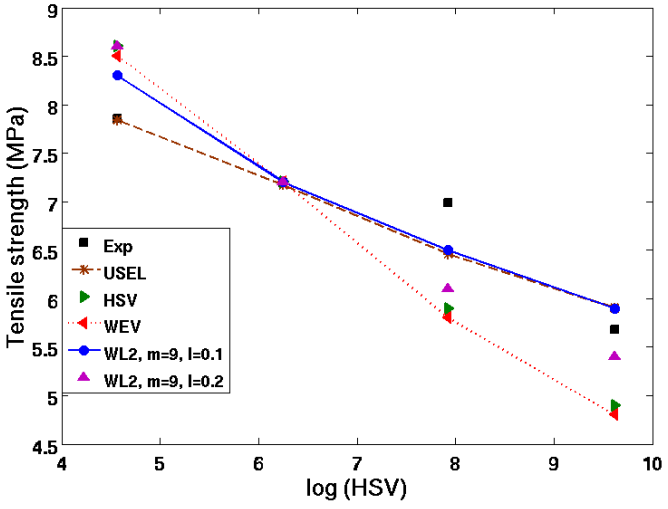

FIGURE 3.9: Estimation of the tensile strength as function of log HSV for Hoover and Bažant [2014a] series for different values of the scale length

In the case of Grégoire et al. [2013] series where d_{max} = 10 mm, the first beam having ($177.1 \times 50.6 \times 50$ mm^3) as dimensions is chosen to be the reference volume. For this case, a comparison with the HSV and the WEV methods is done. As seen for the case of Hoover and Bažant [2014a] series, the HSV and the WEV methods are not able to reproduce the mean of the tensile strength for the largest beams (see Figure 3.10). As

for the WL2$_A$ approach, only the highest value of m in its proposed range given by Table 3.3 is used and two values of l_I are considered. A very slight difference between the results obtained using $l_I = 0.2$ m and $l_I = 0.3$ m is observed in Figure 3.10.

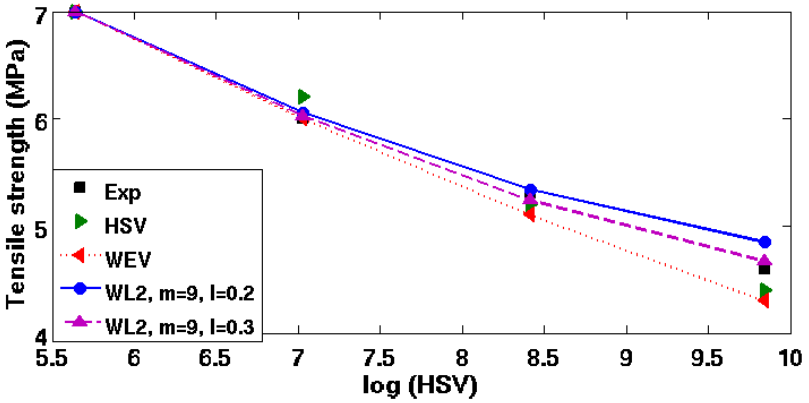

FIGURE 3.10: Estimation of the tensile strength as function of log HSV for Grégoire et al. [2013] series for different values of the scale length

3.2.2 Prediction of the dispersion of the tensile strength

For the identification of the standard deviation of the tensile strength, the variabilities on the reference tensile strength and the Weibull modulus must be known. For the Weibull modulus, a coefficient of variation equal to 30 % is considered (Danzer et al. [2007]). As for the variation of the reference tensile strength, it varies from one concrete series to another. After the identification of these parameters, Monte-Carlo simulations are used to propagate the variabilities of $f_{t/ref}$ and m using Equation 3.7.

First, the standard deviation of tensile strength is identified for Rossi et al. [1994] series. The chosen reference volume is the first concrete specimen. The concrete mix having a compressive strength equal to 35 MPa has a coefficient of variation of the reference tensile strength equal to 20.8 %. As for the second concrete mix with a compressive strength equal to 55 MPa, the coefficient of variation of the reference tensile strength is equal to 19.6 %. The used scale length is equal to 0.2 m. Consequently, Figures 3.11 and 3.12 present the numerical and experimental dispersion for Rossi et al. [1994] series corresponding respectively to $f_c = 35$ MPa and $f_c = 55$ MPa. The vertical bar in theses figures correspond to the dispersion of f_t estimated using the analytical approach WL2$_A$ and the red rectangles correspond to the experimental values. Thus, the results obtained by the analytical approach WL2$_A$ are in good agreement with the experimental

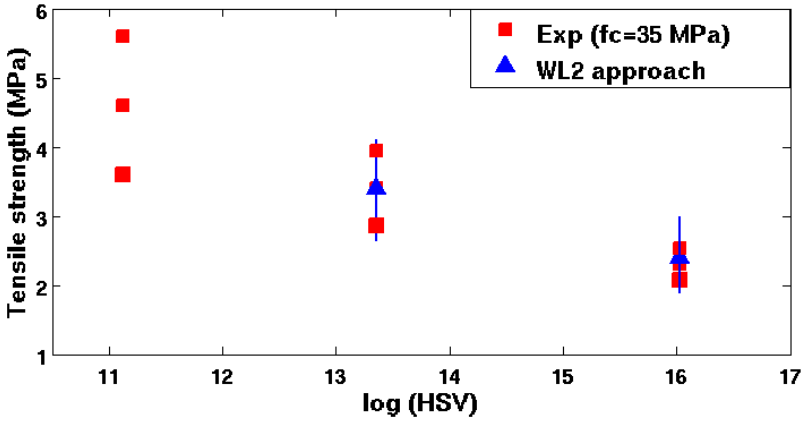

FIGURE 3.11: Estimation of the mean and dispersion of the tensile strength as function of log HSV for Rossi et al. [1994] series corresponding to a concrete mix having $f_c = 35$ MPa.

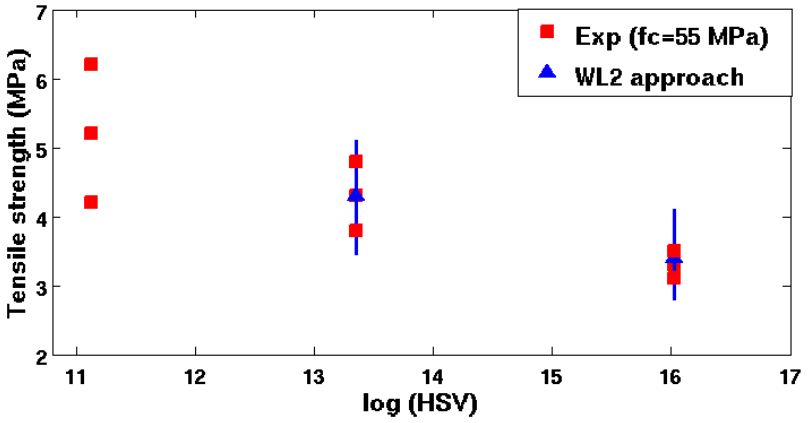

FIGURE 3.12: Estimation of the mean and dispersion of the tensile strength as function of log HSV for Rossi et al. [1994] series corresponding to a concrete mix having $f_c = 55$ MPa.

results.

Moreover, the dispersion of the tensile strength corresponding to Hoover and Bažant [2014a] and Grégoire et al. [2013] series are estimated. The coefficient of variation of the reference tensile strength for Grégoire et al. [2013] series is based on only two tests and it is equal to 13 %. As for Hoover and Bažant [2014a] series, the latest coefficient is equal to 5 % based on 6 specimen tests. The scale length l_I is equal to 0.1 m in the case of Hoover and Bažant [2014a] series and 0.2 m in the case of Grégoire et al. [2013] series (see section 3.2.1.2). Figures 3.13 and 3.14 show the tensile strength dispersion, respectively, for Hoover and Bažant [2014a] series and Grégoire et al. [2013] series.

Figure 3.13 shows that the standard deviation of tensile strength for the Hoover and Bažant [2014a] series does not decrease as the volume increases. This result may be

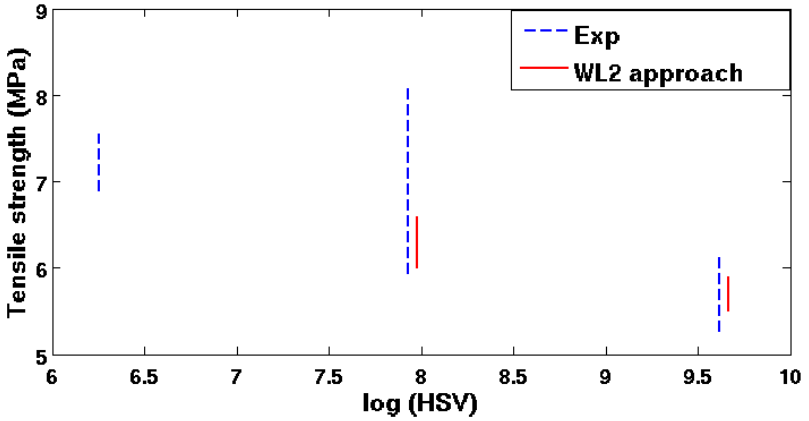

FIGURE 3.13: Evolution of the tensile strength as function of log HSV for Hoover and Bažant [2014a] series.

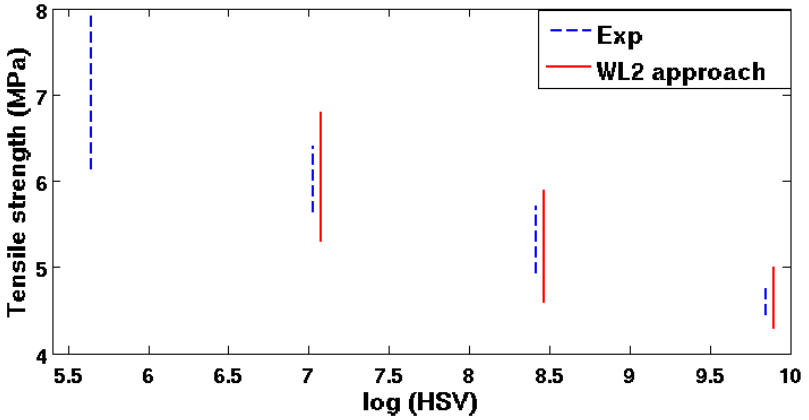

FIGURE 3.14: Evolution of the tensile strength as function of log HSV for Grégoire et al. [2013] series.

ascribed to the relatively small thickness (40 cm) of the beams. However, the analytical size effect approach does appear to reproduce the decrease of the standard deviation of the tensile strength for both concrete series.

3.2.2.1 Influence of the choice of the reference volume

Sellier and Millard [2014] proposed the splitting test as a reference structure. Indeed, splitting tensile strength $f_{ct,sp}$ and uniaxial compressive strength f_c have been widely measured on laboratory tests. Arıoglu et al. [2006] proposed a relation between $f_{ct,sp}$ and f_c (see Equation 3.20) that seems of rather large validity.

$$f_{ct,sp} = 0.387 f_c^{0.63} \tag{3.20}$$

This equation is obtained from hundreds tests on various compressive strengths (4-120 MPa), with respectively 5.6, 4.8 and 2.3 % errors for 20-40, 40-60 and 60-80 MPa, for 0-30^{o}C curing temperatures, Type I, III, cement/fly ash, cement/bottom ash and cement/silica fumes concretes. The ratio water/cement (W/C) was between 0.25 and 0.55. Moreover, Figure 3.15 highlights the HSV, as well as the effective volume in the

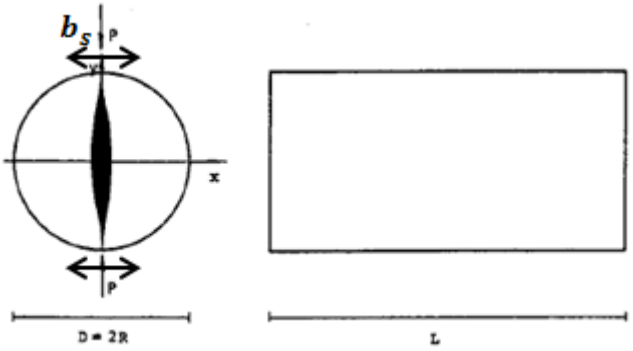

FIGURE 3.15: Cylinder splitting test and its outlined HSV (Torrent [1977]).

case of the splitting test. Torrent [1977] gave an estimation of the HSV for this case (Equation 3.21).

$$HSV = 0.0475D^2L \tag{3.21}$$

As mentioned in Chapter 2, a cylindrical specimen under splitting test is compressed along two diametrically opposed generators so that a nearly uniform tensile stress is induced in the loading plane. Usually, two thin strips having a width equal to b_s are placed between the loading platens and the specimen to distribute the load and avoid local failure in compression. The splitting tensile strength obtained depends directly on the ratio of the width of the load-bearing strips b_s to the diameter of the cylinder D (Rocco et al. [2001]). However, as shown in Equation 3.21, the HSV is estimated as independent of b_s/D and equal to 3.8×10^{-4} m^3 for a cylindrical specimen having a diameter D equal to 16 cm and a length L equal to 32 cm. Moreover, Sellier and Millard [2014] estimated that the effective volume for a cylinder (D = 11 cm and L = 22 cm) is in the order of 3×10^{-4} m^3 and this value is quasi-independent of the choice of the scale length l_I.

An objective is to study the influence of ratio b_s/D on the value of the effective volume of a cylinder (with D=16 cm and L=32 cm) subjected to splitting test. A 2D cylinder was modeled numerically using Cast3m (CEA [2015]). The concrete used has a compressive strength f_c equal to 30 MPa and a Young's modulus equal to 40 GPa. Mazars isotropic

damage model was used to model the concrete. As for the strips, they are considered as wood and their behavior is elastic. Four different ratios of b_s/D are studied: 1/6, 1/10, 1/15 and 1/20. For each ratio, the contouring of the major stress field at the time

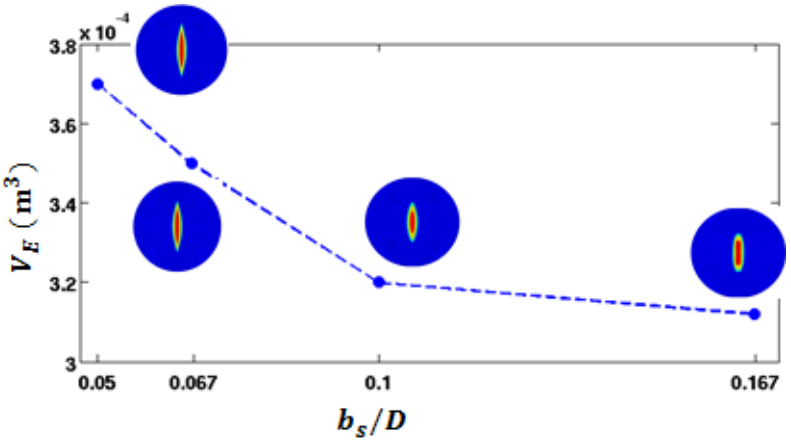

FIGURE 3.16: Evolution of the effective volume V_E as function of the ratio b_s/D and the illustration of the major stress field at the time of rupture for the studied cylinders ($D = 16$ cm and $b_s/D = 1/20, 1/15, 1/10, 1/6$).

of rupture is deduced, in order to estimate the effective volume for each case. Figure 3.16 presents the evolution of the effective volume of the split test as function of b_s/D and the illustration of the major stress field for each ratio. It is shown that the effective volume slightly depends on the width of the strip and a reference volume in the order of 3×10^{-4} m^3 can be generated for the case of splitting test having diameters equal to 11 and a length equal to 22 cm or a diameter of 16 cm and a length equal to 32 cm.

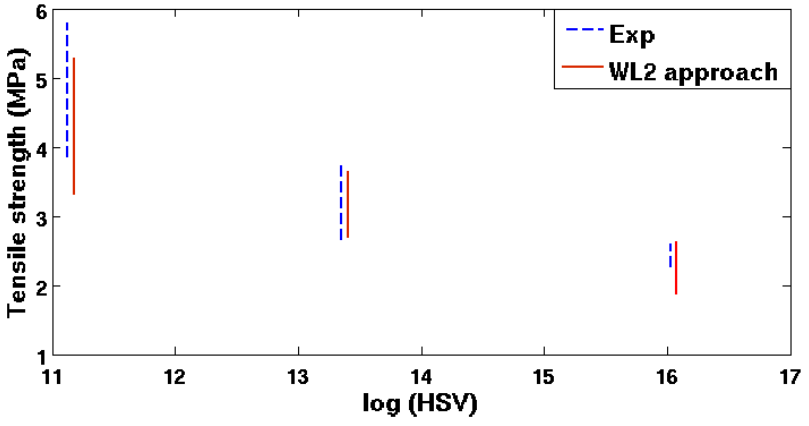

FIGURE 3.17: Estimation of the mean and dispersion of the tensile strength as function of log HSV for Rossi et al. [1994] series corresponding to a concrete mix having $f_c = 35$ MPa, in the case of a splitting test reference volume.

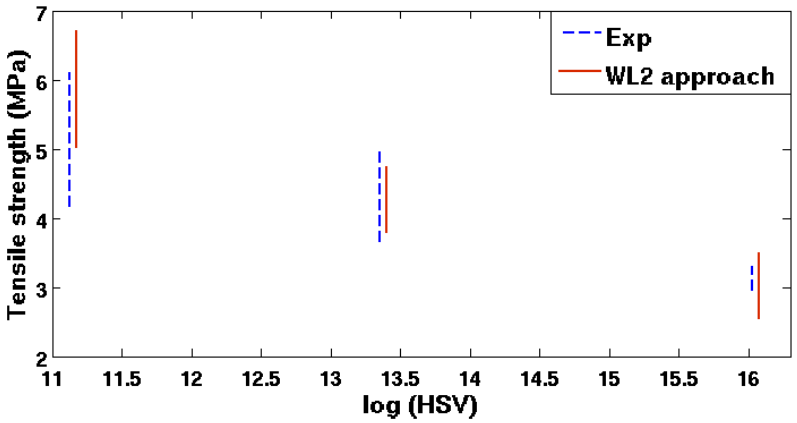

FIGURE 3.18: Estimation of the mean and dispersion of the tensile strength as function of log HSV for Rossi et al. [1994] series corresponding to a concrete mix having $f_c = 35$ MPa, in the case of a splitting test reference volume.

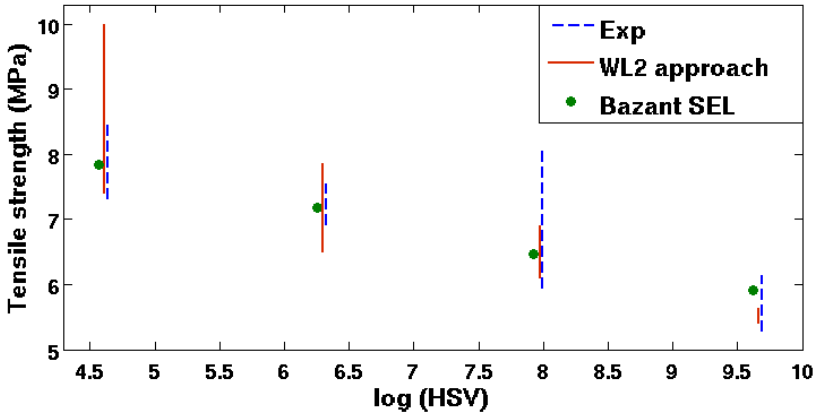

FIGURE 3.19: Evolution of the tensile strength as function of log HSV for Hoover and Bažant [2014a] series, in the case of a splitting test reference volume.

In order to validate this choice of reference volume, the analytical approach WL2_A is applied to Rossi et al. [1994] series and Hoover and Bažant [2014a] series by considering a reference volume equal to 3×10^{-4} m^3 and a reference tensile strength equal to $f_{ct,sp}$. In this case, the coefficient of variation of Y_1 associated to $f_{t/ref}$ is considered equal to a 10 % of variability on f_c (Rossi et al. [1994]). Figures 3.17, 3.18 and 3.19 show the evolution of the experimental tensile strength and the results obtained by the analytical approach WL2_A as function of the HSV for respectively Rossi et al. [1994] series with $f_c = 35$ MPa, Rossi et al. [1994] series with $f_c = 55$ MPa and Hoover and Bažant [2014a] series. For the Hoover and Bažant [2014a] series, Bažant SEL is also applied. It seems that the splitting test can be considered as a reference volume in the analytical approach WL2_A.

Series under 4-point bending loading The bending span in beams subjected to 4-point bending, which corresponds to the length between the two forces, is subjected to direct tension and has the same characteristics as an anchor having uniform loading. Thus, the statistical size effect is predominant in this case of loading. The size effect on the flexural resistance of concrete and RC beams should be studied by scaling the cross section and/or the bending span. Hence, the scaling of bending span highlights the statistical size effect in the beams. However, this loading case suffers from the lack of experimental test series in the literature, specially for concrete series having different volumes. Many authors such as Tanaka and Shimomura [2010], Zhang and Tan [2007] and Adachi et al. [1995] studied the size effect on the shear strength of deep RC beams subjected to 4-point bending. However, the analytical approach $WL2_A$ predicts the tensile strength at first crack of concrete. Therefore, the analytical approach $WL2_A$ is only applied to the two beams of Mazars [1984] and the beams of Koide et al. [2000]. Koide et al. [2000] highlighted a considerable decrease of the flexural resistance when the bending span L_b increases. However, since these three beams have the same section (100×100 mm^2) and the same shear span L_s (200 mm), they reproduced a constant tensile strength f_t equal to 2.9 MPa. Due to the lack of the number of beams having different volumes and subjected to 4-point bending, only the two beams of Mazars [1984] and the smallest beam of Koide et al. [2000] ($L = 600$ mm) are chosen. Since the two compositions of concrete are close and the compressive strength is the same for the two compositions (f_c=30 MPa), the chosen reference volume is a splitting test having fc equal to 30 MPa. Thus, the Weibull modulus is computed using Rossi et al. [1994] formula and it is equal to 6.5. Figure 3.20 shows the predicted dispersion of the tensile strength for the three beams and their corresponding experimental mean value. It is shown that the analytical approach $WL2_A$ is capable of reproducing the mean and the standard deviation of the tensile strength for the case of 4-point bending.

3.3 Application to large structures

The analytical probabilistic approach is applied to the Mivelaz anchor (Mivelaz [1996]), the Malpasset Dam and nuclear containments vessels. For simplification purposes, the cross-section of the reinforced concrete structure is assumed to have been homogenized ($S = [1 + r(n-1)]\, hb$, where r, n, h and b are respectively the reinforcement ratio,

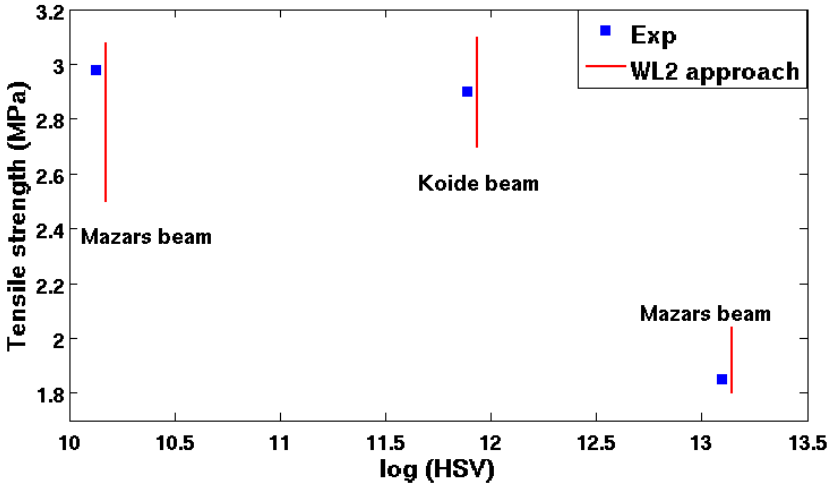

FIGURE 3.20: Evolution of the tensile strength as function of log HSV for the two beams of Mazars [1984] and the smallest beam of Koide et al. [2000] under 4-point bending loading.

the ratio between Young's modulus values for steel and concrete, and the cross-section height and thickness).

3.3.1 Mivelaz anchor

The Mivelaz [1996] anchor is a structure $0.42 \times 1 \times 5$ m^3 in dimension with a reinforcement ratio of 0.86% (see Figure 3.21); it shows a strength reduction of around 50% with respect to the measured tensile strength by means of a splitting test (Sellier and Millard [2014]). The anchor is subjected to uniform loading; the effective volume is defined using Equation 3.4 by considering a homogeneous section and a uniform stress.

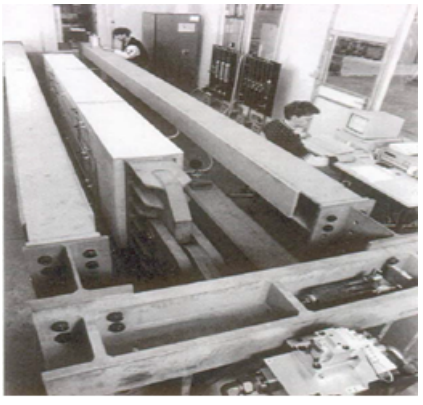

FIGURE 3.21: Mivelaz anchor (Mivelaz [1996]).

In order to apply the analytical size effect approach, the Weibull modulus has been estimated at 8 according to Equation 3.11, as based on the compressive strength of the

TABLE 3.9: Characteristics of Mivelaz anchor Mivelaz [1996]

h (m)	b (m)	L (m)	f_c (MPa)	r (%)	E_b (GPa)	$E_s(GPa)$
0.42	1	5	39.4	0.86	33.4	200

TABLE 3.10: Estimation of the tensile strength for the Mivelaz anchor

	Exp	$WL2_{EF}$ $(m = 10)$	$WL2_A$ $(m = 8)$
$\mu(f_t)$ (MPa)	1.48	1.48	1.46
$Std(f_t)$ (MPa)	-	-	0.1

anchor (Table 3.9). The chosen reference volume V_{ref} corresponds to that studied by Sellier and Millard [2014]: it is the loaded volume of a normalized specimen subjected to the splitting test, i.e. estimated equal to 3×10^{-4} m^3 (see Section 3.2.2.1). Equation 3.7 has been used. Since in this case the splitting test is the chosen reference volume, the coefficient of variation of Y_1 thus corresponds to a 10% coefficient of variation associated with f_c. Y_2 corresponds to a random variable on m on the order of 30% (Danzer et al. [2007]). l_I is set equal to 0.2 m. Table 3.10 lists the tensile strength of the Mivelaz anchor deduced from experimental tests and two numerical methods ($WL2_{EF}$ and $WL2_A$). It is shown that the analytical size effect method is capable of predicting tensile strength in both mean and dispersion.

3.3.2 Malpasset dam

Various reasons explain the collapse of this dam, including failure of igneous and metamorphic rocks as the foundation, very poor properties identified through geotechnical testing both in situ and in the lab, technical rules regarding lift not respected, and failure to execute an independent state control (Gagg [2014], Duffaut [2013]). Two additional causes for the Malpasset accident were the personalities involved in the design and construction of the dam and the rock in the wedge which disappeared from the left bank (Post and Bonazzi [1987]). Figure 3.22 represents an illustration of the Malpasset dam.

Moreover, at the time of construction, the size effect was not being studied for concrete. Bažant et al. [2007] demonstrated that the mean tolerable abutment displacement of the Malpasset Dam would today be about 50% of the value considered safe according to the standard design method in use during the early 1950's. It should be pointed out that in his studies, Bažant introduced 3 values for m, equal to $12, 24$ and 48. In this

FIGURE 3.22: Malpasset dam Gagg [2014].

dam, the concrete displays a compressive strength and Young's modulus of 32.5 MPa and 31.3 GPa, respectively. To apply the analytical probabilistic approach $WL2_A$, the dam is considered as a large fixed arch capable of being simplified to the case of a beam, of height equal 1 m, fixed at one end by a sliding hinge and at the other end by a fixed hinge and subjected to pure bending (see Figure 3.23) (Bažant et al. [2007]).

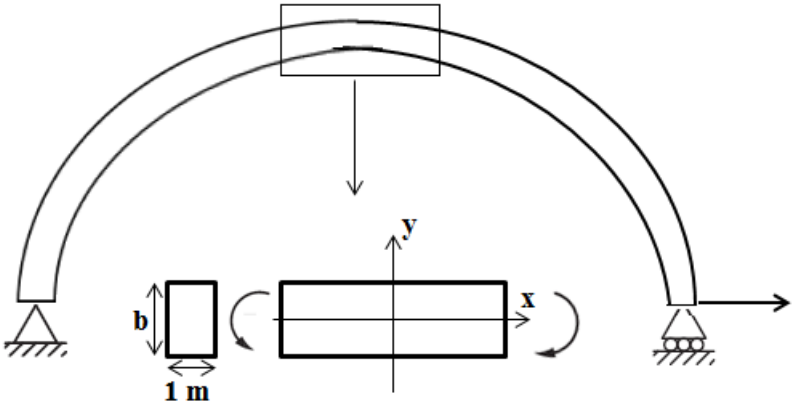

FIGURE 3.23: Sketch of the simplified studied dam.

This hypothesis models the collapse of the arch due to a horizontal abutment displacement. The stress field σ_I is therefore given by the following simplified equation:

$$\sigma_I(x) = \frac{2y}{b}\sigma_{max} \tag{3.22}$$

where $\sigma_{max} = (6M_{max})/b^2$, with M_{max} equal to the maximum bending moment and b is the thickness of the dam ($b = 6.78$ m, $0 < y < \frac{b}{2}$).

Due to the large dam dimensions compared to the scale length, the integral of the weighting function in the effective volume equation (Equation 3.4) can be simplified to: $\sqrt{2\pi}l_I$ (Ceos.fr [2009]). After these simplifications, the effective volume is deduced, for

TABLE 3.11: Estimation of the tensile strength for the Malpasset dam

	Bažant et al. [2007] ($m = 12$)	Bažant et al. [2007] ($m = 24$)	WL2$_A$ ($m = 7$)
$\mu(f_t)$ (MPa)	1.9	2.65	1.96
$Std(f_t)$ (MPa)	-	-	0.7

1 m height, using Equation 3.23:

$$V_E = \frac{\sqrt{2\pi} l_I b}{m+1} \tag{3.23}$$

As for the parameters of Equation 3.7, the Weibull modulus is estimated as equal to 7 according to Equation 3.11. The reference volume and uncertainties in this case are arbitrarily the same as in the case of the Mivelaz anchor. Table 3.11 summarizes the tensile strength of the Malpasset dam, as deduced from Bažant SEL and the analytical approach. Table 3.11 shows that numerical predictions are in good agreement with reference values for the tensile strength of the Malpasset dam, with less use of empirical parameters.

3.3.3 Application to a containment

The applicability of the proposed methodology to a large-scale civil engineering structure is evaluated using a simplified model of a containment having the same dimensions as the 1/3 mock-up of a double-wall containment building of a nuclear reactor (VeRcoRs). This mock-up is realized by EDF (electricity of France), in order to improve the understanding of aging phenomena in nuclear containments. It is constituted of reinforced and prestressed concrete. VeRcoRs is realized using two mock-ups, an internal and an external one. The internal part is constituted of different parts, the main ones being the raft, the gusset, the hatched area and the dome. It has a height of 22 m, an internal radius of 7.3 m, an external diameter of 7.7 m and a thickness of 40 cm. The casting of concrete was done by lifts. In total, the mock-up is constituted of 16 lifts of height around 1.2 m each. For each lift, three cylindrical concrete specimens of length 22 cm and diameter 11 cm was casted and tested using the splitting test method. Thus, in the following, the mechanical properties of concrete (f_c, E and $f_{ct,sp}$) correspond to the values obtained for each lift of VeRcoRs. Hence, the coefficient of variation of the

TABLE 3.12: Characteristics of the concrete at three lifts of VeRcoRs.

	f_c (MPa)	$f_{ct,sp}$ (MPa)	f_t (MPa)	Reduction coefficient (%)
Lift at the Gusset	38.5	4	2.24	38
Ordinary lift	48	4.78	3	30
Lift at the hatch	50	4.67	2.1	50

tensile strength f_t can be evaluated for each lift of the containment. The analytical approach $WL2_A$ is applied to two lifts situated each at the gusset part and the hatch area part and one ordinary lift (not presenting a severe heterogeneity as the hatched areas). Since the nuclear containment is subjected to an internal pressure, it can be simplified, as in the case of a dam, to a beam, having a height equal to 1 m, fixed at one end by a sliding hinge and at another end by a fixed hinge and subjected to pure bending (see Figure 3.23). However, since severe heterogeneities exist in VeRcoRs, the lift at the hatched area should be considered as subjected to the most severe loading, which is direct tension. Thus, in this case, the effective volume is reduced to the following relation:

$$V_E = \sqrt{2\pi} l_I b \tag{3.24}$$

where b is the thickness of the interior mock-up of VeRcoRs.

As a consequence, coefficient of reductions of the tensile strength are concluded for the three chosen lifts. Table 3.12 resumes the compressive strength f_c and the splitting tensile strength $f_{ct,sp}$ measured at the specimen scale, the tensile strength at the chosen lift and the corresponding coefficient of reduction. It is concluded that a coefficient of reduction varying between 30 and 50 % can be observed for large structures.

Finally, the aim of this study is to evaluate the coefficient for different volumes of containments. The concrete characteristics of the ordinary lift of VeRcoRs is considered and different thickness are taken into account (40, 60, 80 and 1.2 m). Figure 3.24 shows that a full scaled nuclear containment can reach a coefficient of reduction of the tensile strength f_t of 43 % from the original measured $f_{ct,sp}$ on splitting test. This reduction of the tensile strength should be taken into account in the construction, in order to avoid any rupture probability of the containments.

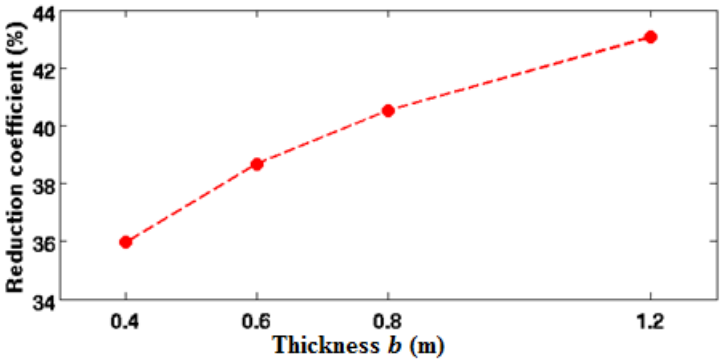

FIGURE 3.24: Evolution of the coefficient of reduction of f_t as function of the thickness b of a containment.

3.4 Conclusions

This work has consisted of developing an analytical probabilistic method, based on the WL2 size effect law (weakest link and localization, Sellier and Millard [2014]), to predict the failure of various series of concrete specimens and structures. This method offers the advantage of accounting for stress redistribution due to the attenuation of elastic stresses, depending on the distance to the weak zone. The originality of this study lies in the following proposals.

1. The identification of a scale length that is linked with the variability of concrete tensile strength, through the use of various experimental results, collected on different concrete specimens under uniaxial tension and 3-point bending loading. An interval for the scale length has been deduced ([0.1-0.3] m), thus confirming the estimations by Sellier and Millard [2014] and Bažant et al. [2007].Therefore a mean scale length equal to 20 cm and equivalent to a scale of fluctuation of 50 cm is concluded.

2. The propagation of uncertainties, such as the reference tensile strength $f_{t/ref}$ and Weibull modulus m. A sensitivity analysis has been conducted on m using four methods, applied to experimental data, allowing for deduction of a confidence interval on the order of 7-12. While this interval is consistent with the statistical variability of about 20-30%, which serves to deduce a size effect law in dispersion, it also tends to confirm the value of 12 used in various studies, instead of values of 24 or 48 for the same type of concrete.

3. The reference volume proposed in the analytical approach $WL2_A$ may be the smallest volume in the series, if dimensions are not on the order of aggregate diameter. For the case of larger structures however, the recommended reference volume of Sellier and Millard [2014] from the cylindrical splitting test can be used.

4. The prevision of a reduction coefficient associated to the tensile strength of concrete for large structures. The analytical probabilistic approach $WL2_A$ is applied to large structures such as Mivelaz anchor, the Malpasset dam and containments. This method proved to be capable of predicting the coefficient of reduction of the tensile strength f_t of the structure, using the cylindrical splitting test as a reference volume. These results are in agreement with Ceos.fr [2009] project, which proved the necessity of attributing a coefficient of reduction to the tensile strength of concrete, when dealing with large structures.

In continuation, the next chapter studies the effect of accounting for the spatial variability of concrete in FE models using random fields and thus, the possible relations between the identified scale length and the autocorrelation length of discretized random fields generated on the input mechanical properties of concrete (f_t, E) that could be used in FE structural models.

Chapter 4

Accounting for size effect in FE models of RC structures

Size effect is a relevant phenomenon influencing cracking in large massive Reinforced Concrete (RC) structures. It is important, then, to consider this effect in Finite Element (FE) models. Moreover, Chapter 3 enhanced the importance of accounting for the variability of the tensile strength in order to reproduce the size effects phenomena and mainly the statistic one. Thus, modeling spatial variability of tensile strength in FE models can be a method to account for size effect on f_t. Hence, this chapter aims to propose a Stochastic Finite Element (SFE) method, based on the generation of realizations of discretized random fields. First, the appropriate autocorrelation characteristics of the random field are chosen based on experimental results of concrete beam series under 4-point bending loading (Koide et al. [2000]). Secondly, under these hypotheses, the method is applied using SFE simulations to series of concrete beams under 4-point bending loading (Mazars [1984]) and 3-point bending loading (Hoover and Bažant [2014a]) and to an anchor under uniaxial tension (Clement [1987]). Eventually, the capability of reproducing the size effect on the tensile strength using SFE method is discussed.
Moreover, since this thesis is a part of MACENA project aiming to study the behavior of a massive RC structure, an application to the simplified model of a concrete containment is done.

4.1 Proposed method

One of the main objective of the thesis is to predict the beginning of cracking in RC structures and to estimate, using FE models, the position of the first crack and the spacing between the cracks. Moreover, a SFE method that accounts for the size effect in large massive structures is developed. This method consists on modeling the spatial variability of the tensile strength in concrete by defining it using discretized random field in FE models. Therefore, the method is summarized by the following steps:

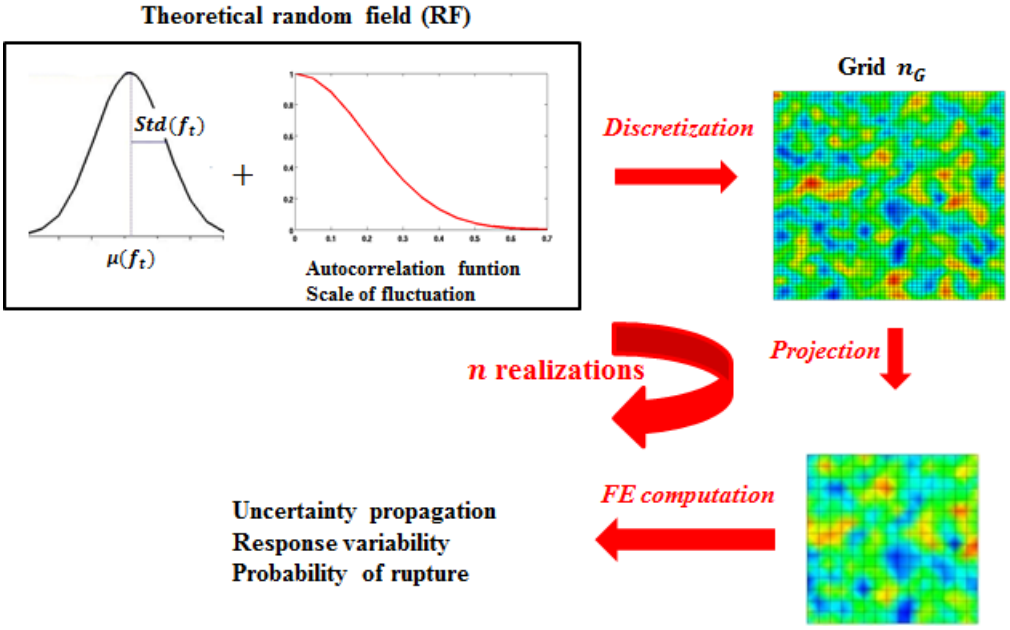

FIGURE 4.1: Sketch for the proposed SFE method.

- prepare a reference deterministic FE model;
- identify the theoretical random field that characterizes f_t;
- generate realizations of discretized random fields on a 2D or 3D grid;
- project the discretized random field realizations on the FE mesh.

Figure 4.1 presents a sketch for the different steps needed to define the discretized random field. Each step of the method is presented in the following sections.

4.1.1 Reference deterministic FE model

The FE model is built at different scales using the FE code Cast3m (CEA [2015]). The structures are modeled in 2D under plane stresses or in 3D. The concrete behavior is modeled using Mazars isotropic damage model (Mazars [1986]), which despite its simplicity is known for its efficiency to describe the concrete behavior and a non-local method is used: the stress-based regularization method (Giry et al. [2011]). Deterministic FE calculations, at different scales, are first done in order to best fit Mazars parameters with the experimental results.

Mazars model has been widely used to represent an elastic isotropic damage behavior (Mazars [1986]). This model is characterized by a single damage scalar D and presents the advantage of distinguishing the tensile and compressive damages. Thus, the load surface is controlled by a state variable U and an equivalent strain $\varepsilon_{eq} = \sqrt{\sum_{i=1}^{3} \langle \varepsilon_i \rangle_+^2}$, where $\langle \varepsilon_i \rangle_+$ are the positive parts of the principal strains $(\varepsilon_1, \varepsilon_2, \varepsilon_3)$, as shown in the following Equation:

$$f(\varepsilon_{eq}, U) = \varepsilon_{eq} - U \tag{4.1}$$

The variable U is initially taken equal to the strain threshold ε_{D0} (defined as f_t/E in the model). Then, during loading, it is equal to the maximum between the equivalent strain and the damage threshold. The asymmetry of the mechanical response of the material between tension and compression is taken into account using the damage variable D, which represents a combination of traction damage D_t and compression damage D_c ($D = \alpha_c D_c + \alpha_t D_t$). Since, structures failing due to tension are modeled, in this thesis, the estimation of the traction damage is a main interest (Equation 4.2).

$$D_t = 1 - \frac{\varepsilon_{D0}(1 - A_t)}{U} - \frac{A_t}{\exp(B_t(U - \varepsilon_{D0}))} \tag{4.2}$$

where ε_{D0}, A_t and B_t are parameters that should be identified using experimental results. Furthermore, the Stress-Based Non-Local (SBNL) method is used. Giry et al. [2011] developed this non-local regularization method, that consists on taking into account the stress state in the medium by averaging a mechanical quantity in its neighborhood using a weight function, defined in Equation 4.3.

$$\phi(x - s) = \exp\left(-\left(\frac{2||x - s||}{l_c \rho(x, \sigma_{prin}(s))}\right)^2\right) \tag{4.3}$$

where $\rho\left(x, \sigma_{prin}(s)\right)$ is equal to the radial coordinate of the ellipsoid associated with the stress state of the point located at s in the direction $(x - s)$ and l_c is an internal length usually taken equal to 3 times the maximum aggregate (the size of FPZ).
In this manner, the SBNL approach allows describing the progressive decrease of nonlocal interactions across the FPZ during failure. Thus, damage and strain, at failure, are well localized. Results are then supposed to be mesh independent.
Once the deterministic FE model is built, the definition of the discretized random fields can start.

4.1.2 Identification of the theoretical random field

First, the theoretical random field $V(x)$ ($x \in \Omega$, where Ω is an open set of R^d ($d = 1, 2, 3$) describing the geometry), that is considered as the key point to build a SFE model, should be defined (Baroth [2005]). The random field $V(x)$ is completely described by its mean μ, variance Std^2 and covariance matrix ($C_{VV}(x, x') = Std(x)Std(x')\rho_v(x, x')$, where ρ_v is an autocorrelation function). The description of the random field is detailed in the section 2.3.2. The SFE method is characterized by defining the spatial variability of the tensile strength f_t of the concrete, thus a random field modeling f_t. As a consequence, for the first part of the method, the mean and the standard deviation of f_t should be determined. Moreover, an appropriate autocorrelation function and autocorrelation length should be defined. The modeling of the tensile strength of concrete f_t requires the use of univariate multidimensional and stationary fields. This means that the random field takes values in a countable subset ($x_1, x_2... \in \mathrm{R}^d$, where d is higher than 1). Moreover, it does not depend on time.
Usually, the value of the tensile strength f_{ctm}, used in the FE models, is taken equal to 90 % of the value of the splitting tensile strength measured on a cylindrical specimen $f_{ct,sp}$ (CEN [2005]). However, in Chapter 3, the decrease of the measured f_{ctm} when dealing with large structures is highlighted and an analytical approach allowing to estimate the reduction of this value is developed. Thus, the influence of attributing or not a coefficient of reduction on the direct tensile strength measured on laboratory specimen, in FE models, is studied in the following sections. The reduced tensile strength f_t is evaluated using the analytical probabilistic approach WL2, denoted $\mathrm{WL2}_A$.
As for the coefficient of variation of the tensile strength $CV(f_t)$, the experimentally estimated value is directly used.

In addition, for the definition of the theoretical random field $V(x)$, the use of autocorrelation functions is required to model the spatial variability of the tensile strength f_t. Various types of autocorrelation functions and different associated autocorrelation lengths (a, b or c) exist in the literature (Carmeliet and de Borst [1995], De Larrard et al. [2010], Colliat et al. [2007] and Giry [2011]). The main autocorrelation functions are:

- Gaussian autocorrelation function (Type A): $\rho_A(x) = \exp\left(-\left(\frac{x}{a}\right)^2\right)$
- Exponential autocorrelation function (Type B): $\rho_B(x) = \exp\left(-\left(\frac{x}{b}\right)\right)$
- Sinusoidal autocorrelation function (Type C): $\rho_C(x) = \frac{\sin\left(-\left(\frac{x}{c}\right)\right)}{\left(-\left(\frac{x}{c}\right)\right)}$

Therefore, we aim to choose the autocorrelation function which fits best with the experimental results.

In order to compare the different autocorrelation functions, an equivalence between their lengths should be defined. The scale of fluctuation υ criteria (see Equation 2.32) can be used. For example, Figure 4.2 allows to compare the shapes of the three types of

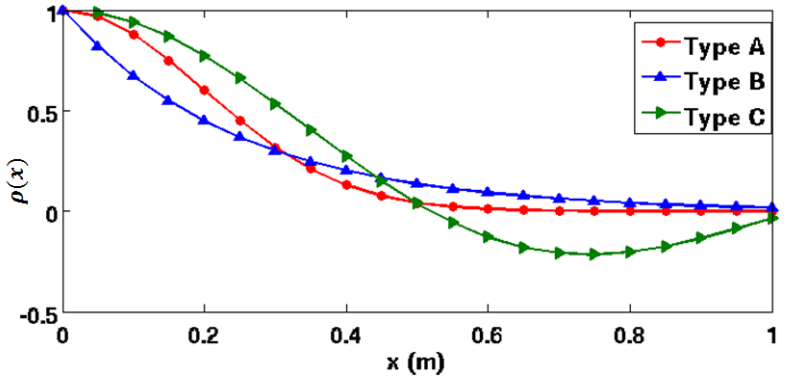

FIGURE 4.2: Autocorrelation functions (scale of fluctuation $\upsilon = 50$ cm).

autocorrelation functions, with a constant scale of fluctuation (arbitrarily $\upsilon = 50$ cm). This figure shows that Type B autocorrelation function, used in most of SFE applications, suffers from its lack of smoothness and the need of more refined mesh (Sudret [2007]). Thus, it is not used in the following work. Hence, in the following, Type A and Type C autocorrelation functions are compared. Also, Gaussian and log-normal distributions are discussed. Table 4.1 gives the values of the Gaussian and sinusoidal autocorrelation lengths, respectively a and c, corresponding to a scale of fluctuation equal to 50 cm. Indeed, this value of scale of fluctuation has been selected in Chapter

3 to account for the spatial variability of the tensile strength. Comparisons with other values of autocorrelation length are discussed in the following section.

TABLE 4.1: Estimation of the Gaussian and sinusoidal autocorrelation lengths equivalent to a scale of fluctuation equal to 50 cm.

Function	Scale of fluctuation ($\upsilon = 50$ cm)	Autocorrelation length
Type A	$\sqrt{\pi} \times a$	$a = 28$ cm
Type C	$\pi \times c$	$c = 16$ cm

4.1.3 Discretized random field

Secondly, the theoretical random field representing the spatial randomness of the tensile strength is spatially discretized on a 2D or 3D grid with n_G nodes (Equation 4.4). A discretization method consists of approximating the original random field $V(x)$ by an approximated finite set of random variables $\tilde{V}_G(x)$ gathered in a random vector $\{V_{G_k}, k = 1, \ldots, n_G\}$:

$$V(x) \overset{Discretization}{\rightarrow} \tilde{V}_G(x) = \{V_{G_k}, k = 1, \ldots, n_G\} \tag{4.4}$$

Covariance function $C_{VV}(x, x')$ is transformed to a covariance matrix C_{ij}, using Cholesky decomposition, which is applied to the covariance matrix. This covariance matrix, given by the Equation 4.5, is an assembly of the values of the covariance function computed between two points i and j of the discretized random field, whose positions are respectively x_i and x_j.

$$C_{VV}(x, x') \overset{Discretization}{\rightarrow} C_{ij} = Std^2.\rho_v\left(x_i - x_j\right) \tag{4.5}$$

Briefly, Cholesky decomposition consists on expressing the vector $\tilde{V}_G(x)$ as a sum of the expected mean value of the random field and a linear combination of standard Gaussian random variables $Y = \{Y_k, k = 1, \ldots, n_G\}$, having a unit variance and zero mean:

$$\tilde{V}_G(x) = \mu + BY \tag{4.6}$$

where B is a square matrix such as $C_{ij} = BB^T$.

This methodology can be seen as a simplification of the Karhunen-Loève decomposition used in some applications as in De Larrard et al. [2010], Colliat et al. [2007] and

Vořechovskỳ [2007]. This method is detailed in appendix B. Moreover, Cholesky decomposition method is already implemented in Cast3m (CEA [2015]).

An advantage of the Cholesky decomposition is the capability of generating also log-normal random fields. A way to generate log-normal random fields is done using two steps: since in Equation 4.6, the random variables Y_k are stochastically independent, first the discretization of the random field can be done using the decomposition of Cholesky and a Gaussian random vector of independent coefficients. Then, the Gaussian realization is transformed into a log-normal one using the following relation: $\tilde{K}_G = \exp\left(\tilde{V}_G\right)$. It is well known that a disadvantage of the point discretization methods is their dependency on the density of the studied grid, more precisely the dependency between the autocorrelation length (a or c) and the grid density (Li and Der Kiureghian [1993]). In order to avoid the error due to the choice of the density of the random field grid, this latter is supposed equal at least to $a/2$ or $c/2$ depending on the chosen type of the autocorrelation function, which means that a smaller autocorrelation length requires a refined grid density.

4.1.4 Projection of the discretized realization on the FE mesh

The concept of projection method is highlighted, hereafter. The discretized random field defined on a 2D or 3D grid is projected onto the different FE meshes, built for the deterministic case (e. g. beams at different scales). Thus, the dependency between the FE mesh and the autocorrelation length is eliminated. The number of nodes in the FE mesh is denoted n_{FE}. This projection procedure prevents the problem of defining boundary conditions or considering boundary layer effects. In addition, the FE mesh density n_{FE} does not depend directly on the autocorrelation length, since this dependency is considered on the grid in which the discretization is done.

$$\tilde{V}_G(x) = \{V_{G_k}, k = 1, \ldots, n_G\} \overset{Projection}{\rightarrow} \tilde{V}_{FE}(x) = \left\{V_{FE_p}, p = 1, \ldots, n_{FE}\right\} \tag{4.7}$$

As to better explain the concept of projection of discretized random field, an example is done on a square FE model of dimensions 100×100 cm^2. The objective is to estimate the error on the mean and standard deviation of the random field values between the grid nodes and the FE mesh nodes. Therefore, the tensile strength is defined arbitrary by a theoretical random field with a mean of 2.9 MPa, a standard deviation of 0.29 MPa,

a Gaussian autocorrelation function (Type A) and an autocorrelation length equal to 28 cm. Then, the random field is discretized on a grid of dimensions 120×120 cm^2 and a density equal to 10 cm ($< 28/2$ cm). Finally, the discretized random field is projected on the FE mesh. Different densities are chosen for the FE mesh. The coefficient N presents the ratio between the grid density d_G and the FE mesh density d_{FE} ($N = \frac{d_G}{d_{FE}}$). $\mu(\tilde{V}_G)$ and $Std(\tilde{V}_G)$ represent respectively the mean and the standard deviation of the random field discretized on the grid. $\mu(\tilde{V}_{FE})$ and $Std(\tilde{V}_{FE})$ define respectively the mean and the standard deviation of the projected discretized random field on the FE mesh. Thus, the error on the mean and standard deviation of the random field between the grid and the FE mesh are estimated using the following equations:

$$Err(\mu) = \frac{\mu(\tilde{V}_G) - \mu(\tilde{V}_{FE})}{\mu(\tilde{V}_G)} \times 100 \tag{4.8}$$

$$Err(Std) = \frac{Std(\tilde{V}_G) - Std(\tilde{V}_{FE})}{Std(\tilde{V}_G)} \times 100 \tag{4.9}$$

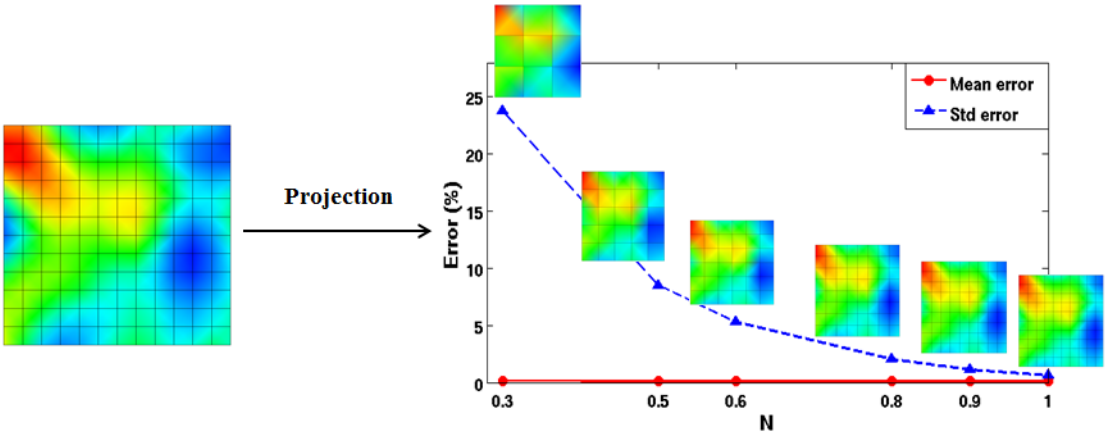

FIGURE 4.3: The discretized random field on a grid (left) and the evolutions of the error on the mean and standard deviation for different values of N.

Figure 4.3 displays one realization of the discretized random field on the grid and its projection on the different FE meshes. Also, the evolutions of the error on the mean and on the standard deviation for different values of N are plotted. In this case, that the projection method keeps the properties of the discretized random field from a coefficient N equal to 0.7 (error on the mean and the standard deviation, respectively equal to 0 % and 4 %).

4.2 Reference SFE model

The previously developed SFE method consists of generating realizations of discretized random fields on a 2D or 3D grid, which will be projected, then, to the FE mesh of the studied structure. First, the investigation of the role of spatial variability of the tensile strength on the size effect is done on series of 4-point bending beams (Koide et al. [2000]), having the same geometry, the same section ($S = 100 \times 100$ mm^2), the same shear span $L_s = 200$ mm and scaled along bending length ($L_b = 200 - 400 - 600$ mm) (see Appendix A). The different parameters of the random field (covariance function and probability distribution law) are characterized using these series of beams. These series are chosen, since experimental CDFs of the rupture force, for each beam, are provided. Thus, the objective is to compare the results obtained from SFE simulations and the experimental obtained results.

4.2.1 Reference FE model

As mentioned before, Koide et al. [2000] series of beams are chosen for the characterization of the discretized random field. Deterministic FE models of the three beams are considered as the reference FE models. These beams are modeled in 2D under the hypothesis of plane stresses. For each beam, quadrilateral mesh of size 8 mm is used. The same concrete having a compressive strength f_c, at 28 days, of 30 MPa is used for the three beams. The Mazars isotropic damage model Mazars [1986] is applied to concrete. Mazars parameters A_T and B_T are inspired from Dufour et al. [2012], they are equal to 0.9 and 20×10^3 respectively. However, the deterministic simulations are not able to reproduce the experimental decline of the rupture force as the length of the beam increases even after trying to fit A_T and B_T (see Figure 4.4). This error can be linked to the randomness of the concrete parameters (statistical size effect). Moreover, using deterministic computation, two symmetrical cracks are formed, unlike the experimental results where only one crack appears first (see Figure 4.5). Thus, the tensile strength is chosen to be modeled as a random field, in the following section.

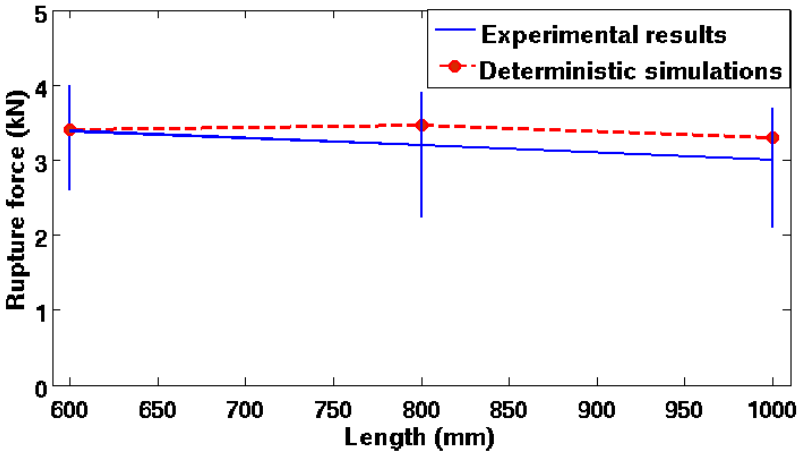

FIGURE 4.4: Evolution of the rupture force obtained by experimental results (Koide et al. [2000]) and deterministic simulations.

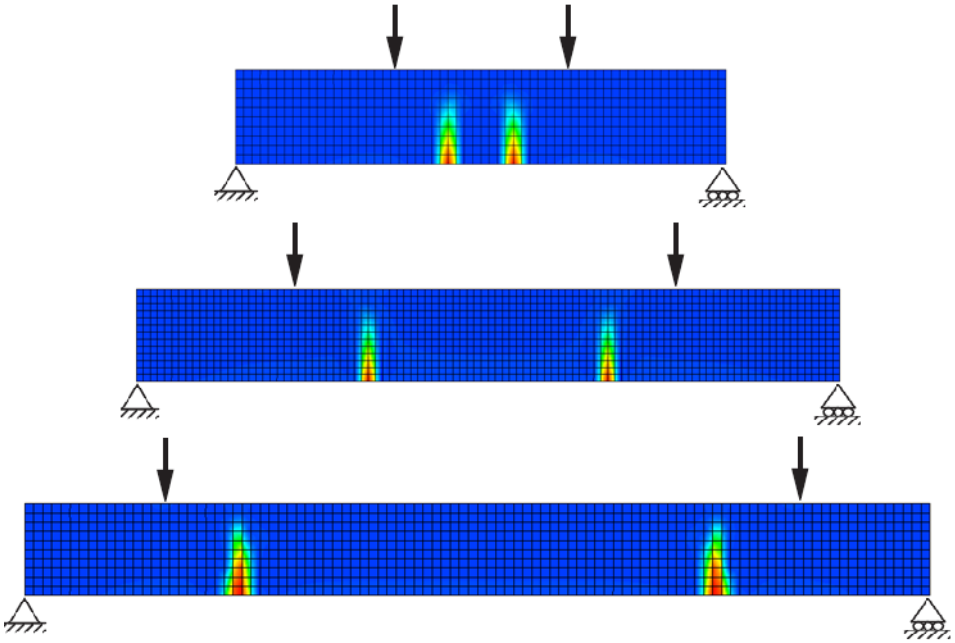

FIGURE 4.5: Equivalent strain evolution obtained for each beam.

4.2.2 Influence of the autocorrelation parameters

By applying the $WL2_A$ approach, the mean of the tensile strength $\mu(f_t)$ is found constant for the three beams and equal to 2.9 MPa, which corresponds to 90% of the splitting tensile strength calculated using Equation 3.20. Therefore, the tensile strength of these series of beams are not affected by a coefficient of reduction. Furthermore, a coefficient of variation of 14 % is experimentally observed by Koide et al. [2000]. Thus, the same random field is considered for the three beams ($\mu(f_t)$ =2.9 MPa and $CV(f_t)$ =14 %). Although tensile strength is not affected by the size effect phenomenon, this concrete series

is chosen since it provides experimental CDFs of the rupture force for each beam (based on around 50 tests for each beam). Therefore, comparison with experimental results can be done to better characterize this random field. The influence of the autocorrelation length, the autocorrelation function and the probability law are, then, studied.

4.2.2.1 Influence of the autocorrelation length

First, the choice of the autocorrelation length is studied. In this study, Gaussian discretized random fields are generated on the tensile strength with type A autocorrelation function. Four possible autocorrelation lengths a are studied. The first chosen autocorrelation length corresponds to the scale of fluctuation of 50 cm, which is equivalent to the 20 cm scale length deduced in the $WL2_A$ approach. This autocorrelation length a is equal to 28 cm (see Table 4.1). Also, two autocorrelation lengths a equal to 1 and 8 cm are chosen. The 1 cm autocorrelation length is used by Giry [2011] for the definition of random fields in cylindrical tensile specimens. As for the 8 cm autocorrelation length, it is adopted by Vořechovskỳ [2007] for the definition of random fields in dog-bone specimens under uniaxial tension. Finally, Sellier and Millard [2014] deduced a 40 cm length that models the variability of concrete. Thus, the possibility of using this length as an autocorrelation length in random field generation is studied. It is worth noting that the grid density changes from one autocorrelation to another and it is equal to $a/2$. Figure

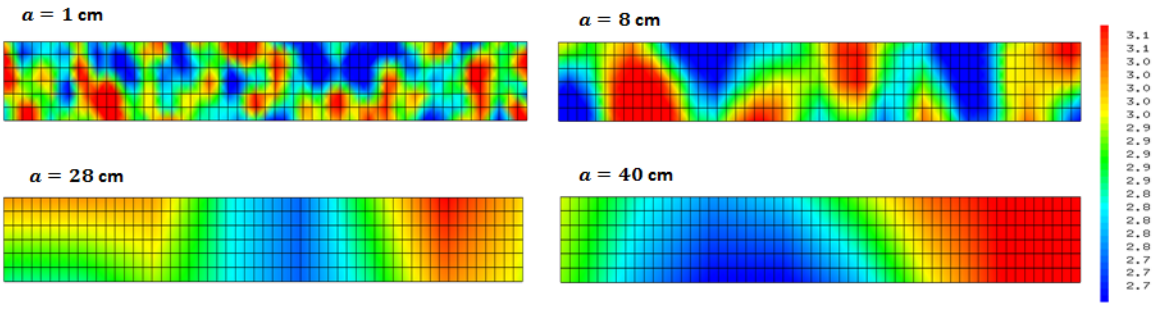

FIGURE 4.6: Examples of random field realizations on f_t obtained using four different autocorrelation lengths a and corresponding to the third beam.

4.6 presents four realizations of discretized random fields, on the FE model, with different autocorrelation lengths a, corresponding to the third beam. As seen in this figure, the FE mesh density is kept constant and equal to 8 mm. 30 random fields realizations of the tensile strength are generated for each autocorrelation length to ensure the convergence of the statistics (mean, standard deviation and coefficient of variation). Figure

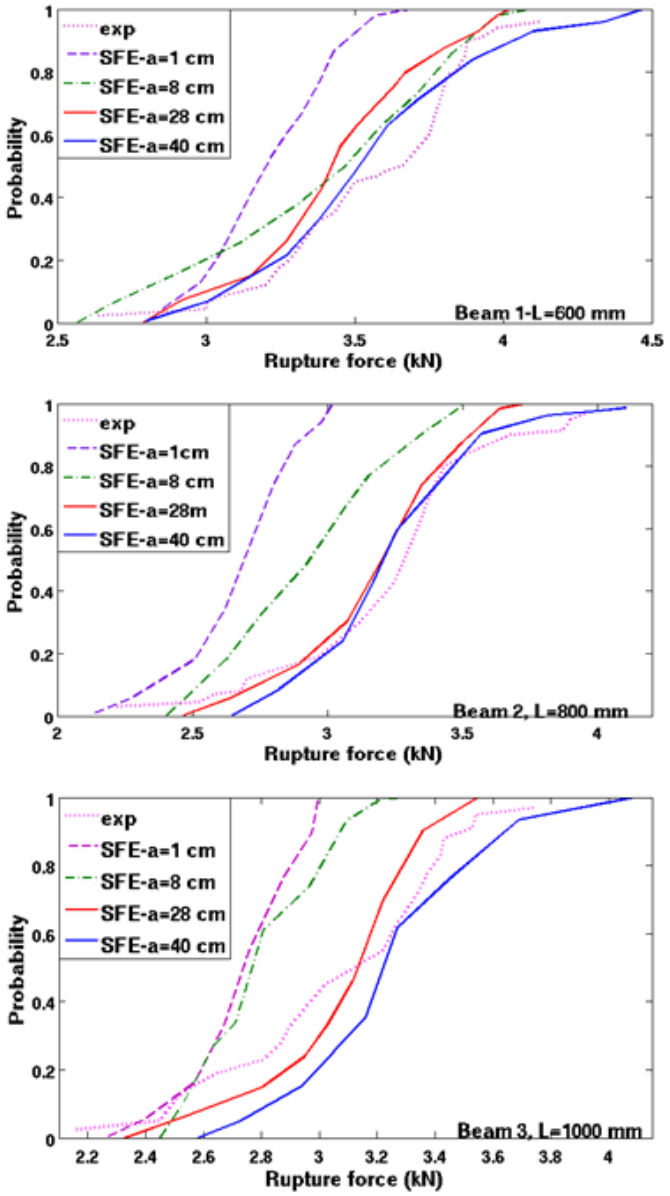

FIGURE 4.7: Evolution of the experimental CDFs (Koide et al. [2000]) and the numerical ones obtained using various autocorrelation lengths ($a = 1, 8, 28$ and 40 cm) for the three beams.

4.7 presents the CDFs corresponding to the numerical and experimental results for the three beams. It shows that, for small structures, the choice of the autocorrelation length is insignificant and more precisely, the use of discretized random field is unnecessary. By studying the influence of the autocorrelation length on the output of interest (rupture force) in the two larger beams, it is shown first that the 1 cm and 8 cm autocorrelation lengths tend to decrease the mean of the rupture force with increasing structural volume. This result seems to show that the used discretized random field does not aim to reproduce the heterogeneities of concrete in terms of aggregates. Also, the 28 cm and

40 cm autocorrelation lengths seems to give numerical results closer to the experimental ones, which can be related to the physical meaning of the random field, aiming to model the variability of the tensile strength. Therefore, in order to be in agreement with the result obtained in Chapter 3, the autocorrelation length $a = 28$ cm can be generated for the three volumes. Hence, the weighting function used in the analytical approach $\mathrm{WL2}_A$ and autocorrelation function of the random field used in SFE method account both for the spatial variability of f_t. $\mathrm{WL2}_A$ method leads to an average size effect, whereas the random field generation is related to crack position.

4.2.2.2 Influence of the autocorrelation function

The influence of the autocorrelation function is also studied. Only types A and C are considered. Comparisons are done on the third beam. Thus, 30 realizations of discretized autocorrelated random fields are generated using type C autocorrelation function. The previous section shows that $a = 28$ cm and equivalent to a scale of fluctuation of 50 cm (see Table 4.1) seems to be accurate to model the spatial variability of the tensile strength. Thus, for this scale of fluctuation, an equivalent parameter c equal to 16 cm is estimated for the type C autocorrelation function. Figures 4.8 and 4.9 show two realizations of discretized random fields, using respectively Type A and Type C autocorrelation functions and their corresponding fracture position. Unlike the deterministic case, using SFE method, the first crack happens at a weak point in the sense of the variability of the mechanical properties of concrete, thus only one crack appears at the peak load. Figure 4.10 illustrates the evolution of the experimental and numerical CDFs corresponding to both types A and C. From this figure, a negligible effect on the rupture force is observed.

Thus, to better understand the influence of the autocorrelation functions, the errors

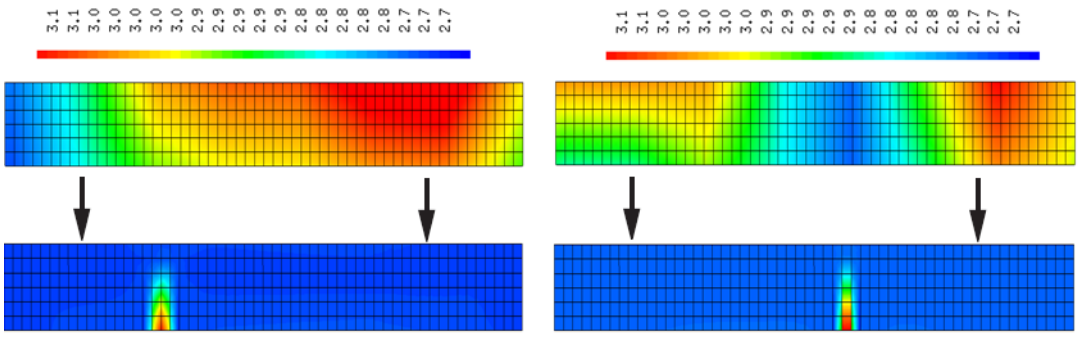

FIGURE 4.8: Two realizations of random field on f_t on the third beam, using type A autocorrelation function and their corresponding fracture positions.

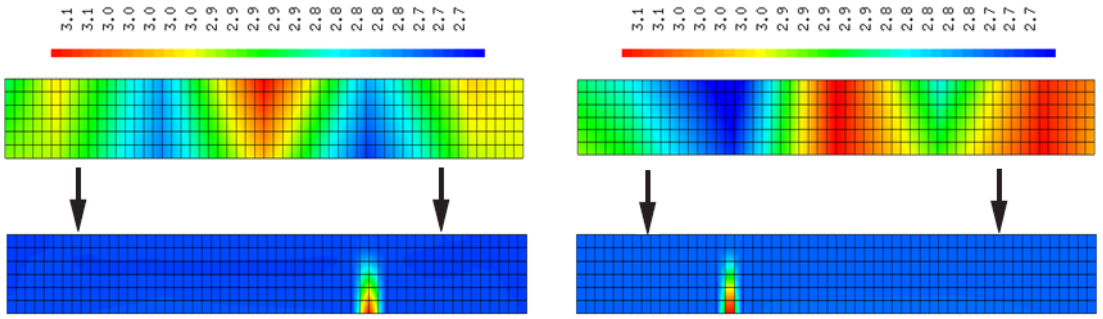

FIGURE 4.9: Two realizations of random field on f_t on the third beam, using type C autocorrelation function and their corresponding fracture positions.

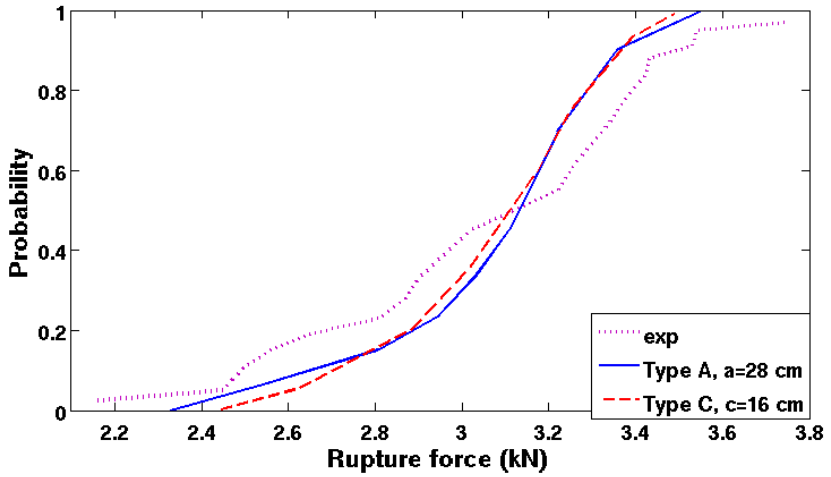

FIGURE 4.10: Evolution of the experimental and numerical CDFs obtained for type A and C autocorrelation functions for the largest beam (with $v = 50$ cm).

between the mean and the standard deviation of the tensile strength estimated on the grid and the FE mesh are evaluated. Therefore, errors on the mean and the standard deviation are estimated, respectively, using Equations 4.8 and 4.9.

Thus, for the type A autocorrelation function, the errors on both mean and standard deviation are respectively in the order of 0.5 % and 3 %. As for the type C autocorrelation function, the error on the mean remains low with a value of 0.5 %, but the error on the standard deviation increases to around 10 %.

Another criteria to compare the two autocorrelation functions is the number of realizations which provides the numerical convergence of the SFE simulations, i.e. the number of realizations that provides satisfying relative errors on the mean and the standard deviation of the output of interest (rupture force). Figure 4.11 shows the evolutions of the relative error on the mean and the standard deviation of the rupture force as functions of the number of realizations for both types of autocorrelation functions. For type A, the relative error on the mean and the standard deviation of the rupture force slightly

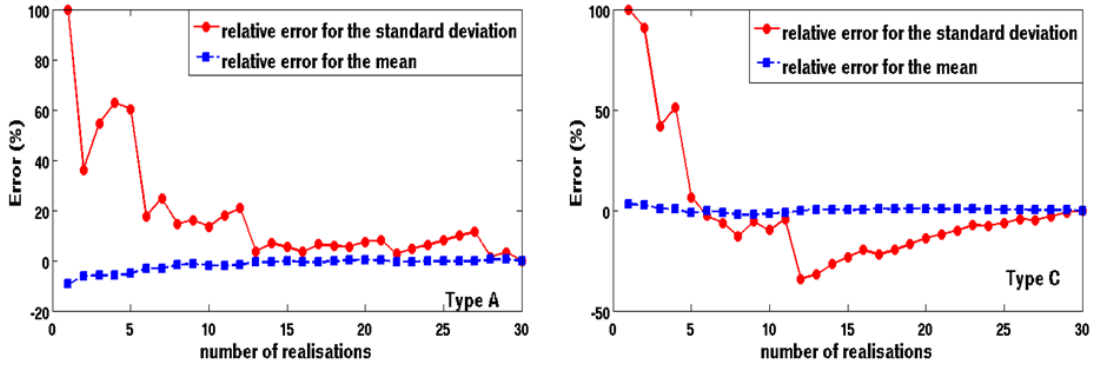

FIGURE 4.11: Evolution of the relative error on the mean and the standard deviation of the rupture force as function of the number of realization for type A autocorrelation function (left) and type C autocorrelation function (right).

decrease from around 15 realizations, which seem to be enough to ensure the numerical convergence of the SFE simulations. However, for type C, more than 25 realizations are necessary to reproduce the convergence on the statistics of the rupture force. It has been checked that using other series of 30 simulations th same relative error evolutions are obtained.

Therefore, the type A autocorrelation function is conserved due to the negligible errors found on the mean and the standard deviation of the projected discretized random field on the FE mesh and the lower number of realizations required to ensure the numerical convergence.

4.2.2.3 Influence of the probability law

One can consider also the log-normal field $\tilde{K}_G$ ($\tilde{K}_G = \exp\left(\tilde{V}_G\right)$). Equations 4.10 and 4.11 provide respectively the mean and the standard deviation of the Gaussian distributions as function of the mean and the coefficient of variation of the log-normal distributions (De Larrard et al. [2010]). In these equations, $\mu(\tilde{V}_G)$ and $Std(\tilde{V}_G)$ are the expected mean value and the standard deviation of the Gaussian field. $\mu(\tilde{K}_G)$, $Std(\tilde{K}_G)$ and $CV(\tilde{K}_G)$ are the mean, the standard deviation and the coefficient of variation for the log-normal field.

$$\mu(\tilde{V}_G) = \ln\left(\frac{\mu(\tilde{K}_G)}{\sqrt{1 + CV(\tilde{K}_G)^2}}\right) \tag{4.10}$$

$$Std(\tilde{V}_G)^2 = \ln\left(1 + CV_{\tilde{K}_G}^2\right) \tag{4.11}$$

In addition, a relation between the autocorrelation length of the Gaussian distribution $a_{\tilde{V}_G}$ and the autocorrelation length of the log-normal distribution $a_{\tilde{K}_G}$ is defined in Equation 4.12 (De Larrard et al. [2010]).

$$a_{\tilde{V}_G} = -\left(\ln\left(\frac{1}{Std(\tilde{V}_G)^2}\left(\ln\left(\frac{Std(\tilde{K}_G)^2}{\mu(\tilde{K}_G)^2}\exp\left(-\frac{1}{a^2_{\tilde{K}_G}}\right)+1\right)\right)\right)\right)^{-\frac{1}{2}} \tag{4.12}$$

By applying this equation, the difference between the autocorrelation lengths of the Gaussian distribution and the log-normal distribution is insignificant. Thus, $a = 28$ cm is taken for both Gaussian and log-normal distribution. Therefore, the log-normal

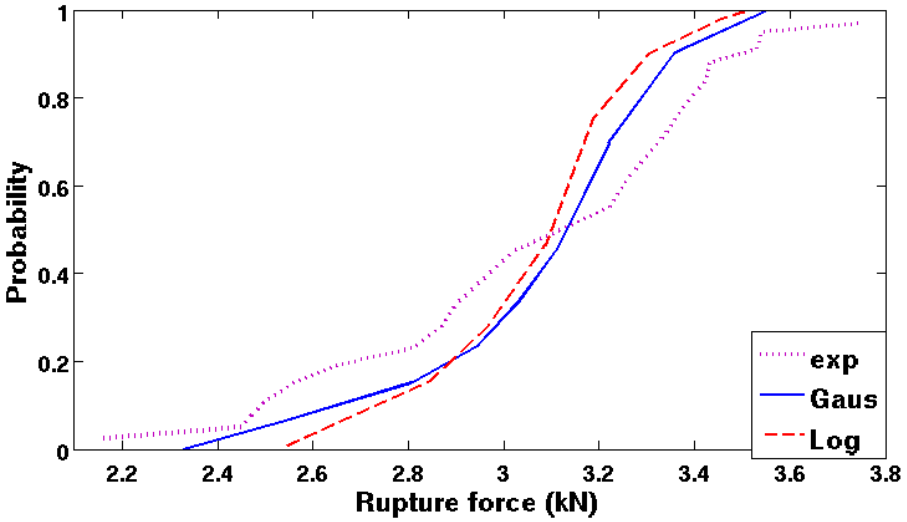

FIGURE 4.12: Evolution of the experimental and numerical CDFs obtained for Gaussian and log-normal distributions on the third beam.

field is applied to the third beam with an autocorrelation function of type A and an autocorrelation length a equal to 28 cm. Also, 30 realizations of random fields on f_t are used for the mechanical FE calculation. Figure 4.12 shows the evolution of the experimental and numerical calculations corresponding to both Gaussian and log-normal distributions. It is highlighted that the choice of the probability law seems to show a negligible effect on the rupture force. For the sake of simplicity, the Gaussian law is arbitrarily chosen in the following.

4.2.3 Statistical size effect

The idea of this study is, mainly, to test if the modelisation of the spatial variability of the tensile strength in FE models is a mean to characterize the size effect. After

choosing to characterize the discretized random field using a Gaussian law with the type A autocorrelation function and a scale of fluctuation of 50 cm, a mean and a standard deviation of the rupture strength can be deduced from the 30 SFE realizations conducted on each beam. Figure 4.13 shows that the SFE simulations are able to reproduce the experimental values of the rupture force on the contrary of the deterministic simulations. SFE simulations can, also, provide CDFs of the rupture strength for the three beams.

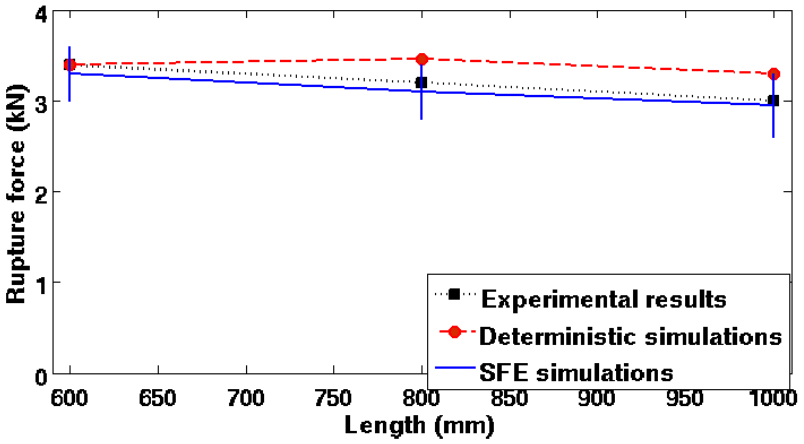

FIGURE 4.13: Size effect in the three 4-point bending beams from experimental results, deterministic and SFE simulations. The vertical bars correspond to the mean ± the standard deviation of the rupture force, obtained from the random field simulations.

Moreover, the analytical approach $WL2_A$ is a mean to plot CDFs of the rupture strength, using Equation 3.3. In order to apply this equation, a scale length l_I equal to 20 cm and a parameter m equal to 8.5 (using Equation 3.12) are chosen. The analytical CDFs of the rupture strength for the three beams are plotted and compared with the obtained one from the SFE simulations (see Figure 4.14). The SFE simulations show a slight size effect on the rupture strength as the analytical approach $WL2_A$ do not show any size effect on the tensile strength. It is worth noting that only a slight size effect on the rupture force is experimentally observed on this beam series, which may be related to the constant shear span considered for the three beams. Nevertheless, both methods are able to reproduce the experimental CDFs for this beam series. Also, SFE method shows to be a solution to model size effect in FE models.

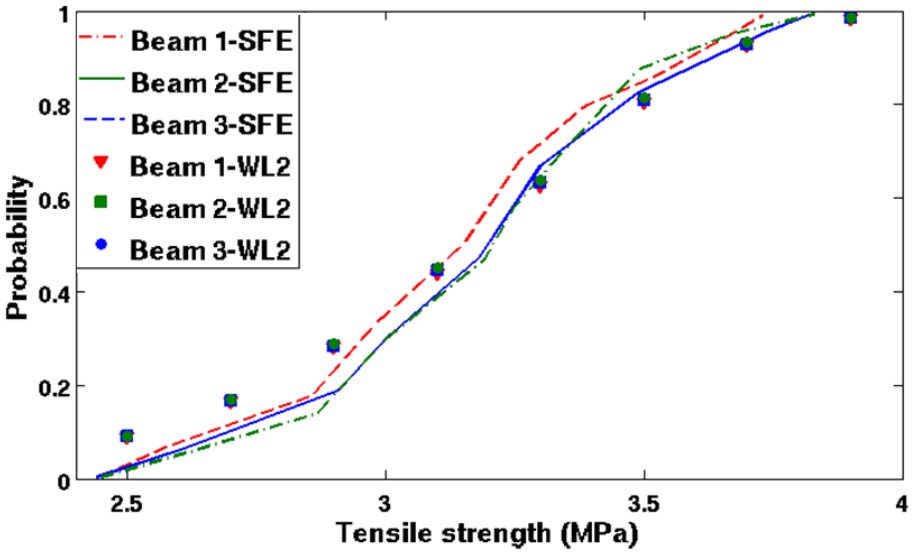

FIGURE 4.14: CDFs of the 3 beams obtained from the SFE simulations and the analytical approach of WL2 ($WL2_A$).

4.3 Application to series of concrete structures

After the study of the influence of the autocorrelation function and the probability law of the random field on the output parameters, Gaussian autocorrelated random fields with a scale of fluctuation of 50 cm seem to accurately model the spatial variability of the tensile strength of concrete. Thus, SFE method using discretized random fields needs to be validated for different types of structures under different loading cases. Moreover, in order to validate the capability of SFE method using discretized random fields to reproduce the size effect, it is applied to series of beams having the same geometry and different volumes. Briefly, the method is applied to Mazars [1984] series of beams under 4-point bending loading and Hoover and Bažant [2014a] series of beams under 3-point bending loading.

4.3.1 Application to series of beams under 4-point bending

Due to the lack of the investigation on the size effect of concrete beams under 4-point bending loading, only two beams, with different sizes, were found in Mazars [1984]. The first beam has a section equal to 100×100 mm^2, a length equal to 300 mm and a shear span equal to 100 mm. As for the second beam, it has a section equal to 150×220 mm^2, a length equal to 1400 mm and a shear span equal to 400 mm. Both beams are casted using the same concrete having a compressive strength f_c (at 28 days) equal to

30 MPa and a maximum aggregate size equal to 10 mm. Thus, a third numerical beam, having the same concrete characteristics as the beams of Mazars [1984], a section equal to 250×250 mm^2, a length equal to 1800 mm and a shear span equal to 500 mm, is numerically modeled.

4.3.1.1 Reference FE model

The beams are modeled in 2D using quadrilateral meshes of size 1 mm. Mazars isotropic damage model (Mazars [1986]) is used to describe the concrete behavior. First, deterministic FE computations are done to estimate the best experimental fit for the parameters A_t and B_t, found equal respectively to 0.8 and 20000. Moreover, in order to ensure the localization, stress based non-local method is used with a characteristic length equal to 3 cm.

For the deterministic case, the tensile strength value should be defined. One method consists on using directly the value deduced from the splitting test conducted on a cylinder specimen with a compressive strength equal to 30 MPa. Thus, the tensile strength, in this case denoted f_{ctm}, is equal to 2.9 MPa (90 % of the value of the splitting tensile strength calculated using Equation 3.20). Another method consists on considering for each beam a reduced value of the tensile strength f_t, evaluated using the analytical approach WL2$_A$. The value of the tensile strength for the two beams of Mazars [1984] are estimated, using the analytical probabilistic approach WL2$_A$, equal to 2.79 MPa for the small beam and 1.92 MPa for the second beam (see Chapter 3). The cylinder splitting test is considered as the reference volume ($V_{ref} = 3 \times 10^{-4}$ m^3). Hence, the mean tensile strength corresponding to the third numerical beam is also estimated using the analytical probabilistic approach WL2$_A$, by considering the same reference volume chosen for Mazars beams. The deduced tensile strength for the numerical beam is, then, equal to 1.66 MPa.

Thus, for each beam, two deterministic FE simulations are done; deterministic FE simulations with f_{ctm} deduced from splitting test (2.9 MPa) and deterministic FE simulations with f_t evaluated using the WL2$_A$ approach. Figure 4.15 presents the values of the tensile strengths obtained from these deterministic simulations. This figure highlights that by using a reduced tensile strength, deterministic FE simulation reproduce the decrease

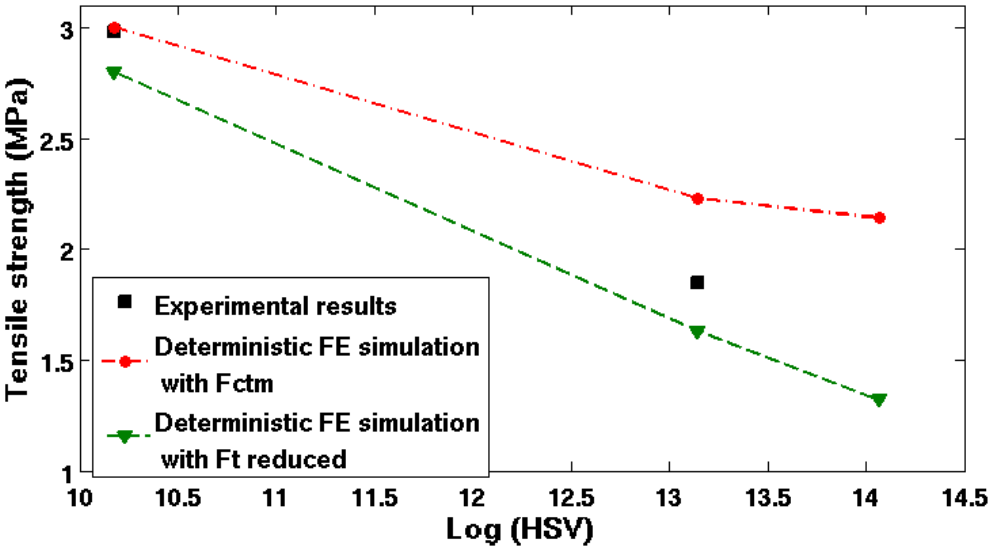

FIGURE 4.15: Evolution of the tensile strength of the three beams resulting from the experiments and the numerical simulations: deterministic simulation with f_t reduced and deterministic simulation with f_{ctm} deduced from splitting test.

of the tensile strength when the volume increases, on the contrary of the case of deterministic FE simulations with f_{ctm}.

In the following, the SFE method is used in order to obtain different crack positions.

4.3.1.2 Application of SFE method

The SFE method using discretized random fields, is applied to the three beams. Thus, the tensile strength is modeled using a discretized random field. Moreover, the aim of this study is to investigate the importance of attributing a coefficient of reduction to the mean of the tensile strength of concrete. Hence, as in the case of deterministic simulations, two choices can be taken for the mean tensile strength of the random field:

- Case 1: the mean values of the random fields are not the same for the three beams and they are equal to the mean tensile strength calculated using the $WL2_A$ approach for each beam.
- Case 2: the mean values of the random fields are equal to the direct tensile strength f_{ctm} deduced from the splitting test.

Moreover, in order to estimate the standard deviation for each beam, the experimental coefficient of variation of the tensile strength must be known. As this information is

not found in Mazars [1984], a coefficient of variation of the tensile strength equal to 10 % is arbitrarily considered for the three beams. Thus, for the case 1, the mean and the standard deviation of the tensile strength, used to define the random field for each beam, are resumed in Table 4.2. As for the second case, it is applied only to the second

TABLE 4.2: The values of the mean and the standard deviation of the tensile strength used in the definition of the random fields corresponding to case 1 for the two beams of Mazars [1984] and the numerical beam (beam 3).

	$\mu(f_t)$ (MPa)	$Std(f_t)$ (MPa)	$CV(f_t)$ (%)
Beam 1 ($L = 300$ mm)	2.79	0.3	10
Beam 2 ($L = 1400$ mm)	1.92	0.2	10
Beam 3 ($L = 1800$ mm)	1.66	0.17	10

beam of Mazars [1984] and the numerical beam. Both beams are affected by the same random field on the tensile strength, having a mean equal to 2.9 MPa and a standard deviation equal to 0.3 MPa.

Gaussian autocorrelated random field with a scale of fluctuation equal to 50 cm are considered for both cases. For each SFE simulation, 30 realizations of Gaussian random fields are conducted. Figure 4.16 presents two realizations of random field on the tensile strength, corresponding to the case 1, for the bigger beam of Mazars [1984] and their corresponding crack position. In the case of 4-point bending loading, the statistical size effect is preponderant, due to the homogeneous stress state between the two applied force. Thus, the crack position is different from one realization to another, depending on the position of the weakest point.

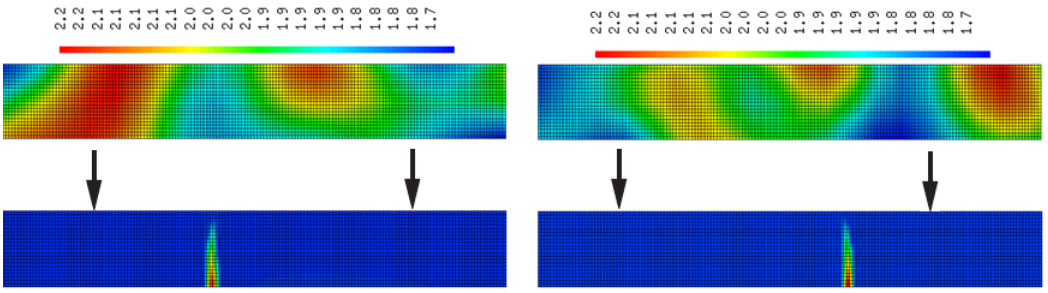

FIGURE 4.16: Two examples of random fields on the tensile strength corresponding to the second beam of Mazars [1984] and their fracture position.

Figure 4.17 shows the dispersion of the tensile strength for the three beams under 4-point bending loading. The case where the mean tensile strength is affected by a coefficient of reduction corresponds to the legend "f_t reduced" and the case where the mean tensile

strength is equal to the direct tensile strength estimated on a splitting test corresponds to the legend "f_{ctm} splitting test". From Figure 4.17, it seems obvious that the mean

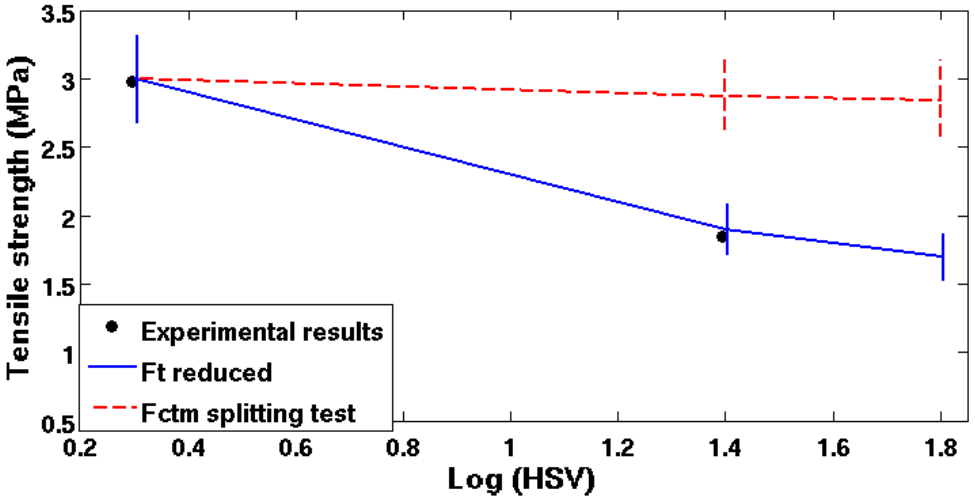

FIGURE 4.17: The dispersion of the tensile strength for the three beams under 4-point bending loading for the case where f_t is reduced and the case where f_{ctm} is used.

tensile strength used in the definition of the random field should be calculated using the WL2$_A$ approach, in order to better estimate the size effect. Thus, the random field generations alone are not capable on reproducing the decrease of the structural tensile strength.

Thus, after showing that the case 1 should be taken into account, Figure 4.18 resumes the confidence interval obtained from both WL2$_A$ approach and SFE simulations. It is shown that both methods are capable of reproducing the decrease of the mean and the standard deviation of the tensile strength as the volume increases. Moreover, the rupture

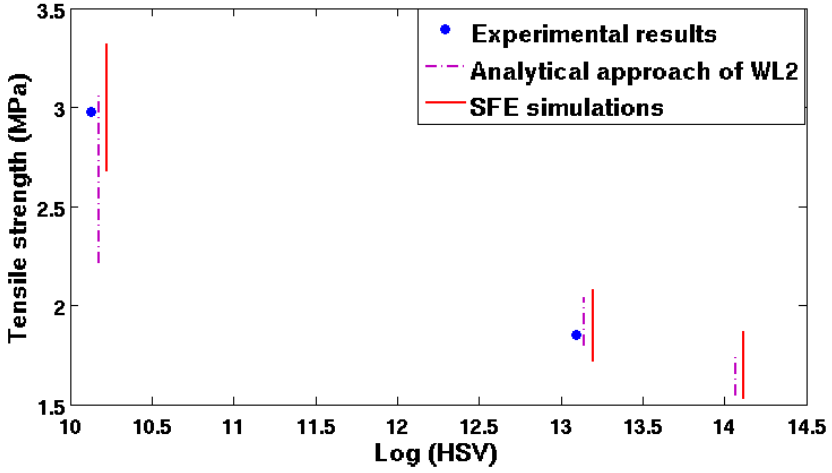

FIGURE 4.18: Computation of the size effect for the two beams of Mazars [1984] and the numerical beam, using WL2$_A$ approach and SFE simulations.

probability CDFs are plotted using both $WL2_A$ approach and the SFE simulations. Therefore, Equation 3.3 is used to plot the CDFs of the rupture probability of the three beams under 4-point bending loading. The reference volume used is the splitting test corresponding to a compressive strength equal to 30 MPa. As for the Weibull modulus, the Weibull definition method is used, since few informations are found on the concrete characteristics Mazars [1984] beams. Thus, a Weibull modulus equal to 12 corresponds to a coefficient of variation of the tensile strength of 10 % (Table 3.2). Figure 4.19 shows the CDFs obtained for the three beams under 4-point bending loading, from SFE simulations and $WL2_A$.

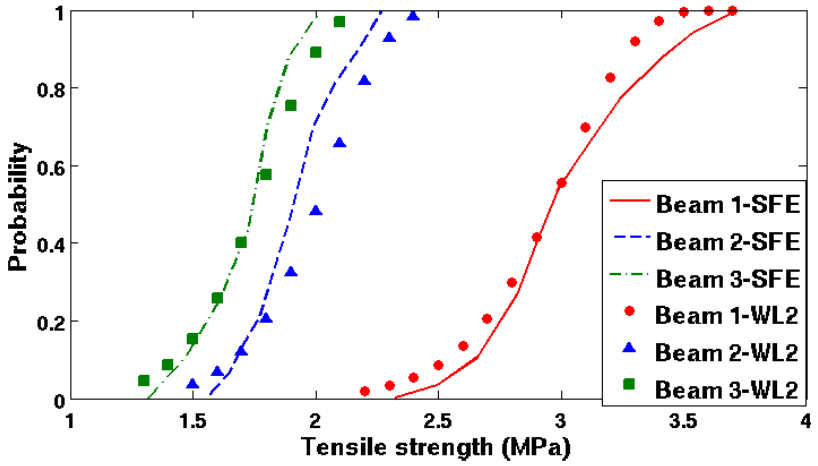

FIGURE 4.19: CDFs of the 3 beams under 4-point bending loading obtained from the SFE simulations and the analytical approach of WL2 ($WL2_A$).

From this figure, we can deduce that both methods reproduce almost the same rupture probability distributions, using a scale of fluctuation equal to 50 cm. Hence, the link between the size effect phenomenon and the spatial variability of the tensile strength seems to be highlighted.

4.3.2 Application on series of beams under 3-point bending loading

SFE simulations are done on 3-point bending beams corresponding to Hoover and Bažant [2014a] series. These beams are all geometrically similar with a constant thickness of 40 mm and a length-to-depth ratio of 2.4, and their depths are 40, 93, 215 and 500 mm, corresponding to a size range of 1:12.5 (see Appendix A). This experimental series showed a strong size effect on the mean and the standard deviation of the tensile strength. In this case, statistical and mainly energetic size effect are involved. The aim of this study

is to test the relevance of modeling the material randomness by means of random field to reproduce the size effect on f_t for this type of loading. As in Chapter 3, the first beam is not considered due to its very small dimensions 96×40 mm^2 compared to the diameter of the maximum aggregate ($d_{max} = 10$ mm). In the previous section, it is shown that the tensile strength of concrete, for each beam, must be affected by a coefficient of reduction. Thus, the reduced tensile strength is calculated using WL2$_A$ approach, for each beam of the series. By considering the second beam as the reference volume, the mean of the tensile strength of each beam, computed in Chapter 3, is summarized in Table 4.3 (the used Weibull modulus is equal to 9). As for the coefficient of variation of the tensile strength, an experimental coefficient of variation of 13 % is observed. At first, deterministic FE calculations are done for the three beams. These beams are

TABLE 4.3: The values of the mean, the standard deviation and the coefficient of variation of the tensile strength used in the definition of the random fields for the three beams of Hoover series Hoover and Bažant [2014a].

	$\mu(f_t)$ (MPa)	$Std(f_t)$ (MPa)	CV(f_t) (%)
Beam 2	7.2	0.93	13
Beam 3	6.3	0.8	13
Beam 4	5.7	0.74	13

also modeled in 2D, using quadrilateral meshes of size 4 mm. The concrete is modeled using Mazars isotropic damage model (Mazars [1986]). For each beam, different strain thresholds ε_{D0} are used depending on the value of the corrected tensile strength using WL2$_A$ approach. The FE calculations are done using stress based non-local method (Giry et al. [2011]) with a characteristic length equal to 3 cm which is relative to three times the maximum aggregate. The deduced tensile strength from the deterministic simulation and the experimental interval of the tensile strength for the three studied beams are given in Figure 4.20. On the contrary of the case of 4-point bending loading, it is shown, that only by using, for each beam, the value of the tensile strength deduced from WL2$_A$ approach as an input parameter in the FE model, deterministic models are capable of reproducing the experimental results. However, in order to predict the dispersion of the tensile strength, the use of a probabilistic approach (analytical or numerical with SFE simulations) is required. Therefore, random field realizations, for each beam, are generated by considering the first and the second statistical moment as respectively the mean $\mu(f_t)$ and the standard deviation $Std(f_t)$ of the tensile strength, given in Table 4.3. Gaussian discretized random fields with an autocorrelation function

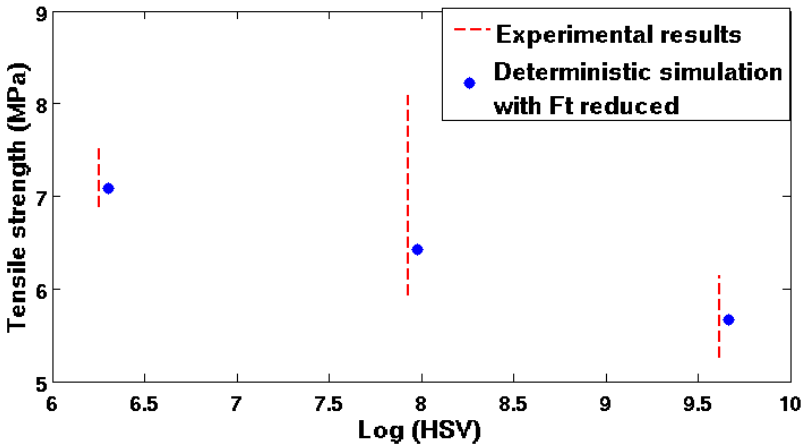

FIGURE 4.20: Experimental and deterministic evolution of the tensile strength for the four beams.

of type A and a scale of fluctuation $v = 50$ cm are used. Also, 30 realizations of random fields are generated for each beam. Figures 4.21 and 4.22 show two different realizations of the random field with their corresponding fracture positions, respectively for the third and fourth beam. Unlike the case of 4-point bending, 3-point bending load induces a stress concentration able to force the position of the first crack. Thus, all the random field realizations induce a crack at the center of the beam.

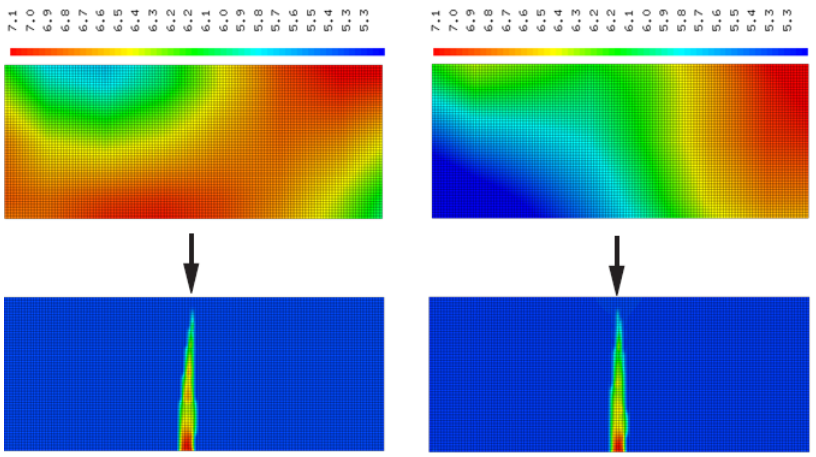

FIGURE 4.21: Two realizations of random field on the tensile strength for the third beam with the corresponding equivalent strain.

Consequently, the capability of SFE simulations on reproducing the size effect, in the case of 3-point bending, is studied. As Hoover and Bažant [2014b] developed a Universal Size Effect (USE) law, their method is applied to this experimental series. Figure 4.23 presents different methods to compute for the size effect in these series of 3-point

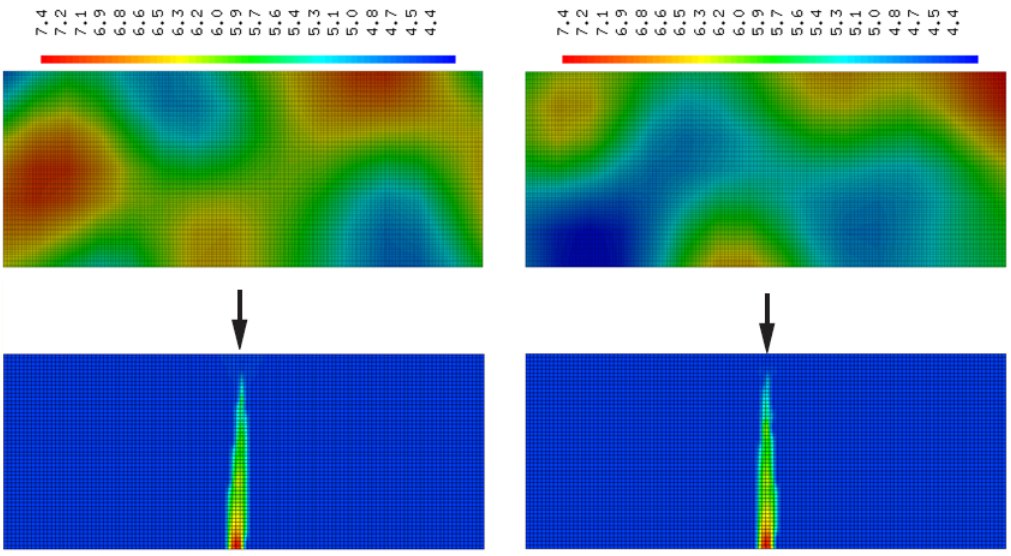

FIGURE 4.22: Two realizations of random field on the tensile strength for the fourth beam with the corresponding equivalent strain.

bending load (USE law (Hoover and Bažant [2014b]), WL2$_A$ approach and SFE simulations). On the one hand, Bažant USE law is able to estimate the mean of the tensile strength, but the standard deviation of the tensile strength is not evaluated. However, the evaluation of the tensile strength using the USE law is complicated and depends on many numerical parameters that can be obtained by fitting. On the other hand, both WL2$_A$ approach and SFE simulations are able to reproduce the dispersion of the tensile strength. In addition, the CDF of the tensile strength are obtained using WL2$_A$

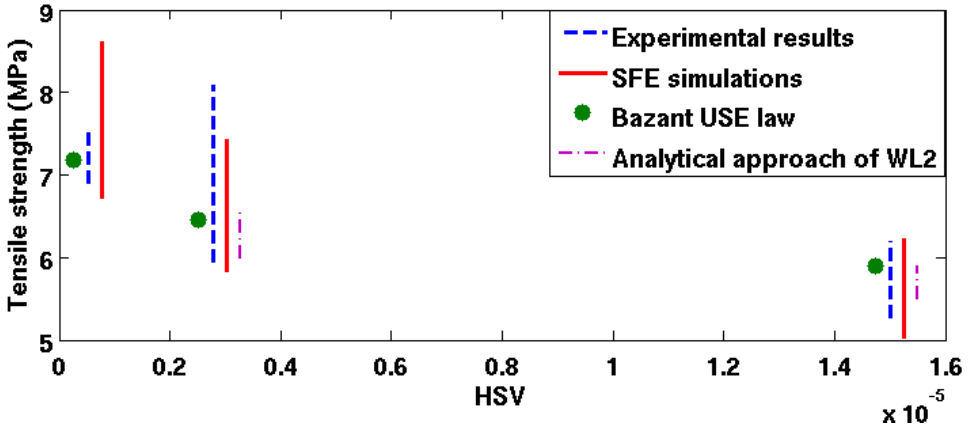

FIGURE 4.23: Computation of the size effect for the three beams of Hoover and Bažant [2014a] using probabilistic simulations, the USEL of Bažant (Hoover and Bažant [2014b]) and the analytical approach of WL2 (WL2$_A$).

approach (Equation 3.3) and the SFE simulations. In the case of WL2$_A$ approach, the reference structure, on which the reference volume and reference tensile strength are

evaluated, is the second beam. The scale length l_I is taken equal to 0.3 m and m=9 (see chapter 3). Figure 4.24 shows the CDFs of the third and fourth beams estimated using WL2$_A$ and the SFE simulations. It is shown that the CDFs of rupture strength obtained from both methods are not similar. It is worth noting that the SFE simulations using discretized random fields seem to be unnecessary for the case of 3-point bending where the stress concentration is preponderant on the spatial randomness of the concrete properties. Thus, for this case of loading, deterministic FE models using f_t estimated by the analytical approach WL2$_A$ are enough to account for the size effect phenomenon.

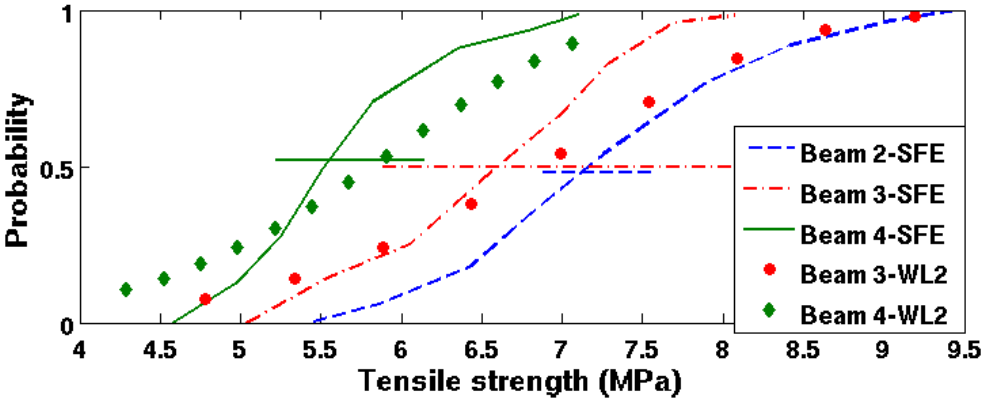

FIGURE 4.24: CDFs of the 3 beams obtained from the SFE simulations and the WL2$_A$ approach with the horizontal bars corresponding to the experimental values of the tensile strength (Hoover and Bažant [2014a]).

4.4 Application to RC structures

After the application of SFE method on series of concrete structures, the aim in view is also to apply this method to large complex structures. First, the method is applied to Clement [1987] anchor, since it provides confidence interval of the position of the first crack. Moreover, the SFE method is applied to a simplified model of a containment.

4.4.1 Application to Clément's anchor

An anchor subjected to direct tension is influenced mostly by the randomness of the material properties, since the applied stress is homogeneous. Therefore, the usefulness of the SFE simulations can be validated for this type of loading. Clement [1987] tie is

chosen to be numerically modeled, since it provides informations on the position of the first crack.

Before testing the $0.1 \times 0.1 \times 0.68$ m^3 RC tie (composition given in Appendix A), three tests on 16×32 cm^2 cylindrical concrete specimens provided the nominal strength in tension and compression (characteristics given in Appendix A). The steel reinforcement is described by only one steel bar of diameter 10 mm. The tests on the tie under direct tensile load are performed by imposing monotonically an increasing displacement at each part of the steel bar. For each test, a single crack appears. The position of this single crack, measured from the edge of the tie, is between 21 and 31.5 cm for the three experimental tests (Figure 4.25.a). Furthermore, the distance between two cracks can be computed using the formula of EC2 (CEN [2005]):

$$S_{r0} = \frac{\phi}{4} r \frac{f_{ctm}}{f_{bd}} \tag{4.13}$$

where ϕ is the diameter of the bar (0.01 m), r is the reinforcement ratio (7.85×10^{-3}),

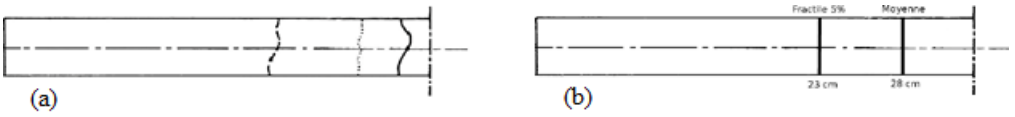

FIGURE 4.25: Fracture positions: a) Experimental model (Clement [1987]), fracture between 21 et 31.5 cm from the edge of the tie, b) EC2 model, Fracture at 28 cm from the edge (90 % confidence interval varying from 23 to 36 cm).

f_{ctm} is the mean value of the tensile strength of the concrete (2.8 MPa) and f_{bd} is the adhesion stress of the concrete-steel (3.2 MPa).

A distance of 27.8 cm is obtained between the edge of the tie and the crack. A probabilistic analysis of the Equation 4.13 is conducted considering the parameters ϕ, f_{ctm} and f_{bd} as log-normal random variables, in order to obtain an interval for the crack position. A mean of 27.8 cm from the edge of the anchor and a 90 % confidence interval varying from 23 to 36 cm are deduced.

For the numerical modelisation, Clément's tie test (Clement [1987]) was modeled in a 3D representation using the FE code Castem (CEA [2015]). It is modeled over its entire length and over a quarter of its section with 3D tetrahedral linear elements. A displacement is imposed on each side of the steel, to be as close as possible to the actual boundary conditions imposed by the experiment. The FE model is composed using four sections: the concrete, modeled with the Mazars damage model (Mazars [1986]), the steel bar,

modeled with an elasto-plastic model, a concrete layer with a thickness of 1 cm, which models the steel/concrete interface and two elastic bands, modeled on both sides, which allow a regular load repartition. Figure 4.26 compares the force-displacement evolutions for the experimental tests and the deterministic FE local model. Three distinct zones

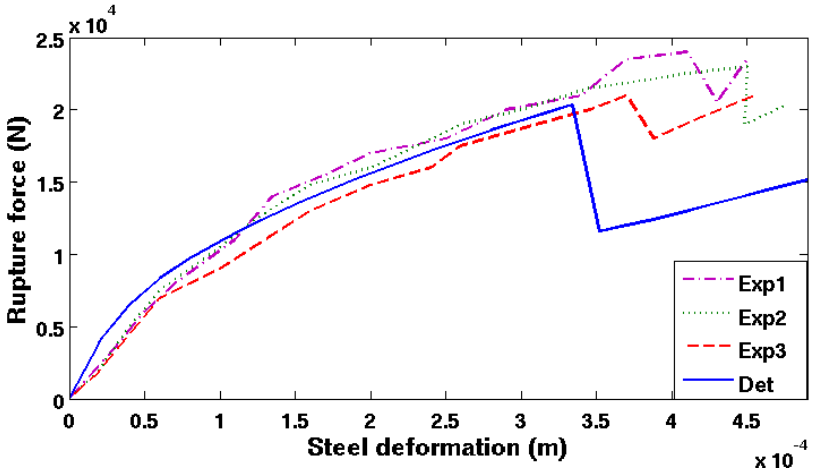

FIGURE 4.26: Force-displacement evolution for the experimental tests and the FE calculation.

can be identified: an elastic zone reaching a displacement of 0.25 mm, where the tensile stresses are distributed in the concrete and steel; a plastic zone, where only the steel supports loading and a sudden drop in the applied force, corresponding to the appearance of a macro crack. The first macro crack occurs in the reference model for a similar loading for the three experimental tests but corresponds to a lower steel elongation. One should note the difficulty of getting a displacement measure for such a test, as elongation of the steel can go on after the crack occurrence. FE elongation corresponds to the damage. Figure 4.27 allows the visualization of the damage field at the appearance of

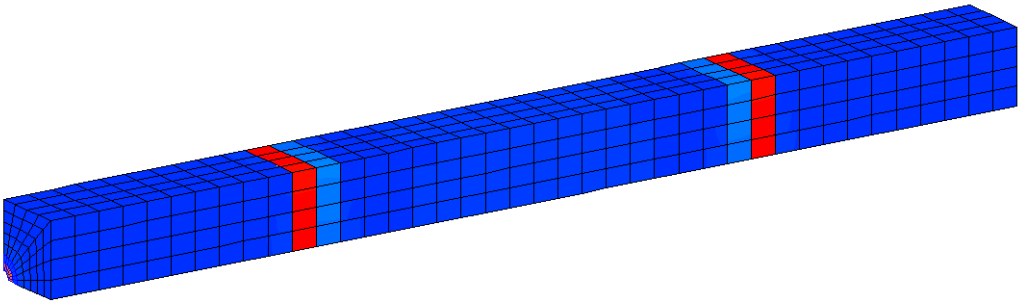

FIGURE 4.27: Fracture position in deterministic FE calculation.

the first crack. From the distribution of the damage, the exact positions of two theoretical macro-cracks can be estimated: a first crack extends between 0.22 and 0.29 m

from the left edge of the tie, the same for the second crack located on the right side of the tie (see Figure 4.27). The specific loading of the tie creates a plane of symmetry at the center. The distance between the two theoretical cracks, thus, corresponds to the average spacing deduced by the EC2 and the experimental tests.

As the stress supported by the concrete is gradually transmitted to the steel through the interface, the transfer length depends directly on the mechanical characteristics of this interface. The space between two cracks is then conditioned by the quality of the interface. Therefore, the first crack will happen at a weak point in the sense of the variability of the mechanical properties of concrete (Young's modulus or tensile strength). Thus, it becomes useful to model the tensile strength f_t, using a discretized random field.

Gaussian random fields using Gaussian autocorrelation function with a scale of fluctuation equal to 50 cm are used. First, to determine the mean of the tensile strength, used to define the random field, the WL2_A approach is applied to the tie. The splitting tensile strength $f_{ct,sp}$ equal to 2.8 MPa is considered as the reference tensile strength and a corresponding reference volume equal to 3×10^{-4} m^3 is used. Since an experimental coefficient of variation on f_t equal to 9 % was observed, the Weibull modulus m is computed using Weibull definition (Table 3.2) and it is equal to 13. Thus, the mean tensile strength is evaluated equal to 2.2 MPa, using the WL2_A approach. Moreover, the standard deviation of f_t, used in the definition of the random field, is equal to 0.2 MPa (based on $CV(f_t)$=9 %).

After defining the mean and the standard deviation of f_t, the SFE simulations are applied to Clément's anchor. Thus, 30 random fields of the tensile strength are generated. Figure 4.28 presents relative errors for the means and standard deviations of the rupture force as function of the number of random field realizations. An average of 21 kN (corresponding to f_t equal to 2.1 MPa) and a standard deviation of 2.5 kN are obtained on the rupture force which corresponds to the experimental results that has a mean value equal to 22 kN. So for a coefficient of variation of 9 % for the tensile strength, a coefficient of variation of 11 % for the rupture force is obtained. In addition, 15 realizations are sufficient to obtain a relative error on the mean of 0.3 % and a relative error on the standard deviation of 9 % (see Figure 4.28).

Figure 4.29 shows two realizations of random field on the tensile strength and their corresponding crack position. A single crack, corresponding to the weak point, is obtained, in the case of SFE simulations. Furthermore, a study of the crack position is possible.

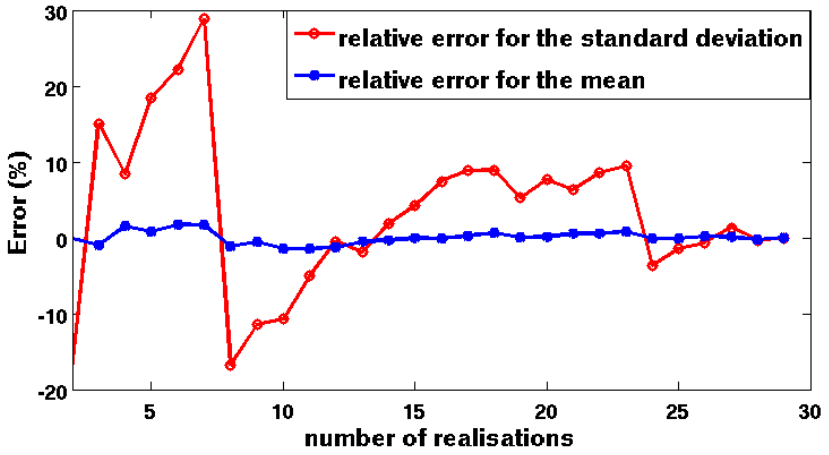

FIGURE 4.28: Evolution of the relative error for the mean and the standard deviation of the maximum rupture force as function of the number of realizations.

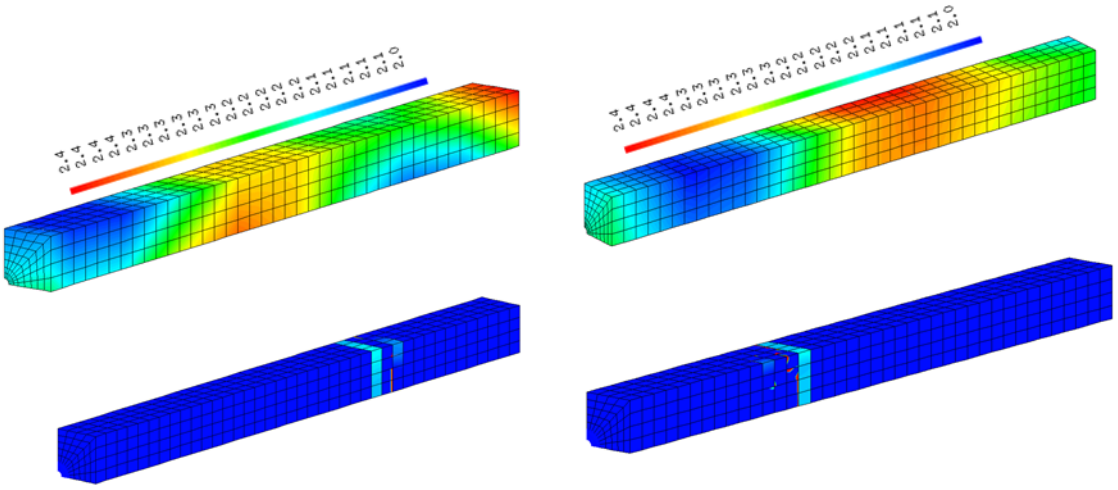

FIGURE 4.29: Two realizations of random field on the tensile strength and their corresponding crack position.

From 30 realizations of random fields, the mean value of the position of the crack from the edge of the tie is equal to 21 cm. The minimum and maximum values of the position of the crack from the edge of the tie correspond, respectively, to 19 and 31 cm. Thus, a valid interval for the crack position is reproduced, using SFE simulations, due the necessity of such a model to better predict the crack pattern in RC structures.

4.4.2 Application to a containment vessel

One major objective is to apply the developed SFE method using discretized random fields to the case of large concrete structures. More specifically, this method is applied to the case of a concrete containment vessel, in order to evaluate the capability of such

method to give information on damage and thus cracks position for such structure. This study is based on VeRCoRs mock-up. To simplify our study, we choose to focus on the concrete mechanical property. Thus, the chosen containment has the same dimensions and concrete characteristics as VeRCoRs, since information on its concrete mechanical properties are provided. As a consequence, this exercise gives quantitative estimation of the size effect on the tensile strength.

4.4.2.1 Reference FE model

A brief description on the dimensions of the mock-up is done in Chapter 3. The height of the containment is 20 m. However, the pouring of concrete in massive structures is not continuous; it is casted on 15 lifts having a height equal to 1.2 m each. Table 4.4 resumes, at each lift, the external temperature, the mean and standard deviation of the Young's modulus and the mean and standard deviation of the tensile strength. The concrete characteristics are deduced from splitting tests on three 11×22 cm^2 cylinders, casted for each lift. Table 4.4 shows a variation in concrete properties from one lift to

TABLE 4.4: Characteristics of the concrete at each lift.

	T^oC	$\mu(E)$ GPa	$Std(E)$ GPa	$\mu(f_t)$ MPa	$Std(f_t)$ MPa
Lift 14	0.4	35	1.85	4.7	0.25
Lift 13	8.3	31.3	3.25	3.7	0.1
Lift 12	8.8	37.1	2.67	3.7	0.17
Lift 11	8.5	37.2	1.36	4.9	0.21
Lift 10	3.6	37.2	0.97	5	0.21
Lift 9	10.9	37.2	1.13	4	0.23
Lift 8	10.1	36.2	0.63	4.2	0.1
Lift 7	9	35.8	0.98	4.8	0.2
Lift 6	14.1	38.9	1.42	4.3	0.15
Lift 5	16.7	37	2.06	3.9	0.42
Lift 4	14.4	36.9	2.58	4.3	0.35
Lift 3	20.6	40.3	0.57	4.3	0.43
Lift 2	29.6	45.5	0.9	4.5	0.15
Lift 1	20.6	34.3	0.53	4.1	0.15
Raft	30.9	36.8	1.7	3.6	0.21

another. Therefore, a main objective is to study the effect of accounting for concrete variabilities on the appearance of fracture, at early age.

The method, then, consists on defining, at each lift, the tensile strength as autocorrelated Gaussian random field. These random fields are supposed independent from one lift to

another. Thus, a simplified cylinder is modeled using Cast3m CEA [2015], with a height of 20 m, an internal radius of 7.3 m and a thickness of 40 cm. Note that only concrete is modeled, prestressed cables and reinforcement are not considered.

First, a deterministic model is conducted. This model consists on defining at each lift the tensile strength to the mean values given in Table 4.4. As for the Young's modulus, in order to reduce the environmental effect, it is considered equal, at each lift, to the deduced Young's modulus at 20^oC using the formula of the CM2010 (Code [2012]):

$$E_{ci} = \frac{E_{ci}(T)}{1.06 - 0.003T} \tag{4.14}$$

where E_{ci} is the Young's modulus at 20 ^oC and $E_{ci}(T)$ is the Young's modulus at temperature T, at lift i.

It is worth noting that the aim of this qualitative study is to show the effect of applying the SFE method on large structures, since it allows to model the spatial variability of the weakest spot of the concrete.

Mazars isotropic damage model is used to describe the behavior of concrete (Mazars [1986]). Table 4.5 resumes the parameters of Mazars used in the FE model. The strain

TABLE 4.5: Parameters of Mazars isotropic damage model.

ν	A_T	B_T	A_C	B_C
0.2	0.9	10^4	1.1	1300

threshold $\varepsilon_{D0} = \frac{f_t}{E}$ is not defined in the table, since it is not a constant and it takes different values from one lift to another, depending on the values of f_t and E. The cylinder is considered subjected to internal pressure of 4.9 bar. Also, the raft is considered fixed and its stiffness is increased to neutralize the damage in this area.

Figure 4.30 shows the values of the strain threshold at each lift and the damage occurrence after a deterministic calculus. It is shown that the damage occurs in three lifts corresponding to lifts 5, 9 and 13. These three lifts have a low strain threshold equal to 1×10^{-4}.

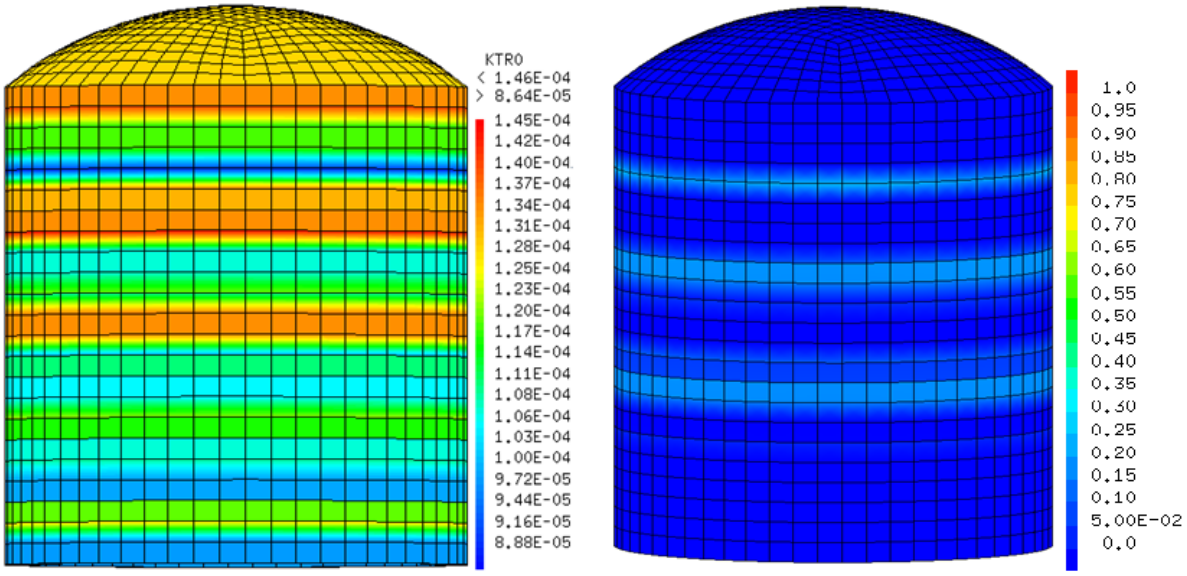

FIGURE 4.30: The evolution of the strain threshold (right) and the damage occurrence.

4.4.2.2 Application of SFE method

Since the deterministic FE model is not capable of predicting the crack position and gives an estimation only of the position of the weakest lift, SFE method using discretized random fields may be a solution. Therefore, at each lift, the tensile strength is defined as autocorrelated Gaussian discretized random field with an autocorrelation length equal to 40 cm (having a volume higher than 1 m^3). The used autocorrelation length is increased to 40 cm, instead of 28 cm, because in section 4.2.2.1, it seems that an autocorrelation length equal to 40 cm can be considered valid for large structures. The mean of the tensile strength, is estimated, for each lift, using the analytical approach $WL2_A$, where the reference tensile strength is equal to the values given in Table 4.4 from cylindrical specimen (see Section 3.3.3)

As at each lift the tensile strength of concrete is modeled using discretized random fields, the strain threshold value ($\varepsilon_{D0} = \frac{f_t}{E}$) defined in Mazars isotropic damage model is also modeled using random field generations. Thus, Figure 4.31 shows an example of a random field realization on ε_{D0} at the sixth lift of the containment. This example corresponds to the random field grid. For this calculation, only 10 realizations of random fields are conducted. The objective is to estimate the number of damaged zones, the mean, the maximum and the minimum angle between two "cracks" (e.g. locally damaged zones). Figure 4.32 shows two realizations of random fields on the grid and their projection on the FE mesh and their corresponding damage fields. On the contrary

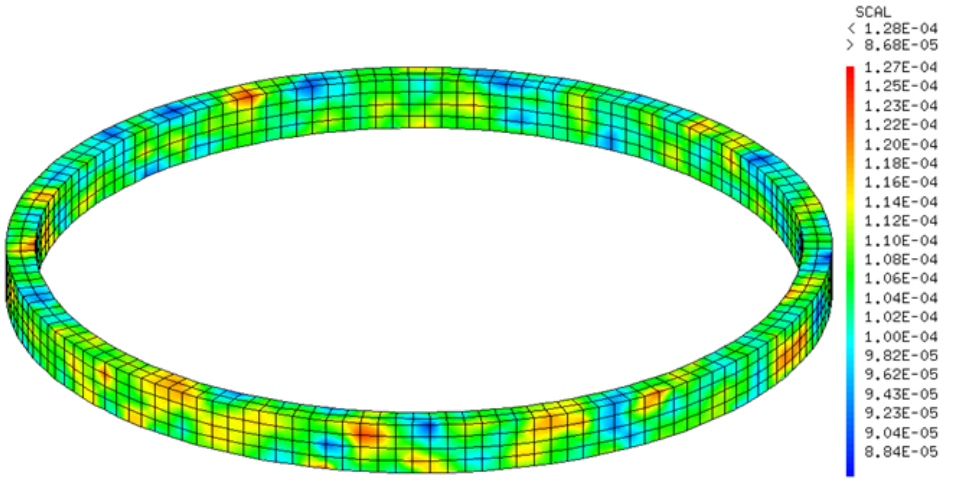

FIGURE 4.31: Realization of random field on ε_{D0} at the sixth lift of the concrete containment vessel.

of the deterministic case, SFE simulations are able to reproduce an estimation of the position of the crack. Table 4.6 presents the numerical number of damaged zones, mean, minimum and maximum angle between two cracks. Therefore, SFE simulations allow

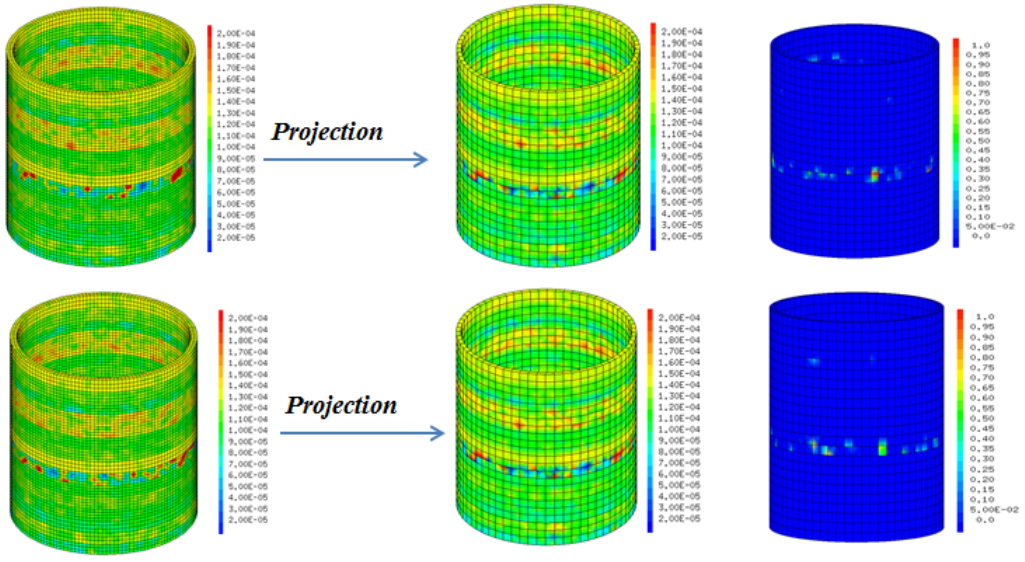

FIGURE 4.32: Two realizations of random fields on the grid, their projection on the FE mesh and their corresponding damage field.

TABLE 4.6: Numerical values of the number of damage zone, the mean, the maximum and the minimum angle between two cracks.

	Number of damaged zones	$\mu(S_r)$	$\max(S_r)$	$\min(S_r)$
SFE simulations	14	21^o	79^o	6^o

a preliminary estimation of the number of damaged zones and the position of cracks.

4.4.2.3 Sensitivity analysis

De Larrard et al. [2010] used discretized random fields to define the spatial variability of the Young's modulus of concrete in a simplified FE model of a nuclear containment. In their simulations, De Larrard et al. [2010] adopted autocorrelation lengths varying from 10 to 60 m and Karhunen-Loève discretization method. Therefore, two sensitivity analysis that seem important are: the effect of the autocorrelation length and the effect of considering the Young's modulus modeled as a random field instead of the tensile strength.

Influence of the autocorrelation length In the previous section, an autocorrelation length of 40 cm was associated to Gaussian autocorrelation function defined to model the variability of the tensile strength. To study the influence of the autocorrelation length, three different values of a are investigated: 60, 80 and 150 cm. For each case, 30 realizations of discretized random fields are associated to the variation of the tensile strength f_t. Figure 4.33 presents three different random field realizations corresponding to the three autocorrelation lengths. As in the previous section the number

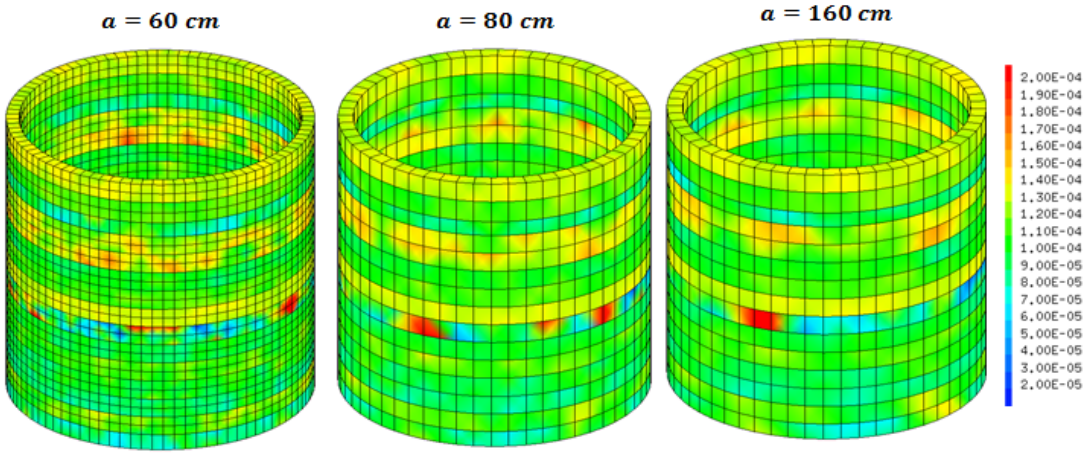

FIGURE 4.33: Examples of random fields realizations for different autocorrelation lengths a.

of damaged zones, the mean, minimum and maximum distance between two cracks are summarized in Table 4.7. It is shown that the lowest the autocorrelation length is, the

higher is the number of damage zones, since the weakest zones are more concentrated when the autocorrelation length decreases.

TABLE 4.7: Experimental and numerical values, corresponding to the three different autocorrelation length, of the number of damage zone, the mean, the maximum and the minimum angle between two cracks.

	Number of damaged zones	$\mu(S_r)$	$\max(S_r)$	$\min(S_r)$
$a = 60$ cm	16	18^o	84^o	6^o
$a = 80$ cm	14	21^o	90^o	6^o
$a = 160$ cm	11	25^o	112^o	6^o

Young's modulus modeling as random field Table 4.4 shows a variability on the Young's modulus, at each lift. Its mean values are varying from 31 to 46 GPa and its standard deviations are varying between 0.5 to 3 GPa, giving a coefficient of variation of around 5 % on each lift. Thus, the variability on E is investigated by defining discretized random field on this mechanical property. Hence, as in the case of random fields on f_t, independent autocorrelated random fields are defined on E at each lift. The standard deviation of E is defined, for each lift, in Table 4.4. As for its mean value, it is calculated using Equation 4.14. Gaussian autocorrelation function with a scale of fluctuation equal to 58 cm (corresponding to $a = 40$ cm) are used to define the discretized random fields. Figure 4.34 presents an example of two different random field realizations on the Young's modulus and their corresponding damage fields. Table 4.8 shows that

TABLE 4.8: Numerical values, corresponding to random fields defined on E, of the number of damage zone, the mean, the maximum and the minimum angle between two cracks.

	Number of damaged zones	$\mu(S_r)$	$\max(S_r)$	$\min(S_r)$
SFE simulations	16	18^o	84^o	6^o

modeling the variability on E is also a possible solution for running SFE simulations. However, the Young's modulus is a value influenced by external temperature and environmental conditions. Thus, its estimation is complicated, since the measured values must be decorrelated from external conditions.

Briefly, this study is done on a concrete containment vessel without considering the

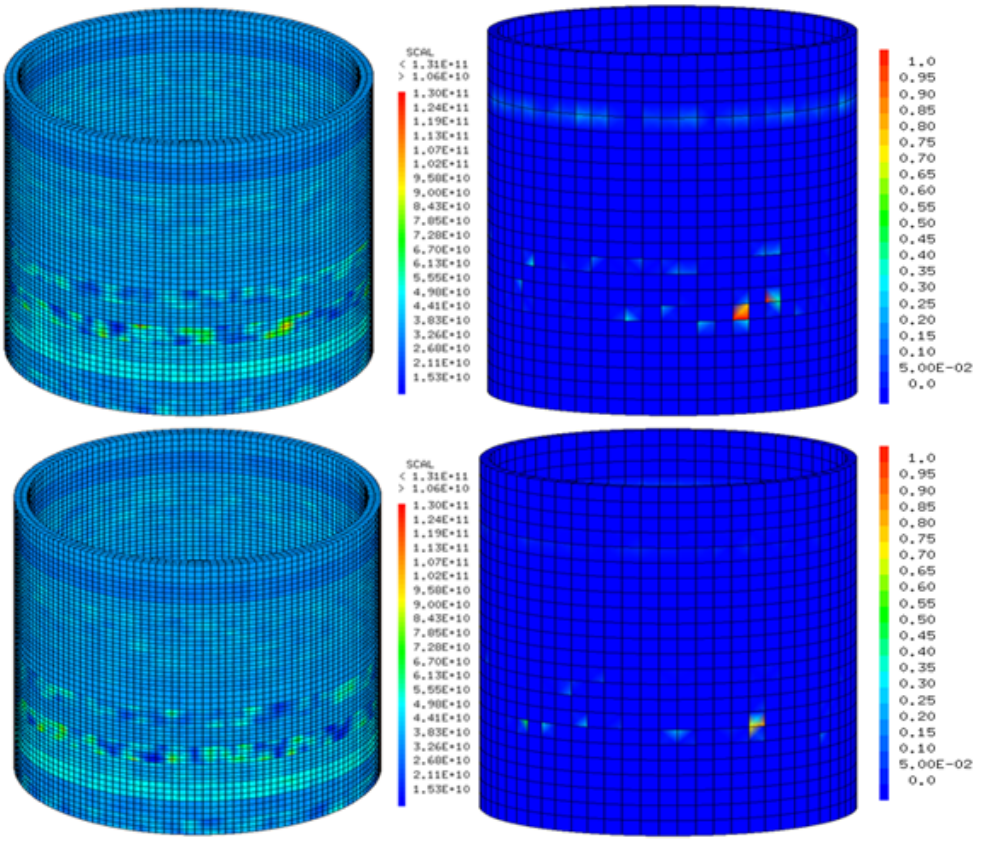

FIGURE 4.34: Examples of random fields realizations on E with their corresponding damage fields.

prestressed cables and the reinforcement. Its objective is only to demonstrate the possibility of obtaining the spatial distribution of the concrete heterogeneities and its effect on reproducing the damage field in the structure and its crack position. Therefore, the SFE method demonstrate to be an effective method in modeling the spatial variability of the tensile strength of concrete and thus different crack positions are obtained.

4.5 Conclusions

The use of discretized random fields to model the spatial variability of the tensile strength of concrete in FE models is explored. For this, discretized autocorrelated random field using Cholesky decomposition are generated. This methodology allows the estimation of the size effect on the tensile strength. However, the definition of the random field depends on various parameters. Experimental results from test series of concrete beams under 3-point bending loading and 4-point bending loading are used to validate the methodology. Mazars isotropic damage model is used to model the concrete behavior

and the non-local stress based method is adopted to limit the spreading of non-local damage.

First, the discretized random field used to model the variability of the tensile strength in concrete is characterized. Its parameters are chosen based on experimental CDFs of the rupture force for the three beams of Koide et al. [2000] under 4-point bending loading. The influence of parameters such as the law, the autocorrelation function and the autocorrelation length are studied. Hence, the influence of the autocorrelation length is investigated on the three beams. It is shown that a decimeter autocorrelation length is required. A scale of fluctuation of 50 cm is chosen. In addition, the choice of the autocorrelation function is studied. The Gaussian autocorrelation function proves to be more convenient than the exponential and the sinusoidal autocorrelation functions. Also, two laws of random fields distribution are compared (the Gaussian and the log-normal) and negligible differences between the two distributions are highlighted. Thus, Gaussian random fields with Gaussian autocorrelation function and a scale of fluctuation of 50 cm are chosen. Therefore, the link between the size effect and the definition of concrete tensile strength variability is validated.

Secondly, SFE method using discretized random fields are applied on two campaigns of experimental test series subjected to two types of loading (Mazars [1984] series and Hoover and Bažant [2014a] series). First, it is shown on Mazars [1984] series that the mean of the tensile strength used in the theoretical random field must be reduced by applying $WL2_A$ approach. Thus, different random fields are built for each structural size. SFE simulations seem to be necessary to reproduce the experimental results in the case of 4-point bending loading. However, as in the case of 3-point bending loading the applied force induces a strong stress concentration, deterministic FE simulations with reduced tensile strength seem to be sufficient to reproduce the experimental values of the tensile strength. Moreover, the SFE method seems able to account for size effect.

The applicability of discretized random field to characterize the variability of the tensile strength on RC structures such as Clement [1987] anchor is also studied. The SFE model of Clement [1987] anchor highlights the importance of applying SFE simulations to estimate the position of the first crack. The use of proper model that accounts for steel-concrete bond behavior is required to study the post-peak behavior. Finally, SFE method using discretized random field is applied to a large concrete containment vessel using the concrete properties of VeRCoRs. This containment has no reinforcement or prestressing. The aim of this last study is to demonstrate the necessity of using

random fields in order to model the variability of concrete. Thus, the effect of accounting for concrete variabilities on the appearance of crack position is highlighted by defining independent autocorrelated random fields on each lift of the containment. Finally, SFE simulations were able to estimate the number of locally damaged zones, the mean, the maximum and the minimum angle that separate two cracks. The sensitivity of the scale of fluctuation has also been studied.

Chapter 5

Conclusions and perspectives

5.1 Conclusions and results

This thesis deals with the problematic of using the concrete characteristics measured at the specimen scale with lab tests to estimate the concrete mechanical parameters to be used in models representative of structural scale. Particularly, the tensile strength of concrete shows direct dependency with the structural size, more precisely with the considered volume under tensile stresses (this idea is detailed in Chapter 2). Therefore, first, an analytical simplified version of WL2 (Sellier and Millard [2014]), denoted $\mathrm{WL2}_A$, is developed. This approach aims to estimate with an analytical method the decrease of the tensile strength when the loaded concrete volume increases. Then, the variability on the tensile strength is propagated using a Stochastic Finite Element (SFE) method based on discretized random fields.

In Chapter 3, the $\mathrm{WL2}_A$ approach, allowing a fast estimation of the distribution of concrete tensile strength at first crack is proposed. Thus, using this method, the decrease of the mean and standard deviation of the tensile strength as the volume increases is evaluated. This approach is applied to structures failing in mode I mechanism. It introduces a weighting function to the Weibull integral and thus accounts for the stress redistributions due to the attenuation of the elastic stresses around the weakest point. Therefore, one originality of this analytical method lies on the estimation of a scale length in the weighting function, based on various experimental databases. This scale length is related to the spatial variability of f_t in a homogeneous concrete, it does not

correspond, then, to the granulate heterogeneities. As this simplified method aims to identify the dispersion on the tensile strength, the uncertainty on the Weibull modulus and the experimental uncertainty on the reference tensile strength are taken into account. Each parameter of the method is identified through experimental concrete series under different types of loading. Two possible choices have been considered for the reference structure; the smallest specimen from the tested concrete series or the 16×32 cm^2 splitting cylindrical specimen. Another focal point of this method is the estimation of the Weibull modulus using four different methods found in the literature. The concluded interval of validity of the Weibull modulus (between 7 to 12) made some estimations proposed in the literature questionable (24-48). This modulus is concluded to be a material parameter and depends on the concrete mechanical properties, that is why it is considered as variable. Its mean value is estimated using an appropriate method, depending on the concrete mix or the experimental results. As for the scale length, it is determined using an inverse analysis done on series under uniaxial loading and series under 3-point bending loading. Thus, a mean value equal to 20 cm, equivalent to a scale of fluctuation equal to 50 cm, and a standard deviation equal to 10 cm are deduced. This variation of the scale length can be assessed to the geometry of the structure, its stress state or to the lack of experimental statistics ...
The method is applied to the concrete of large RC structures, such as Mivelaz [1996] anchor, Malpasset dam (Bažant et al. [2007]) and a containment. A coefficient of reduction of the tensile strength varying from 20 % to 50 % is concluded for the case of containments (by considering a simplified concrete containment).

After showing that accounting for variability of the concrete tensile strength is a mean to model the size effect, a SFE method allowing to define the spatial variability of concrete tensile strength using discretized random field is developed in Chapter 4. This method is able to account for size effect in FE models of concrete or RC structures and gives an estimation of the crack pattern.
First, the reference (deterministic) FE model is built, using Mazars mechanical damage model and the stress based non local approach. Secondly, the theoretical random field on the tensile strength is defined. Then, Cholesky method is used to discretise the random field on a 2D or 3D grid, whose mesh refinement depends on the chosen autocorrelation length. Finally, the discretized random field is projected onto the FE

mesh. The characteristics of the random field (probability law, autocorrelation function and autocorrelation length) are determined using Koide et al. [2000] experimental concrete series under 4-point bending loading. Gaussian autocorrelated random fields with a scale of fluctuation of 50 cm provided results in agreement with the experimental results. The originality of this method lies in the justification of the autocorrelated parameters, which are found to be different from an author to another (see Chapter 2). Furthermore, it is shown that the mean tensile strength, used in the definition of the random field must be calculated using the $WL2_A$ approach. As for the standard deviation of the tensile strength, it is supposed equal to the experimental coefficient of variation of the tensile strength. In conclusion, the deduced discretized random field is consistent with the weighting function defined for the analytical approach, since both functions requires the use of the same scale of fluctuation.

Moreover, the capability of both methods to reproduce the size effect is discussed for the concrete test series, studied in this chapter. They, both, seem to be capable on reproducing the size effect. The analytical approach $WL2_A$ gives a fast estimation of the size effect on f_t. As for the SFE method, it uses the $WL2_A$ approach to calculate the reduced tensile strength used as a mean value in the random field generation. It allows to both estimate for the size effect on f_t in FE models and obtain an estimation for the crack position. However, the necessity of using a SFE method for the case of 3-point bending loading is questionable, since the stress concentration induced in this type of loading is important. Thus, for this loading case, deterministic FE models with the reduced tensile strength evaluated using the analytical approach can be used to reproduce the experimental results.

Finally, the behavior of a concrete containment vessel (no reinforcement or prestressing) having the same concrete properties as the 1/3 mock-up VeRCoRs is studied using the SFE method, in order to show the capability of random fields in modeling the variability of concrete. For each lift of the structure, an independent autocorrelated random field is defined on the tensile strength of concrete. Using this method, the weakest lift can be identified, as well as an estimation of the number of damaged zones, the minimum, the maximum and the mean angle between two cracks.

In conclusion, a method accounting for concrete size effect resulting from the spatial variability of f_t is introduced in the mechanical FE modeling of large massive structures. Therefore, a better characterization of the crack pattern in RC structures is

obtained.

5.2 Improvements of the proposed methods

On the one hand, the WL2$_A$ approach presents a limited study domain (only uniaxial loading). Thus, a generalization of this method is discussed hereafter. On the other hand, the possibility of coupling between the SFE method using discretized random fields and other effects influencing the crack pattern in large massive structures is highlighted.

5.2.1 Generalization of the WL2$_A$ method

The WL2$_A$ method is limited to the size effect on f_t, for the case of structures failing in mode I. Hence, this variability is taken into account using a scale length l_I defined in the direction of the first principal stress σ_I. In the case of more complex failure modes, a multiaxial stress state should be perhaps introduced using scale lengths defined in the directions of the three principal stresses (σ_I,σ_{II},σ_{III}). Thus, the weighting function can be rewritten, in the following form:

$$\psi_1 = \psi\left(l_I, x\right)\psi\left(l_{II}, y\right)\psi\left(l_{III}, z\right) = \exp\left(-\frac{1}{2}\left(\frac{x^2}{l_I^2} + \frac{y^2}{l_{II}^2} + \frac{z^2}{l_{III}^2}\right)\right) \tag{5.1}$$

Also, in this analytical method, heterogeneities linked only to the concrete mix properties are considered. However, other heterogeneities exist in the structures, related to stress concentration, geometry discontinuities, the presence of steel and/or pre-stressed steel (reinforcement ratio r), the loading rate $\dot{\varepsilon}$ that can influence the value of the Weibull modulus, the boundary conditions ... Thus, an idea is to introduce regularization functions able to model each heterogeneity ($\psi_1\left(\Delta\sigma\right)$ modeling the stress state, $\psi_2\left(\Delta\dot{\varepsilon}\right)$ modeling the influence of the loading rate, $\psi_3\left(r\right)$ modeling the effect of r ...).

$$V_E = \int_V \left\langle \frac{\sigma_I + \sigma_{II} + \sigma_{III}}{\sigma_{max}} \right\rangle^m \psi_1\left(\Delta\sigma\right)\psi_2\left(\Delta\dot{\varepsilon}\right)\psi_3\left(r\right)dV \tag{5.2}$$

5.2.2 On the definition of discretized random fields

The modeling of the tensile strength using a discretized random field showed to be a tool to represent its consequence on crack pattern in concrete. However, a limit of the

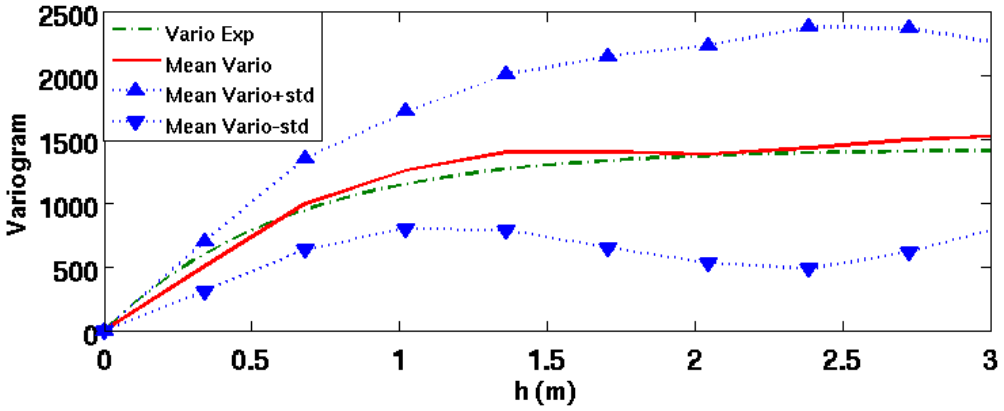

FIGURE 5.1: Mean, maximum and minimum theoretical and experimental (Gomez-Cardenas et al. [2015]) variograms corresponding to ultrasonic pulse velocity measurements done on a nuclear containment wall, using non-destructive techniques.

SFE method is the absence of experimental measures on the local in field mechanical properties of concrete, done on a defined surface of a massive structure. These experimental measures could be directly used for the estimation of an appropriate random field. For example, EVADEOS project presents an optimal methodology to estimate concrete mechanical properties, using non-destructive techniques, in the field of a real structure. Using this method, an experimental variogram of the measured quantities with non-destructive techniques is provided. The idea is then to reproduce the experimental variogram using random fields, that can be used later in the SFE models. Gomez-Cardenas et al. [2015] gives the variogram distribution of ultrasonic pulse velocity measurements, done on a nuclear containment wall. From this variogram, the autocorrelation function and its corresponding length can be deduced, using the correlation length criteria (see Chapter 2). Then, a fit between experimental and numerical variograms is possible after generating 30 random fields with the deduced type of autocorrelation function and autocorrelation length. However, the remaining question is the link between the measured values, such as ultrasonic pulse velocity and the mechanical properties of concrete (E and f_t).

Figure 5.1 shows the maximum, minimum and mean theoretical and experimental variograms. It is shown that the experimental variograms can be reproduced. Thus, more realistic random field generations are evaluated.

5.3 Perspectives

For massive structures, more precisely for nuclear containment vessels, crack pattern and crack widths are important factors to estimate the leakage rate. Using SFE simulations, a prediction of the crack width should be possible. Bouhjiti et al. [2017] demonstrates that taking a coefficient of variation of 10 % on f_t leads to 18 cracks occurrence, which is more or less in agreement with our study that predicted 16 potential damaged zones. In addition, he showed that a 60 % increase on the value of the crack width can be obtained with probabilistic simulations. Furthermore, the recent study carried by Bouhjiti et al. [2017] considers a Thermo-Hydro-Mechanical (THM) coupling at early age. In their method, Bouhjiti et al. [2017] use a regularization method, based on the principles of WL2, to estimate the reduced tensile strength that should be used in the FE calculus. Therefore, the mechanical study developed for the initial state of the structure can be generated for large massive structures including a coupling with the thermal and hydration behavior of concrete.
In addition, various proposals could allow improvements to the methodology developed in this thesis:

- Both tensile strength and Young's modulus are variable concrete mechanical properties. Indeed, spatial variability on Young's modulus, rather than the tensile strength is considered by other authors (e. g. Breysse [1991] and De Larrard et al. [2010]). Therefore, the effect of accounting for the variability of the Young's modulus seems to be necessary, since it is an important parameter for the definition of the elastic behavior of concrete. Bouhjiti et al. [2017] have chosen to model the variability on the Young's modulus rather than the tensile strength in their study on a nuclear containment behavior. Moreover, modeling the variability on the Young's modulus or the tensile strength in Mazars isotropic damage model, should induce various influence on the output response, depending of random fields characteristics and their correlation. Thus, Bouhjiti et al. [2017] studies the possible correlation between these two parameters.

- Lamon and Evans [1983] present a size effect approach applied to ceramics under multiaxial loading. In their approach, the effective volume is influenced by both the stress state and the direction of the applied stress. A parameter accounting

for the direction of the applied stress is, then, introduced in the effective volume formula (Equation 3.4). Thus, this method can be generalized to concrete like materials. Hence, different characteristic lengths defined in the direction of the applied stress (σ_I, σ_{II}, σ_{III}) can be involved in size effect methods and these characteristic lengths can influence the crack propagation in the structure. Therefore, the characterization and the modeling of the interactions between the different characteristic lengths involved in crack propagation mechanisms could be studied in a new PhD research (F. Vilette, 3SR, 2017-2020). The experimental campaign in this PhD thesis will be carried on papers, which present fibrous aggregates that are created during its manufacture.

- The case of structures, where high stress concentrations exist such as in splitting tests and notched beams, are not presented in this thesis. The study of such type of structures requires special care for the chosen characteristic length, used in the weighting function (Equation 3.2). Hence, the weighting function, in this case of loading, is linked directly to the Fracture Process Zone (FPZ). This centimeter value can be obtained when fitting the $WL2_A$ approach with series of notched beams or splitting tests.

- For the case of RC structures, the reinforcement ratio is taken into account, using the formula of a homogenized section. However, the presence of steel can increase the scale length value. Thus, it is important to study series of RC beams, such as Tanaka and Shimomura [2010]. In this case, different rupture modes can be obtained and the analysis is not limited only to mode I rupture.

- The definition of the $WL2_A$ approach as function of strain state, such as Mazars [1984] approach, rather than stress state is possible.

- The application of the SFE method to splitting tensile tests is being processed. However, for this case of test, the 50 cm scale of fluctuation is not valid anymore, since the aggregate distribution is more pertinent. Hence, a smaller scale of fluctuation is required.

- When applying SFE method to RC structures, an appropriate steel-concrete bond model is required. The coupling between these two models should give a better estimation of the crack pattern. Hence, the estimation of crack position is not limited only to the first crack.

Appendix A

Synthesis of experimental concrete or RC series or structures

In this Appendix, the different test series studied and mentioned, in this thesis, are presented and described. These test series are divided into different categories, depending on their type of loading (direct tensile loading, 3-point bending or 4-point bending).

A.1 Series of concrete specimens under uniaxial tension

A.1.1 Rossi et al. [1994] series

The aim of the conducted experimental series by Rossi et al. [1994] is to investigate the size effect in direct tensile tests. Thus three sizes of cylinders, with a slenderness ratio equal to 2 and diameters equal to 30, 60, 150 mm were cored from large rectangular blocks of concrete. To investigate the effect of material properties on the scale effect, three concrete compositions were tested. The composition of the three types of concrete are summarized in Table A.1. Consequently, Table A.2 resumes the number N of specimens for each geometry, the mean μ and the standard deviation Std of the tensile strength f_t and the Young's modulus E for the three different concrete compositions.

TABLE A.1: Compositions of the three types of concrete with $d_{max} = 20$ mm (Rossi et al. [1994]).

Compositions	Concrete 1	Concrete 2	Concrete 3
Crushed silico-calcareous gravel, 5/20 mm	1114	1236	
Calcareous gravel 4/20 mm	-	-	1265
Silico-calcareous sand 0/4 mm	774	-	652
Silico-calcareous sand 0/5 mm	-	667	-
Cement	300 (CPJ 45)	350 (CPA HP)	421 (CPA HTS)
Water	185	158	112
Silica-fume	-	-	42.1
Superplasticizer	-	7	7.6

TABLE A.2: Results for concrete 1, 2 and 3 (Rossi et al. [1994]).

	Concrete 1			Concrete 2			Concrete 3		
D (mm)	30	60	150	30	60	150	30	60	150
N	15	15	16	18	8	9	12	17	7
$\mu(f_t)$ (MPa)	4.8	3.2	2.4	5.1	4.3	3.1	6.4	6.0	6.0
$Std(f_t)$ (MPa)	1	0.6	0.2	1	0.7	0.2	0.9	0.7	0.2
$\mu(E)$ (GPa)	35.6	39.0	39.8	42.4	44.2	45.3	52.3	51.8	53.9
$Std(E)$ (GPa)	3.4	1.8	0.8	3.1	1.8	1.5	2.7	1.6	1.1

A.1.2 Van Vliet and Van Mier [2000] series

The experimental results of the "dog bone" specimens of Van Vliet and Van Mier [2000] showed that the tensile strength depends not simply on the specimen dimensions but also on the curing conditions. In order to investigate the size effect on strength and fracture energy of concrete and sandstone, Van Vliet and Van Mier [2000] performed many uniaxial tension experiments on specimens having six different dimensions in a scale range of 1:32, having all the same dog bone shape (see Figure A.1). The behavior incorporated by the dog bone shape is similar to the behavior of a notched specimen. However, the dog bone shape presents many advantages, by applying circular bays, the cross section in the middle is reduces, thus the stress concentrations are smaller and easy to reproduce for many specimen sizes. Also, in the case of dog bone specimens, the area where failure may occur is larger compared to notched specimens. Failure is therefore more likely to occur at the weakest spot in the material. The choice of concrete mixture depends on the size of the smallest specimen chosen that is related to the maximum aggregate size. The concrete chosen has an average cube compressive strength f_c of 50

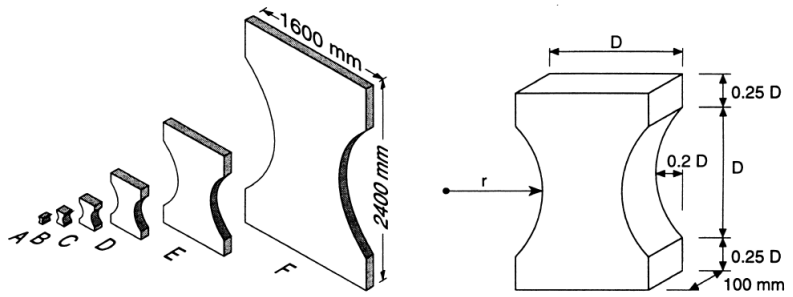

Type	A	B	C	D	E	F
D (mm)	50	100	200	400	800	1600
r (mm)	36.25	72.5	145	290	580	1160

FIGURE A.1: Specimens geometry (Van Vliet and Van Mier [2000]).

MPa and a maximum aggregate diameter d_{max} of 8 mm. Concrete compositions are given in Table A.3. The strength and the stiffness of small concrete specimens can vary

TABLE A.3: Compositions of concrete (Van Vliet and Van Mier [2000]).

Compositions	Unit content (kg/m^3)
Aggregate size 8/4 mm	540
Aggregate size 4/0 mm	363
Aggregate size 2/1 mm	272
Aggregate size 1/0.5 mm	272
Aggregate size 0.5/0.25 mm	234
Aggregate size 0.25/ 0.125 mm	127
Portland cement, type B	375
W/C	0.5

strongly with the presence or absence of large aggregates in the smallest cross section. Besides of the effect of the largest aggregate in the smallest cross section, the small specimen presents a distinct wall effect, so the results of the specimen A are not reliable. The size effect on the strength f_t for the dry series is presented in the Table A.4. A

TABLE A.4: Mean valuesand standard deviation for the tensile strength of the concrete tests of the dry series (Van Vliet and Van Mier [2000]).

Type	A	B	C	D	E	F
N	10	4	7	5	4	4
$\mu(f_t)$ (MPa)	2.54	2.97	2.75	2.3	2.07	1.86
$Std(f_t)$ (MPa)	0.41	0.19	0.21	0.09	0.12	0.16

wet test was performed to five specimens of type A, B, C and D. Only four strength results are obtained due to glue failure. In addition to the lower strength obtained, also the size effect on strength varied from wet to dry series. The concrete cured under

water has a lower strength than the concrete cured in air. Table A.5 gives the concrete strength for the different type of dog-bone. In conclusion, this series showed that drying

TABLE A.5: Mean values and standard deviation for the tensile strength of the concrete tests of the dry series (Van Vliet and Van Mier [2000]).

Type	A	B	C	D
N	5	5	5	4
$\mu(f_t)$ (MPa)	2.17	2.23	2.48	2.37
$Std(f_t)$ (MPa)	0.25	0.13	0.16	0.06

is an important phenomenon that should be well understood to avoid problems during concrete casting. Temperature and humidity rate influences the curing process of the concrete, which may induces map cracking. In the figure A.2, the size effect is reflected for the two dry and wet series.

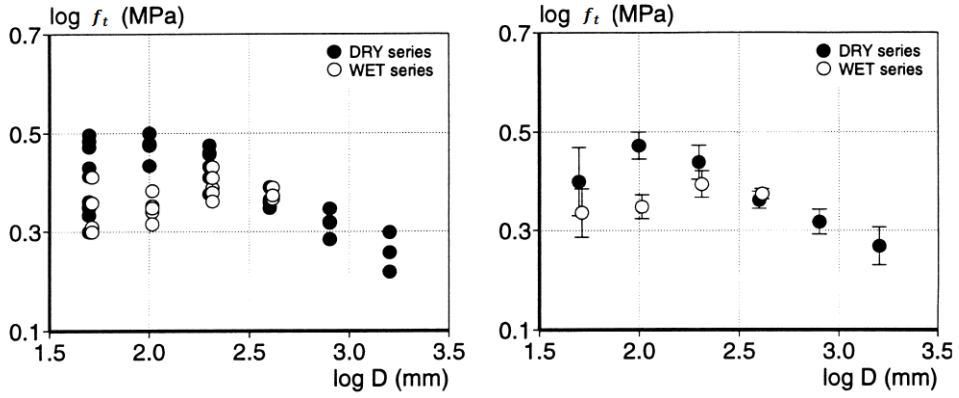

FIGURE A.2: Individual value (left) and mean value (right) of f_t vs D for dry and wet series (Van Vliet and Van Mier [2000]).

A.1.3 Clement [1987] anchor

The first studied anchor is done by Clement [1987]. The structure studied is a cuboid anchor of the following dimension $0,1 \times 0,1 \times 0,68$ m^3 (see Figure A.3). The steel reinforcement is described by only one steel bar of diameter 10 mm. The tests performed on this anchor reproduce the realistic behavior of an anchor under uniaxial tension at each part of the steel bar by imposing monotonically increasing displacement. The steel and concrete deformations are first measured, then the displacements at the border of the steel bar are measured. Finally, the tensile strength is deduced. The composition of the concrete used is given in the Table A.6, in which the aggregate size is lower than 10 mm.

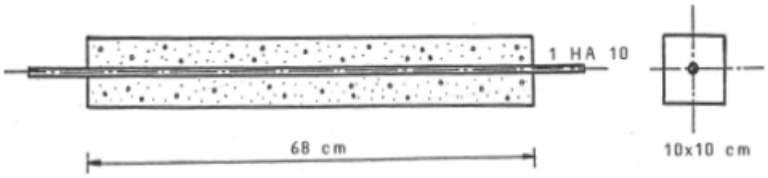

FIGURE A.3: A sketch of Clement's anchor (Clement [1987]).

TABLE A.6: Compositions of the concrete (Clement [1987]).

Components	Density (kg.m^{-3})	mass %
Sand 0.1	625	26.5
Sand 1.4	155	6.5
Gravel 4.1	1019	43.3
Cement (CPJ 45)	365	15.5
Water	194	8.2

Before testing the RC anchors, 3 tests on 16×32 cm^2 cylindrical concrete specimens provide the nominal strength in traction and compression of the concrete (see Table A.7). Finally, after the test conducted on the anchor, a mean rupture force equal to 22 kN is found.

TABLE A.7: Concrete Characteristics (Clement [1987]).

	f_c (MPa)	$f_{ct,sp}$ (MPa)
Test 1	29.15	2.76
Test 2	28	3.02
Test 3	33.42	2.58
Mean	30.2	2.8
CV	9.5	7.9

A.1.4 Farra [1994] anchors

Farra [1994] studied the effect of reinforcement ratio on the mechanical behavior of the anchor. 135 cuboid anchors of the following dimensions $1.15 \times 0.1 \times 0.1$ m^3 were casted, with a single steel bar at the center (see Figure A.4). Steel bars S500 were used in the experiments; the steel bar was tested to verify its quality. The steel Young's modulus varies between 192 and 206 GPa. 16 different types of concrete were used in this study. The results corresponding for N20 concrete are selected, in which N corresponds to Portland cement CPN, the first number corresponds to the cement dosage, i.e the number 2 corresponds to 300 kg/m^3 and the second number corresponds to the dosage

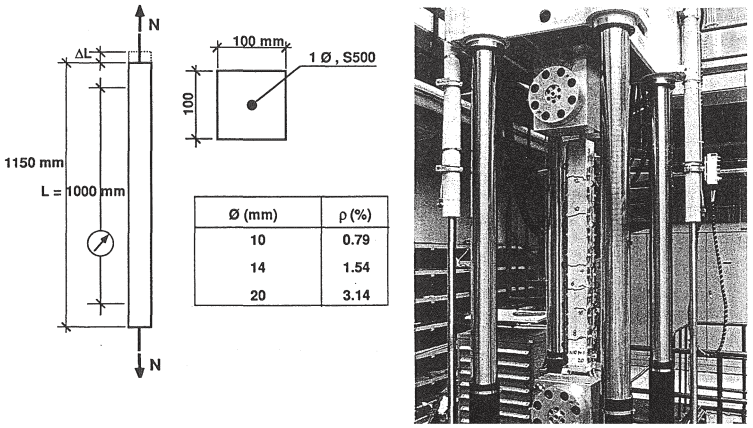

FIGURE A.4: Test on RC anchor (Farra [1994]).

of silica, i.e. 0 corresponds to 0 %. Thus, only concrete of type N20 with steel bars of diameters 10, 14 and 20 mm are considered. The main components and characteristics of N20 concrete are given in Tables A.8 and A.9 respectively. Finally, the rupture

TABLE A.8: Compositions of the concrete (Farra [1994]).

Components	Mass (kg)
Sand 0-3	29.4
Gravel 3-8	16.4
Gravel 8-16	16.4
Gravel 16-32	37.7
Cement (CPN)	300
Water	148.8

TABLE A.9: Characteristics of the concrete (Farra [1994]).

	Mean	Standard deviation
f_c (MPa)	35.7	3.37
E (GPa)	29.2	1.69

strength obtained for each reinforcement ratio r is shown in Table A.10.

TABLE A.10: Rupture strength of the anchor (Farra [1994]).

Reinforcement ratio r (%)	Tensile strength f_t (MPa)
0.8	1.8
1.5	1.9
3.1	2.1

A.1.5 Mivelaz [1996] anchors

The last studied anchor corresponds to the Mivelaz [1996] anchor. Two types of concrete, three reinforcement ratios and two different distributions of the steel bars were tested. The studied anchor, in this thesis, has $0.42 \times 1 \times 5$ m^3 dimensions and it represents a massive structure. The steel distribution of the studied anchor is described in Figure A.5, where the reinforcement ratio corresponds to 0.86 %. The concrete used is IBAP

FIGURE A.5: Reinforcement in the Mivelaz anchor and transversal section with longitudinal reinforcement (Mivelaz [1996]).

concrete, which corresponds to an ordinary concrete of class C30/C37 in Eurocode2 (CEN [2005]). The principal components of this concrete are given in Table A.11. The main characteristic of the IBAP concrete is given in Table A.12. The anchor was

TABLE A.11: Compositions of the concrete (Mivelaz [1996]).

Components	Mass (kg)
Sand 0-3	587
Gravel 3-8	329
Gravel 8-16	329
Gravel 16-32	755
Cement (CPN)	300
Water	148

subjected to axial traction forces. The first meter from each border of the anchors is reserved to the penetration of forces only, so the deformation measurement is limited at only 3 m in the longitudinal direction. Finally, a rupture strength equal to 1.48 MPa is deduced.

TABLE A.12: Characteristics of the concrete (Mivelaz [1996]).

	Mean	Standard deviation
f_c (MPa)	37.9	4.4
f_{ctm} (MPa)	2.6	0.3
E (GPa)	31.8	1.2

A.2 Series of concrete beams under 3-point bending loading

A.2.1 Hoover and Bažant [2014a] series

The US department of transportation provided major funding to conduct a series of concrete fracture tests. 164 concrete specimens were casted from the same batch of mixed concrete, thus the material properties of all the specimens were the same. 128 beams of 4 different sizes were also casted, these beams are all geometrically similar and have a constant thickness of 40 mm and a length-to-depth ratio of 2.4, and their depths were equal to 40, 93, 215 and 500 mm, corresponding to a size range of 1:12.5. Notches of 1.5 mm wide and five different relative depths $\alpha = a/D = 0.025, 0.075, 0.150$ and 0.3 were cut into the beams, where a is the notch depth (Hoover and Bažant [2014a]). The properties of the concrete used in theses fracture tests are presented in Table A.13. The tensile strength was calculated for all the beams from the measured dimensions,

TABLE A.13: Compositions of the concrete (Hoover and Bažant [2014a]).

Concrete properties	Values
Compressive strength	3 1.03 MPa
Maximum aggregate diameter	10 mm
Water/Cement ratio	0.41
Water/binder ratio	0.35

particularly the actual thickness of each beam over the ligament, which deviated slightly from the design thickness. The average overall thickness of the beams is equal to 39.74 mm with a standard deviation of 1.61 mm and coefficient of variation of 4.06 %. The statistics for family of unnotched beams ($\alpha = 0$) are shown in Table A.14.

TABLE A.14: Mean, standard deviation and coefficient of variation of the tensile strength of each beam of Hoover and Bažant [2014a] series.

Depth D (mm)	$\mu(f_t)$ (MPa)	$Std(f_t)$ (MPa)	$CV(f_t)$ (MPa)
400.1	5.68	0.46	8.3
200	6.99	1.1	15.7
100.9	7.19	0.35	4.9
50.6	7.85	0.61	7.7

A.2.2 Grégoire et al. [2013] series

The aim of this study is to model geometrically similar beams with and without notches, having different volumes and under 3-point bending loading. Figure A.6 presents the different volumes and notches used for this series of beams. Four different volumes are cured with a constant thickness of 50 mm, a depth varying from 50 to 400 mm and a span-to-depth ratio equal to 2.5. As for the notches, three notch-to-depth ratios are considered: 0, 0.2 and 0.5. In total, 34 concrete beams were casted. The concrete mixture used is the same for all the beams and its characterization is presented in Table A.15. Moreover, to characterize the mechanical behavior of the concrete, standardized compressive tests and splitting tests are carried out on 51 standard cylinders. Table A.16 presents the mean, standard deviation and the coefficient of variation of the compressive strength, the Young's modulus, the Poisson ratio and the splitting tensile strength. As only unnotched beams are modeled in this thesis, only mean and standard deviation of the tensile strength corresponding to this case are summarized in Table A.17.

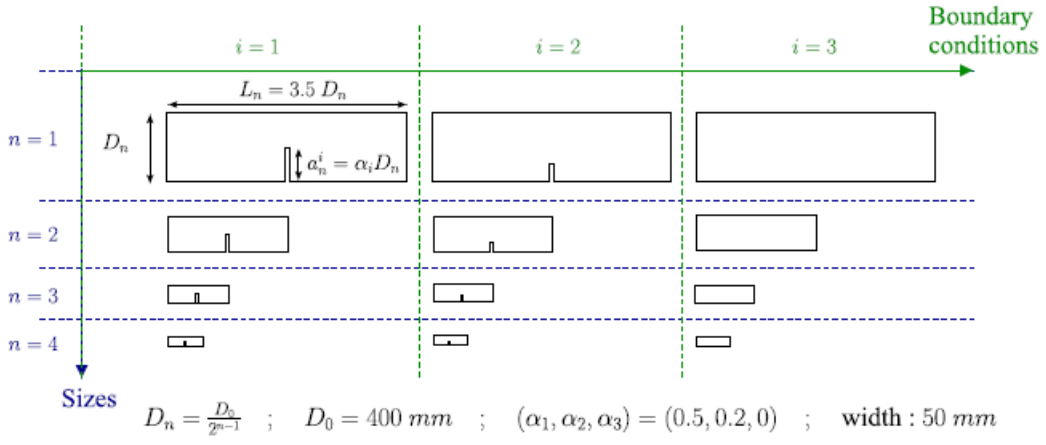

FIGURE A.6: Beams geometry (Grégoire et al. [2013]).

TABLE A.15: Concrete mixture formulation(Grégoire et al. [2013]).

Product	Designation	Mass (kg)
Sand	Cemex 0/4	740
Aggregates	Durruty 4/10	1140
Cement	Calcia CEM II/A	286
Admixture	Axim Cimplast 115	1
Water	Clarified water	179

TABLE A.16: Concrete mechanical properties (Grégoire et al. [2013]).

	μ	*Std*	CV
Compressive strength	42.3 MPa	2.8 MPa	6.6 %
Young modulus	37 GPa	0.9 GPa	2.4 %
Poisson ratio	0.21	0.02	8.7 %
Splitting tensile strength	3.9 MPa	0.2 MPa	6 %

TABLE A.17: Means, standard deviations and coefficient of variations of the tensile strength, corresponding to each beam of Grégoire et al. [2013] series.

Depth D (mm)	$\mu(f_t)$ (MPa)	$Std(f_t)$ (MPa)	$CV(f_t)$ (MPa)
400.1	4.6	0.2	4.4
200	5.3	0.41	7.7
100.9	6	0.4	6.7
50.6	7	0.91	13.1

A.2.3 Torrent [1977] series

Different experimental tests conducted on splitting tests, 3-point bending and 4-point bending are carried out in Torrent [1977]. The objective of these experimental tests is to apply the highly stressed volume approach to different types of tests. Specimens are casted with mortar having different water/cement ratios and different types of aggregates. The cement used has a flexural modulus equal to 8.04 ± 0.35 MPa and a compressive strength of 44.3 ± 1.5 MPa, measured on RC mortar at 7 days. To test the effect of the type of aggregate, fine natural sand, medium natural sand and expanded clay 0-1 mm are used. In this thesis, only three mixes with the same type of aggregates (fine natural sand) and three different water/cement ratios 0.55, 0.67 and 0.8 corresponding respectively to Mix A, Mix B and Mix C are considered. Also, only 3-point bending tests are studied. These tests are done on rectangular beams having different volumes: $25 \times 25 \times 106$ mm^3, $25 \times 25 \times 240$ mm^3, $40 \times 40 \times 106$ mm^3 and $150 \times 150 \times 450$ mm^3. For each mix type, mean and standard deviation values of the tensile strength corresponding to the four different volumes are presented in Table A.18.

TABLE A.18: Means and standard deviations of tensile strength for three different volumes and corresponding to three different mixes (Torrent [1977]).

Volumes	Mix A $\mu(f_t)$ (MPa)	$Std(f_t)$ (MPa)	Mix B $\mu(f_t)$ (MPa)	$Std(f_t)$ (MPa)	Mix C $\mu(f_t)$ (MPa)	$Std(f_t)$ (MPa)
$25\times25\times106$	8.23	0.07	6.43	0.15	4.52	0.0.7
$25\times25\times240$	7.14	0.17	5.9	0.26	4.39	0.07
$40\times40\times106$	6.69	0.19	5.59	0.09	4.5	0.09
$150\times150\times450$	5.12	0.26	3.66	0.06	3.02	0.03

A.3 Series of concrete beams under 4-point bending

A.3.1 Koide et al. [2000] series

Koide et al. [2000] aimed to study the size effect on the flexural resistance of concrete beams from a point of the length of the beam. Therefore, series of concrete beams, with various bending span ($L_m = 200, 400$ and 600 mm), under 4-point bending loading are conducted. The shear span (200 mm) and the cross section (100×100 mm^2) are kept constant for all the three different beams studied. Figure A.7 shows the three different

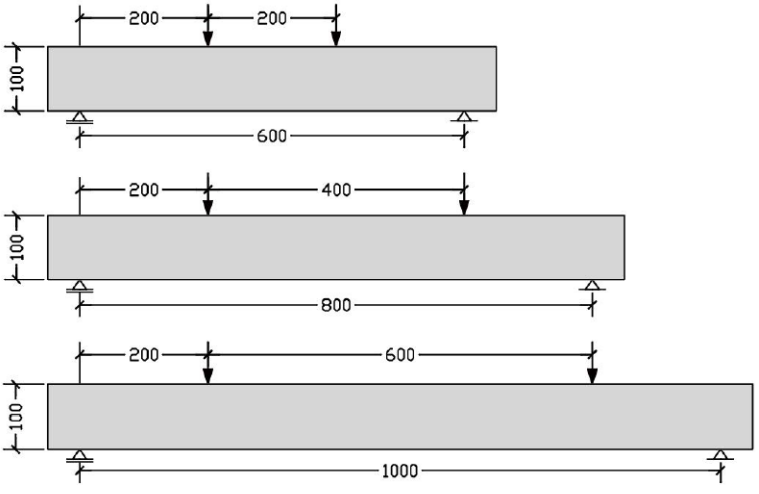

FIGURE A.7: Geometries of Koide beams (Korol [2012]).

geometries of the beams. 120 beams from the same batch of concrete were made and tested. The maximum diameter of aggregate is 20 mm and the compressive strength is equal to 30 MPa. However, concrete properties are not found in the literature. A

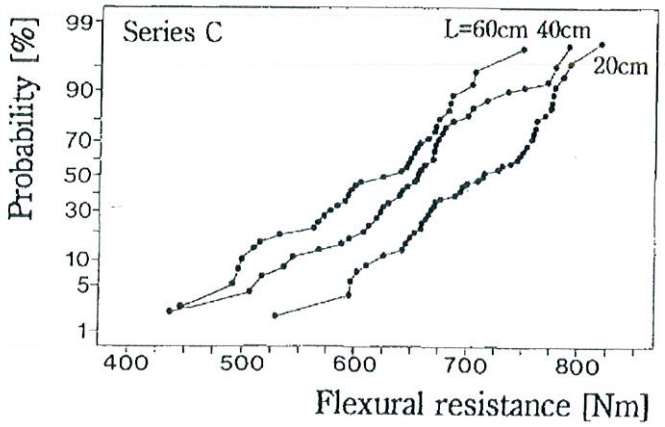

FIGURE A.8: Experimentally determined probability distribution functions (Koide et al. [2000]).

load-control method was applied and the bending moment obtained in the pure bending span is equal to 2.4 Nm/s. Figure A.8 presents the three cumulative density functions corresponding to the three different beams studied.

Appendix B

Probabilistic modelisation of uncertain parameters

B.1 Definition

The definition of random variables and random fields are presented in this Appendix. First, a probability space (Θ, F, P) needs to be defined:

- Θ is a set of outcomes.
- F is a collection of all the considered events.
- P is a function returning an event's probability.

B.1.1 Random variables

In probability and statistics, a random variable, aleatory variable or stochastic variable is a variable whose value is subjected to variations due to chance. A random variable $X : (\Theta, F, P) \rightarrow \mathrm{R}$ is a measurable function from the set of possible outcomes Θ to some set R. f_x and F_x are respectively the probability density function and the cumulative distribution function. The expected value (mean) and the variance are given by Equations B.1 and B.2 respectively.

$$\mu(x) = E[X] = \int_{-\infty}^{+\infty} x.f(x)dx \tag{B.1}$$

$$\sigma_x^2 = E\left[X - \mu_x\right] = \int_{-\infty}^{+\infty} (x - \mu_x)^2 . f(x) dx \tag{B.2}$$

The most familiar measure of dependency between two variables is the correlation coefficient that can be obtained by dividing the covariance of two variables by the product of their standard deviations. The correlation coefficient is defined as:

$$\rho\left(XY\right) = \frac{cov\left[X, Y\right]}{\sigma_X \sigma_Y} = \frac{E\left[\left(X - \mu_x\right)\left(Y - \mu_y\right)\right]}{\sigma_X \sigma_Y} \tag{B.3}$$

B.1.2 Gaussian random field

A random field $V(x)$ is defined as a collection of random variables indexed by a continuous parameter $x \in \Omega$, where Ω is an open set of R^d $(d = 1, 2, 3)$ describing the geometry. The Gaussian random field is completely defined by its mean function $\mu(x)$ and its autocovariance function $C_{VV}(x, x')$ that depends on an autocorrelation function $\rho_v(x, x')$.

$$C_{VV}(x, x') = \sigma(x)\sigma(x')\rho_v(x, x') \tag{B.4}$$

The variance function is defined by $\sigma^2(x) = C_{VV}(x, x)$.

The values in a random field are often spatially correlated. A random field is univariate or multivariate, depending on the nature of $V(x)$ attached to x, which could be a random variable or a random vector. Also, according to the dimension d of x ($d = 1$ or $d > 1$), it is called one-dimensional or multidimensional. In consequence, for modeling the spatial variability of the mechanical properties of the concrete, univariate multidimensional random fields are used. Moreover, a random field is homogeneous if it does not depend on the time; its corresponding autocorrelation function depends only on the relative length between two points:

$$\rho_v\left(x, x'\right) = \rho_v\left(x - x'\right) \tag{B.5}$$

B.2 Different methods of discretized random fields

A discretization method consists on approximating the original random field $V(x)$ by an approximated finite set of random variables $\{V_k, k = 1, \ldots, n\}$ grouped in a random

vector $\tilde{V}(x)$ (Sudret and Der Kiureghian [2000]):

$$V(x) \overset{Discretization}{\rightarrow} \tilde{V}(x) = \{V_k, k = 1, \ldots, n\} \tag{B.6}$$

Different discretization methods are presented in the literature. These methods can be divided into three main groups:

- Point discretization methods: the random variables V_k are specified values defined on a number of selected points x_i (the nodes of the FE mesh, for example).
- Average discretization: the random variables V_k are weighted integrals over a domain V_e (the volume of an element in a FE mesh, for example).
- Series expansion methods: the random variables are defined using series which contain also deterministic spatial functions. The discretization results from the truncation of the series.

B.2.1 Point discretization methods

These methods are usually used in the FE context, where the approximation of the mechanical response of the structures is evaluated by a spatial discretization on the mesh (nodes x_i or elements V_e).

Midpoint method (MP) This method consists on the discretization of the random field at the centroid x_c of the element V_e, by defining a single random variable ($\tilde{V}(x) = V(x_c)$). Thus, the random field is simplified by the following random vector, defined on the centroids of all the elements (N_e is the number of elements):

$$V(x) \overset{Discretization}{\rightarrow} \tilde{V}(x) = \left\{V(x_c^1), \ldots, V(x_c^{N_e})\right\} \tag{B.7}$$

Shape function method (SF) The approximation of $V(x)$ is done, at each element having q number of nodes, using nodal values x_i and shape functions, as follow:

$$\tilde{V}(x) = \sum_{i=1}^{q} N_i(x)\, H(x_i) \tag{B.8}$$

where x_i is the coordinate of the node i and N_i is the associated shape function. In this case, the approximated random field is a set of q random variables, where q is the number of nodes in the mesh.

Optimal linear estimation method This method is also called "Kriging method". In this context, nodal discretization is considered for the approximated field $\tilde{V}(x)$. Thus, a linear function of nodal values $X = \{V(x_1), \ldots, V(x_q)\}$.

$$\tilde{V}(x) = a(x) \sum_{i=1}^{q} b_i(x) X_i = a(x) + b^T(x) X \tag{B.9}$$

where q is the number of nodes, $a(x)$ and $b_i(x)$ are functions determined by minimizing in each point x the variance of the error ($Var\left[V(x) - \tilde{V}(x)\right]$), by considering that $\tilde{V}(x)$ is an unbiased estimator of $V(x)$ in mean ($E\left[V(x) - \tilde{V}(x)\right] = 0$).
Thus, by solving this minimization problem point-wise for $b_i(x)$, the variance of the error is considered the same as the error of the variance or the difference between the variances of $V(x)$ and $\tilde{V}(x)$. Therefore, the approximated field is always under-estimated, since the error variance is a positive value. Moreover, the error and the approximated field should be uncorrelated, in order to minimize the error variance.

B.2.2 Average discretization method

Spatial average (SA) In the FE context, this method provides an approximated field at each element computed as the average of the original field $V(x)$ over the element:

$$\tilde{V}(x) = \frac{\int_{\Omega_e} V(x) d\Omega_e}{\Omega_e} \qquad x \in \Omega_e \tag{B.10}$$

Thus, the random field is a vector of constant values, defined at each element using Equation B.10:

$$V(x) \overset{Discretization}{\rightarrow} \tilde{V}(x) = \{V_1, \ldots, V_{N_e}\} \tag{B.11}$$

This method is applied, only for the case of rectangular elements.

B.2.3 Series expansion method

Karhunen-Loève expansion The key idea of this method is to expand any realization of $V(x)$, defined by the eigenvalue problem:

$$V(x,\theta) = \mu(x) + \sum_{i=1}^{\infty} \sqrt{\lambda_i}\xi_i(\theta)\varphi_i(x) \tag{B.12}$$

Equation B.12 has two main terms, where $\mu(x)$ is the expected value of the random field and the second term accounts for the stochastic and the spatial dependency. The random variables ξ_i account for the stochastic dependency and the covariance kernel eigenmodes (λ_i, φ_i), where λ_i are the eigenvalues and φ_i are the eigenvectors, accounting for the spatial dependency. The eigenvalues and eigenvectors are computed, using the Equation B.13, where $C_{VV}(x,x')$ is the covariance function for the random field V.

$$\int_V C_{VV}(x,x')\varphi_i(x')dV_{x'} = \lambda_i\varphi_i(x) \tag{B.13}$$

It is possible to compute the eigenvalues in a descending series converging to zero. Thus, a set of the largest eigenvalues and their corresponding eigenvectors should be determined. Consequently, the truncated Karhunen–Loève expansion, defined using Equation B.14, gives an approximation for any second-order random field. M is the number of chosen modes, which can be considered as optimal. In Equation B.14, the random variables φ_i, for Gaussian distributions, are normally distributed with an expected value of 0 and a variance equal to 1.

$$\tilde{V}(x,\theta) = \mu(x) + \sum_{i=1}^{M} \sqrt{\lambda_i}\xi_i(\theta)\varphi_i(x) \tag{B.14}$$

Orthogonal series expansion method This method consists on defining a set of orthogonal functions $h_i(x)_{i=1}^{\infty}$ and presents the advantage of avoiding solving the eigenvalue problem. The set of orthogonal functions is considered as orthonormal. Thus, the random field $V(x,\theta)$ is defined by the expected mean function $\mu(x)$ and an expansion by means of the orthogonal functions and zero-mean random variables $X_i(\theta)$.

$$V(x,\theta) = \mu(x) + \sum_{i=1}^{\infty} X_i(\theta)h_i(x) \tag{B.15}$$

With the hypothesis of orthogonality, for a Gaussian random field $V(x)$, the set $X_{i\,i=1}^{\infty}$ is a set of zero-mean Gaussian random variables, which also may be considered as correlated. Consequently, the approximated random field is deduced by choosing the number of terms kept for the discretization M.

$$\tilde{V}(x,\theta) = \mu(x) + \sum_{i=1}^{M} X_i(\theta) h_i(x) \tag{B.16}$$

Bibliography

Adachi, H., Shirai, N., Nakanishi, M., and Ogino, K. (1995). Size effect on strength and deformation of RC beams failing in flexure. *Fracture Mechanics of Concrete Structures, Proceedings of FRAMCOS-2, AEDIFICATIO Publishers, Freiburg*, pages 655–664.

Afferrante, L., Ciavarella, M., and Valenza, E. (2006). Is Weibull's modulus really a material constant? example case with interacting collinear cracks. *International Journal of Solids and Structures*, 43(17):5147–5157.

Arıoglu, Girgin, Z. C., and Arıoglu, E. (2006). Evaluation of ratio between splitting tensile strength and compressive strength for concretes up to 120 MPa and its application in strength criterion. *ACI Materials Journal*, 103(1):18–24.

ASTM, C. (2004). 496, standard test method for splitting tensile strength of cylindrical concrete specimens. *United States: ASTM International*.

Baroth, J. (2005). *Analyse par éléments finis stochastiques de la propagation d'incertitudes dans un modèle mécanique non linéaire*. PhD thesis, Université Blaise Pascal-Clermont II.

Barretta, R. and Barretta, A. (2010). Shear stresses in elastic beams: an intrinsic approach. *European Journal of Mechanics-A/Solids*, 29(3):400–409.

Bažant, Z. P. (1976). Instability, ductility, and size effect in strain-softening concrete. *Journal of the engineering mechanics division*, 102(2):331–344.

Bažant, Z. P. (1984). Size effect in blunt fracture: concrete, rock, metal. *Journal of Engineering Mechanics*, 110(4):518–535.

Bažant, Z. P. (1999). Size effect on structural strength: a review. *Archive of applied Mechanics*, 69(9):703–725.

Bažant, Z. P. and Desmorat, R. (1994). Size effect in fiber or bar pullout with interface softening slip. *Journal of engineering mechanics*, 120(9):1945–1962.

Bažant, Z. P. and Kazemi, M. T. (1991). Size dependence of concrete fracture energy determined by RILEM work-of-fracture method. In *Current Trends in Concrete Fracture Research*, pages 121–138. Springer.

Bažant, Z. P., Kazemi, M. T., Hasegawa, T., and J., M. (1991). Size effect in brazilian split-cylinder tests: Measurements and fracture analysis. *ACI Materials Journal*, 88(4):325–332.

Bažant, Z. P. and Novak, D. (2000). Energetic-statistical size effect in quasibrittle failure at crack initiation. *ACI Mater. J*, 97(3):381–392.

Bažant, Z. P., Vořechovskỳ, M., and Novák, D. (2007). Asymptotic prediction of energetic-statistical size effect from deterministic finite-element solutions. *Journal of engineering mechanics*, 133(2):153–162.

Bergman, B. (1984). On the estimation of the Weibull modulus. *Journal of Materials Science Letters*, 3(8):689–692.

Bornert, M., Bretheau, T., and Gilormini, P. (2001). *Homogénéisation en mécanique des matériaux, Tome 1: Matériaux aléatoires élastiques et milieux périodiques*. Hermes science.

Bouhjiti, E.-M., Baroth, J., Dufour, F., and Masson, B. (2017). Sensitivity analysis of cracking in large reinforced and prestressed concrete structures, case of the veRCoRs mock-up. *23ème Congrès Francais de Mécanique*.

Breysse, D. (1990). Probabilistic formulation of damage-evolution law of cementitious composites. *Journal of engineering mechanics*, 116(7):1489–1510.

Breysse, D. (1991). Numerical study of the effect of inhomogeneities and boundary conditions on the tensile strength of concrete. *Materials Journal*, 88(5):489–498.

Briffaut, M. (2010). *Etude de la fissuration au jeune âge des structures massives en béton: influence de la vitesse de refroidissement, des reprises de bétonnage et des armatures*. PhD thesis, Ecole normale supérieure de Cachan.

Carmeliet, J. and de Borst, R. (1995). Stochastic approaches for damage evolution in standard and non-standard continua. *International journal of solids and structures*, 32(8-9):1149–1160.

Carmona, S., Gettu, R., and Aguado, A. (1998). Study of the post-peak behavior of concrete in the splitting-tension test. *AEDIFICATIO Publishers, Fracture Mechanics of Concrete Structures,*, 1:111–120.

Carpinteri, A. (1989). Decrease of apparent tensile and bending strength with specimen size: two different explanations based on fracture mechanics. *International Journal of Solids and Structures*, 25(4):407–429.

Carpinteri, A., Chiaia, B., and Ferro, G. (1995). Size effects on nominal tensile strength of concrete structures: multifractality of material ligaments and dimensional transition from order to disorder. *Materials and Structures*, 28(6):311–317.

Carpinteri, A. and Cornetti, P. (2002). Size effects on concrete tensile fracture properties: an interpretation of the fractal approach based on the aggregate grading. *Journal of the Mechanical Behavior of Materials*, 13(3/4):233–246.

CEA (2015). Description of the finite element code Cast3m.

CEN (2005). Eurocode 2: Design of concrete structures. *EN 1992*, 4 (04.02):266–269.

Ceos.fr (2009). French national research project for design and assessment of special concrete structure toward cracking and shrinkage.

Clement, J. L. (1987). *Interface acier-béton et comportement des structures en béton armé - Caractérisation – Modélisation.* PhD thesis, Université Paris VI.

Code, M. (2012). Model code 2010-final draft, vol. 1. *Bulletin*, 65.

Colliat, J.-B., Hautefeuille, M., Ibrahimbegovic, A., and Matthies, H. G. (2007). Stochastic approach to size effect in quasi-brittle materials. *Comptes Rendus Mécanique*, 335(8):430–435.

Corbin, M. and Garcia, M. (2015). International benchmark, VeRCoRs: Overview, synthesis and lessons learnt. *EDF Septen*, 65.

Danzer, R., Supancic, P., Pascual, J., and Lube, T. (2007). Fracture statistics of ceramics–weibull statistics and deviations from weibull statistics. *Engineering Fracture Mechanics*, 74(18):2919–2932.

De Larrard, T., Colliat, J., Benboudjema, F., Torrenti, J., and Nahas, G. (2010). Effect of the Young modulus variability on the mechanical behaviour of a nuclear containment vessel. *Nuclear Engineering and Design*, 240(12):4051–4060.

Del Viso, J., Carmona, J., and Ruiz, G. (2007). Size and shape effects on the compressive strength of high strength concrete. In *6th International Conference on Fracture Mechanics of Concrete and Concrete Structures*, pages 1297–1304.

Duffaut, P. (2013). The traps behind the failure of Malpasset arch dam, France, in 1959. *Journal of Rock Mechanics and Geotechnical Engineering*, 5(5):335–341.

Dufour, F. (2017). Advanced concrete mechanics course. *Master 2 Geomechanics civil engineering and risk*.

Dufour, F., Legrain, G., Pijaudier-Cabot, G., and Huerta, A. (2012). Estimation of crack opening from a two-dimensional continuum-based finite element computation. *International journal for numerical and analytical methods in geomechanics*, 36(16):1813–1830.

EN, N. (2001). 12390-8: Norme: Essai pour béton durci–partie 8: Profondeur de pénétration d'eau sous pression. *AFNOR, oct*.

Farra, B. (1994). *Influence du béton et de l'armature sur la fissuration des structures en béton*. PhD thesis, Ecole polytechnique fédéral de Lausanne.

Fisher, R. A. and Tippett, L. H. C. (1928). Limiting forms of the frequency distribution of the largest or smallest member of a sample. In *Mathematical Proceedings of the Cambridge Philosophical Society*, volume 24, pages 180–190. Cambridge Univ Press.

Fréchet, M. (1928). Sur la loi de probabilité de l'écart maximum. In *Annales de la societe Polonaise de Mathematique*. [sn].

Gagg, C. R. (2014). Cement and concrete as an engineering material: an historic appraisal and case study analysis. *Engineering Failure Analysis*, 40:114–140.

Giry, C. (2011). *Modélisation objective de la localisation des déformations et de la fissuration dans les structures en béton armé*. PhD thesis, Université de Grenoble.

Giry, C., Dufour, F., and Mazars, J. (2011). Modified nonlocal damage model based on stress state influence. *IJSS*, 48(25-26):3431–3443.

Gomez-Cardenas, C., Sbartai, Z.-M., Balayssac, J. P., Garnier, V., and Breysse, D. (2015). New optimization algorithm for optimal spatial sampling during non-destructive testing of concrete structures. *Engineering Structures*, 88:92–99.

Grassl, P., Wong, H. S., and Buenfeld, N. R. (2010). Influence of aggregate size and volume fraction on shrinkage induced micro-cracking of concrete and mortar. *Cement and concrete research*, 40(1):85–93.

Grégoire, D., Rojas-Solano, L., and Pijaudier-Cabot, G. (2013). Failure and size effect for notched and unnotched concrete beams. *International Journal for Numerical and Analytical Methods in Geomechanics*, 37(10):1434–1452.

Griffith, A. A. (1921). The phenomena of rupture and flow in solids. *Philosophical transactions of the royal society of london. Series A, containing papers of a mathematical or physical character*, 221:163–198.

Hasegawa, T., Shioya, T., and Okada, T. (1985). Size effect on splitting tensile strength of concrete. In *Proceedings Japan Concrete Institute 7th Conference*, pages 309–312.

Hillerborg, A., Modéer, M., and Petersson, P.-E. (1976a). Analysis of crack formation and crack growth in concrete by means of fracture mechanics and finite elements. *Cement and concrete research*, 6(6):773–781.

Hillerborg, A., Modéer, M., and Petersson, P.-E. (1976b). Analysis of crack formation and crack growth in concrete by means of fracture mechanics and finite elements. *Cement and concrete research*, 6(6):773–781.

Hoover, C. and Bažant, Z. P. (2014a). Universal size-shape effect law based on comprehensive concrete fracture tests. *Journal of Engineering Mechanics*, 140(3):473–479.

Hoover, C. G. and Bažant, Z. P. (2014b). Universal size-shape effect law based on comprehensive concrete fracture tests. *Journal of Engineering Mechanics*, 140(3):473–479.

Irwin, G. (1960). Plastic zone near a crack and fracture toughness. *Proceedings of 7th Sagamore conf.*, 250:63.

Kadleček, V. and Modrỳ, S. (2002). Size effect of test specimens on tensile splitting strength of concrete: general relation. *Materials and Structures*, 35(1):28.

Kanos, A., Kanos, A., and Perdikaris, P. (2006). Size effect on concrete splitting tensile strength and modulus of elasticity. *Measuring, monitoring and modeling concrete properties*, pages 239–246.

Kittl, P. and Diaz, G. (1988). Weibull's fracture statistics, or probabilistic strength of materials: state of the art. *Res Mechanica*, 24(2):99–207.

Kittl, P. and Diaz, G. (1990). Size effect on fracture strength in the probabilistic strength of materials. *Reliability Engineering & System Safety*, 28(1):9–21.

Koide, H., Akita, H., and Tomon, M. (2000). Probability model of flexural resistance on different lengths of concrete beams. *Application of Statistic and Probability*, pages 1053–1057.

Korol, E. (2012). *Theoretical and experimental study on size effect in concrete beams reinforced with steel or basalt bars.* PhD thesis, Doctoral thesis, Gdańsk university of technology.

Kuguel, R. (1961). A relation between theoretical stress concentration factor and fatigue notch factor deduced from the concept of highly stressed volume. In *Proc. ASTM*, volume 61, pages 732–748.

Lamon, J. (1988). Ceramics reliability: Statistical analysis of multiaxial failure using the Weibull approach and the multiaxial elemental strength model. In *ASME 1988 International Gas Turbine and Aeroengine Congress and Exposition*, pages V005T13A004–V005T13A004. American Society of Mechanical Engineers.

Lamon, J. and Evans, A. G. (1983). Statistical analysis of bending strengths for brittle solids: a multiaxial fracture problem. *Journal of the American Ceramic Society*, 66(3):177–182.

Le, J.-L., Bažant, Z. P., and Bazant, M. Z. (2011). Unified nano-mechanics based probabilistic theory of quasibrittle and brittle structures: I. strength, static crack growth, lifetime and scaling. *Journal of the Mechanics and Physics of Solids*, 59(7):1291–1321.

Le, J.-L., Falchetto, A. C., and Marasteanu, M. O. (2013). Determination of strength distribution of quasibrittle structures from mean size effect analysis. *Mechanics of Materials*, 66:79–87.

Lefort, V., Pijaudier-Cabot, G., and Grégoire, D. (2015). Analysis by Ripley's function of the correlations involved during failure in quasi-brittle materials: Experimental and numerical investigations at the mesoscale. *Engineering Fracture Mechanics*, 147:449–467.

Li, C.-C. and Der Kiureghian, A. (1993). Optimal discretization of random fields. *Journal of engineering mechanics*, 119(6):1136–1154.

Małecki, T., Marzec, I., Bobiński, J., and Tejchman, J. (2007). Effect of a characteristic length on crack spacing in a reinforced concrete bar under tension. *Mechanics Research Communications*, 34(5):460–465.

Malhotra, V. (1970). Effect of specimen size on tensile strength of concrete. In *Journal Proceedings*, volume 67, pages 467–480.

Mazars, J. (1984). *Application de la mécanique de l'endommagement au comportement non linéaire et à la rupture de béton de structure*. PhD thesis, Université Pierre et Marie Curie.

Mazars, J. (1986). A description of micro-and macroscale damage of concrete structures. *Engineering Fracture Mechanics*, 25(5):729–737.

Mazars, J., Hamon, F., and Grange, S. (2015). A new 3D damage model for concrete under monotonic, cyclic and dynamic loadings. *Materials and Structures*, 48(11):3779–3793.

Mefisto (2012). Maitrise durable de la fissuration des infrastructures en béton. *Projet ANRT*.

Mesureur, B. (1989). Résistances des bétons: Etude de la relation existant entre la résistance à la traction et la résistance à la compression des bétons courants de batiment. *cahiers du CSTB*, 305.

Michelle-Ponnelle, S. (2015). Description de l'essai PACE1450 et de la maquette veRCoRs à destination du projet MACENA. *EDF R&D analyses mécaniques et acoustique tenue des ouvrages*.

Mihashi, H. and Izumi, M. (1977). A stochastic theory for concrete fracture. *Cement and Concrete Research*, 7(4):411–421.

Mivelaz, P. (1996). *Etanchéité des structures en béton armé: Fuite au travers d'un élément fissuré*. PhD thesis, Ecole polytechnique fédérale de Lausanne.

Momayez, A., Ehsani, M., Ramezanianpour, A., and Rajaie, H. (2005). Comparison of methods for evaluating bond strength between concrete substrate and repair materials. *Cement and concrete research*, 35(4):748–757.

Nemati, K. M. and Gardoni, P. (2005). Microstructural and statistical evaluation of interfacial zone percolation in concrete. *Strength, fracture and complexity*, 3(2-4):191–197.

Neville, A. M. (1995). *Properties of concrete*.

Peirce, F. T. (1926). Tensile tests for cotton yarns:"the weakest link" theorems on the strength of long and of composite specimens. *J. Textile Inst*, 17:T355–368.

Pijaudier-Cabot, G. and Bažant, Z. P. (1987). Nonlocal damage theory. *Journal of engineering mechanics*, 113(10):1512–1533.

Post, G. and Bonazzi, D. (1987). Latest thinking on the Malpasset accident. *Engineering Geology*, 24(1-4):339–353.

Quinn, G. D. (2003a). Weibull effective volumes and surfaces for cylindrical rods loaded in flexure. *Journal of the American Ceramic Society*, 86(3):475–479.

Quinn, G. D. (2003b). Weibull strength scaling for standardized rectangular flexure specimens. *Journal of the American Ceramic Society*, 86(3):508–510.

Rocco, C., Guinea, G., Planas, J., and Elices, M. (2001). Review of the splitting-test standards from a fracture mechanics point of view. *Cement and concrete research*, 31(1):73–82.

Rossi, P. and Piau, J. (1988). The usefulness of statistical models to describe damage and fracture in concrete. In *CNRS-NSF Workshop Strain Localization and Size Effect due to Cracking and Damage, Cachan, France*, pages 91–103.

Rossi, P. and Ulm, F. (1997). Size effects in the biaxial tensile-compressive behaviour of concrete: physical mechanisms and modelling. *Materials and structures*, 30(4):210–216.

Rossi, P., Ulm, F.-J., and Hachi, F. (1996). Compressive behavior of concrete: physical mechanisms and modeling. *Journal of Engineering Mechanics*, 122(11):1038–1043.

Rossi, P., Wu, X., Le Maou, F., and Belloc, A. (1994). Scale effect on concrete in tension. *Materials and Structures*, 27(8):437–444.

Saouma, V. and Fava, G. (2006). On fractals and size effects. *International Journal of Fracture*, 137(1):231–249.

Saouma, V., Natekar, D., and Hansen, E. (2003). Cohesive stresses and size effects in elasto-plastic and quasi-brittle materials. *International journal of fracture*, 119(3):287–298.

Sebsadji, S. and Chouicha, K. (2012). Determining periodic representative volumes of concrete mixtures based on the fractal analysis. *International Journal of Solids and Structures*, 49(21):2941–2950.

Sellier, A. and Millard, A. (2014). Weakest link and localisation WL2: a method to conciliate probabilistic and energetic scale effects in numerical models. *European journal of environmental and civil engineering*, 18(10):1177–1191.

Skarżyński, Ł., Syroka, E., and Tejchman, J. (2011). Measurements and calculations of the width of the fracture process zones on the surface of notched concrete beams. *Strain*, 47(s1).

Stroeven, M., Askes, H., and Sluys, L. (2004). Numerical determination of representative volumes for granular materials. *Computer Methods in Applied Mechanics and Engineering*, 193(30):3221–3238.

Sudret, B. (2007). Uncertainty propagation and sensitivity analysis in mechanical models–contributions to structural reliability and stochastic spectral methods. *Habilitationa diriger des recherches, Université Blaise Pascal, Clermont-Ferrand, France.*

Sudret, B. and Der Kiureghian, A. (2000). *Stochastic finite element methods and reliability: a state-of-the-art report.* Department of Civil and Environmental Engineering, University of California Berkeley, CA.

Syroka-Korol, E., Tejchman, J., and Mróz, Z. (2013). FE calculations of a deterministic and statistical size effect in concrete under bending within stochastic elasto-plasticity and non-local softening. *Engineering Structures*, 48:205–219.

Tanaka, Y. and Shimomura, T. (2010). Role of diagonal tension crack in size effect of shear strength of deep beams. *Proceedings Framcos-7*, pages 198–206.

Tang, X., Zhou, Y., Zhang, C., and Shi, J. (2010). Study on the heterogeneity of concrete and its failure behavior using the equivalent probabilistic model. *Journal of materials in civil engineering*, 23(4):402–413.

Tippett, L. H. C. (1925). On the extreme individuals and the range of samples taken from a normal population. *Biometrika*, 17(3-4):364–387.

Torrent, R. (1977). A general relation between tensile strength and specimen geometry for concrete-like materials. *Matériaux et Construction*, 10(4):187–196.

Van Vliet, M. and Van Mier, J. (2000). Experimental investigation of size effect in concrete and sandstone under uniaxial tension. *Engineering Fracture Mechanics*, 65(2):165–188.

Vanmarcke, E. (2010). *Random fields: analysis and synthesis*. World Scientific Publishing Co Inc.

Von Mises, R. (1936). La distribution de la plus grande de n valeurs. *Rev. math. Union interbalcanique*, 1(1).

Vořechovskỳ, M. (2007). Interplay of size effects in concrete specimens under tension studied via computational stochastic fracture mechanics. *International Journal of Solids and Structures*, 44(9):2715–2731.

Warren, P. (2001). Fracture of brittle materials: effects of test method and threshold stress on the Weibull modulus. *Journal of the European Ceramic Society*, 21(3):335–342.

Weibull, W. (1951). A statistical distribution function of wide applicability. *Journal of applied mechanics*, 18(3):293–297.

Wittmann, F. H. and Zaitsev, Y. V. (2013). Crack propagation and fracture of composite materials such as concrete. In *ICF5, Cannes (France) 1981*.

Wong, H., Zobel, M., Buenfeld, N., and Zimmerman, R. (2009). Influence of the interfacial transition zone and microcracking on the diffusivity, permeability and sorptivity of cement-based materials after drying. *Mag. Concr. Res*, 61(8):571–589.

Wright, P. and Garwood, F. (1952). The effect of the method of test on the flexural strength of concrete. *Magazine of Concrete Research*, 4(11):67–76.

Wu, Q. (2015). Estimation du volume élémentaire représentatif associé à la détermination d'isothermes de désorption sur bétons. In *Rencontres Universitaires de Génie Civil*.

Wu, S., Chen, X., and Zhou, J. (2012). Tensile strength of concrete under static and intermediate strain rates: Correlated results from different testing methods. *Nuclear Engineering and Design*, 250:173–183.

Yi, S.-T., Yang, E.-I., and Choi, J.-C. (2006). Effect of specimen sizes, specimen shapes, and placement directions on compressive strength of concrete. *Nuclear Engineering and Design*, 236(2):115–127.

Zhang, N. and Tan, K.-H. (2007). Size effect in RC deep beams: Experimental investigation and STM verification. *Engineering Structures*, 29(12):3241–3254.